

Quantification of calcium signatures in roots of  
*Arabidopsis thaliana*



# Dissertation

submitted to the  
Combined Faculty of Natural Sciences and Mathematics  
of the Ruperto Carola University Heidelberg, Germany  
for the degree of  
Doctor of Natural Sciences

Presented by

**MSc. Rik Brugman**

Born in: Amstelveen, Netherlands

Oral examination: 27th of September 2019



**Quantification of calcium signatures in  
roots of *Arabidopsis thaliana***

Referees:

Prof. Dr. Karin Schumacher

Dr. Guido Grossmann



# Table of content

<b>Contributions</b> .....	<b>1</b>
<b>Summary</b> .....	<b>2</b>
<b>Zusammenfassung</b> .....	<b>3</b>
<b>1. Introduction</b> .....	<b>5</b>
1.1 Calcium as a second messenger.....	5
1.2 Calcium signatures.....	7
1.3 How are calcium signatures measured? .....	8
1.4 Elicitors of calcium signals.....	9
1.5 'Single file' versus 'network' signaling .....	13
1.6 The aim of this thesis.....	15
<b>2 Results:</b> .....	<b>16</b>
<b>2.1: How to quantify calcium signatures?</b> .....	<b>16</b>
2.1.1: A new method for spatio-temporal quantification of calcium signatures in <i>Arabidopsis</i> roots .....	16
2.1.2: Spatio-temporal quantification of calcium responses in <i>Arabidopsis</i> roots reveals stimulus-specific signatures.....	18
2.1.3: The maximum amount of calcium released into the cytoplasm is the same for different stresses .....	24
<b>2.2: Differences in calcium signatures of biotic and abiotic stresses</b> .....	<b>25</b>
2.2.1: There are distinct biotic and abiotic features in calcium signatures.....	25
2.2.2: The calcium signature can be used to make predictions about the nature of sensing mechanisms .....	33
2.2.3: The calcium response to biotic stresses is not propagated through the root	35
<b>2.3: Different stress responses use overlapping signaling pathways</b> .....	<b>37</b>
2.3.1: Simultaneous exposure to flg22 and C8 results in one unique calcium response.....	38
2.3.2: Exposure to NaCl and flg22 simultaneously results in an intermediate calcium signature .....	39
2.3.3: Calcium signatures in response to simultaneous NaCl and C8 exposure exhibit parameters from both single elicitors.....	41
<b>2.4: ROS plays a role in both biotic and abiotic signaling responses</b> .....	<b>42</b>
2.4.1: ROS play a role in both the initiation and the propagation of calcium signals in response to salt stress.....	43
2.4.2: ROS targets and restricts the biotic calcium response to the elongation zone.....	44
2.4.3: ROS scavenging results in a higher maximum calcium release for C8 .....	46
2.4.4: ROS is produced during salt signaling responses, but not during flg22 or C8 signaling responses .....	47
<b>2.5: Different signaling pathways start their own set of downstream responses</b> .....	<b>49</b>

2.5.1: ROS targets the calcium response to a combination of flg22 and C8 to the elongation zone.....	49
2.5.2: ROS plays a role in the signal initiation and propagation response to combined NaCl and flg22 stress .....	50
2.5.3: ROS plays a role in prioritization between NaCl and C8 stress.....	53
<b>2.6: Crestline: An automated image analysis pipeline for calcium signature analysis.....</b>	<b>54</b>
<b>3 Discussion.....</b>	<b>57</b>
3.1: Global stimulation can be used to examine signal propagation pathways ...	57
3.2: The amplitude of the calcium release is not part of the calcium signature ...	58
3.3 Calcium signature analysis reveals information about the nature of a stress	59
3.4 Local application of stresses show that the flg22 induced calcium signal is not propagated .....	60
3.5 Newly produced ROS is not involved in the flg22 calcium signaling response .....	61
3.6 ROS targets and restricts the biotic calcium signal to the elongation zone ...	62
3.7 Combinations of stresses result in new calcium signatures and stress responses .....	63
3.8 Different branches of signaling pathways influence the calcium signature parameters .....	64
3.9 Is calcium just a chemical switch after all? .....	65
<b>Material and Methods .....</b>	<b>68</b>
4.1 Plant growth conditions.....	68
4.2 Microscopy .....	68
4.3 Image and data analysis.....	70
4.4 Data analysis.....	71
<b>Supplemental information .....</b>	<b>74</b>
<b>Acknowledgements .....</b>	<b>95</b>



## Contributions

The work presented in this thesis has been partially published in the following publications:

Keinath, N. F., Waadt, R., Brugman, R., Schroeder, J. I., Grossmann, G., Schumacher, K., & Krebs, M. (2015). Live Cell Imaging with R-GECO1 Sheds Light on flg22- and Chitin-Induced Transient  $[Ca^{2+}]_{cyt}$  Patterns in Arabidopsis. *Molecular Plant*, 1–13. <http://doi.org/10.1016/j.molp.2015.05.006>

Stanley, C. E., Shrivastava, J., Brugman, R., Heinzelmann, E., van Swaay, D., & Grossmann, G. (2017). Dual-flow-RootChip reveals local adaptations of roots towards environmental asymmetry at the physiological and genetic levels. *New Phytologist*, 217(3), 1357–1369. <http://doi.org/10.1002/sml.201503208>

Stanley, C., Shrivastava, J., Brugman, R., Heinzelmann, E., Frajs, V., Bühler, A., et al. (2018). Fabrication and Use of the Dual-Flow-RootChip for the Imaging of Arabidopsis Roots in Asymmetric Microenvironments. *Bio-Protocol*, 8(18). <http://doi.org/10.21769/BioProtoc.3010>

Wan, W.-L., Zhang, L., Pruitt, R., Zaidem, M., Brugman, R., Ma, X., et al. (2018). Comparing Arabidopsis receptor kinase and receptor protein-mediated immune signaling reveals BIK1-dependent differences. *New Phytologist*, 1, 15140. <http://doi.org/10.1038/nature02485>

Parts of this thesis would not have been possible without the help of other scientists:

Martin Zauser created the Crestline normalization method and wrote the R script that automated the calcium signature quantification.

Milan Župunski provided support with the principle component analysis.

## Summary

Calcium ( $\text{Ca}^{2+}$ ) is an essential second messenger in plant cells linking the perception of stresses at the plasma membrane to the appropriate defense response. The calcium signature theory states that for each perceived stress there is a unique calcium transient that triggers specific downstream responses. It is thought that the signaling specificity is encoded in the spatio-temporal pattern of cytosolic calcium concentration, which is in turn decoded by various intracellular calcium binding proteins. For 25 years now the calcium signature theory has not been conclusively proven, and alternative theories are now appearing. One of the problems remaining is that there is no standard method to quantify these spatio-temporal signals. The aim of this thesis was to develop a standard method to quantify calcium signatures in plants and start constructing a library of calcium signatures in response to different stresses. As a model system I used *Arabidopsis thaliana* roots expressing the R-GECO calcium sensor.

To quantify the spatio-temporal calcium response, the calcium signature was divided into six quantifiable parameters: (a) delay of the first detected calcium signal, (b) location of the first calcium signal, (c) duration of the calcium signal, (d) distance that the calcium wave traveled along the root, (e) velocity with which the calcium wave travels towards the root tip, and (f) velocity with which the calcium wave travels towards the shoot. Principle component analysis (PCA) was used to look for similarities and analyze the data. Responses to eleven elicitors (ATP, chitin, cellobiose, cold, D-serine, elf18, flg22, glutamate, NaCl, nlp20 and PG3) were tested. The results showed that, indeed, each elicitor resulted in a unique composition of the six parameters that together form the calcium signature. Moreover, calcium signatures in response to biotic versus abiotic elicitors formed two distinct groups. While biotic stress caused delayed calcium responses specific to the elongation zone of plant roots, abiotic stresses resulted in immediate and systemic calcium signatures. Further experiments suggested that ROS play a key role in restricting calcium signatures to the elongation zone in response to biotic stress and in propagation of calcium signals through the root in response to abiotic stress, indicating that there is crosstalk between reactive oxygen species (ROS) and calcium signatures to prioritize distinct stresses.

## Zusammenfassung

Kalzium ist ein essentieller sekundärer Botenstoff in Pflanzenzellen, der die Wahrnehmung von Reizen an der Plasmamembran mit der entsprechenden Abwehrreaktion verbindet. Die Kalziumsignaturtheorie besagt, dass es für jeden wahrgenommenen Stress einen einzigartigen Kalzium-Transient gibt, der spezifische Downstream-Reaktionen auslöst. Es wird angenommen, dass die Signalspezifität in dem raum-zeitlichen Muster der zytosolischen Kalziumkonzentration kodiert ist, das wiederum von verschiedenen intrazellulären Kalziumbindungsproteinen erkannt wird. In den letzten 25 Jahren wurde die Kalziumsignaturtheorie noch nicht vollständig bewiesen und es gibt mittlerweile alternative Theorien. Eines der verbleibenden Probleme der Kalzium-Signatur-Theorie besteht darin, dass es keine Standardmethode zur Quantifizierung dieser raum-zeitlichen Kalziumsignale gibt.

Das Ziel dieser Arbeit war es, eine Standardmethode zur Quantifizierung von Kalziumsignaturen in Pflanzen zu entwickeln und eine Bibliothek von Kalziumsignaturen zu erstellen, die von unterschiedlichen Arten von Stress ausgelöst werden. Als Modellsystem wurden Wurzeln aus *Arabidopsis thaliana* verwendet, die den Kalziumsensor R-GECO exprimierten.

Um die raum-zeitliche Kalziumsignatur zu quantifizieren, wurde die Kalziumsignatur in sechs quantifizierbare Parameter unterteilt: (a) Verzögerung des ersten detektierbaren Kalziumsignals, (b) Ort des ersten Kalziumsignals, (c) Dauer des Kalziumsignals, (d) zurückgelegte Entfernung der Kalziumwelle, (e) Geschwindigkeit, mit der sich die Kalziumwelle zur Wurzelspitze bewegte, und (f) Geschwindigkeit, mit der sich die Kalziumwelle zum Spross bewegte. Die Hauptkomponentenanalyse wurde verwendet, um Gemeinsamkeiten der Reaktionsmuster zu identifizieren. Die Reaktionen auf elf Elicitoren (ATP, Chitin, Cellobiose, Kälte, D-Serin, Elf18, Flg22, Glutamat, NaCl, nlp20 und PG3) wurden getestet. Die Ergebnisse zeigten, dass tatsächlich jeder Elicitor zu einer einzigartigen Zusammensetzung der sechs Parameter führte, die zusammen die individuelle Kalziumsignatur ergaben. Darüber hinaus bildeten Kalziumsignaturen

als Reaktion auf biotische beziehungsweise abiotische Elicitoren zwei unterschiedliche Gruppen. Während biotischer Stress eine verzögerte Kalziumreaktionen verursachte, die auf die Zellstreckungszone der Pflanzenwurzeln begrenzt waren, führten abiotische Reize zu sofortigen und systemischen Kalziumsignaturen. Weitere Experimente zeigten, dass reaktive Sauerstoffspezies (ROS) eine Schlüsselrolle bei der Entstehung der Kalziumsignaturen spielen. Die Antwort auf biotischen Stress wird durch ROS auf die Zellstreckungszone beschränkt wohingegen die Weiterleitung der Antwort auf abiotischen Stress durch ROS auf die gesamte Wurzel ausgedehnt wird. Diese Ergebnisse deuten darauf hin, dass ROS und Kalziumsignaturen zusammenarbeiten, um unterschiedliche Reize zu priorisieren.

# 1. Introduction

## 1.1 Calcium as a second messenger

Ionic calcium easily forms complexes with proteins, membranes and organic acids. This feature makes calcium toxic to the cell in high concentrations as it can disrupt enzyme functions and membranes. In addition calcium disrupts the ATP balance by precipitating with the phosphate in ATP (Kass et al. 1999). Therefore, the calcium concentration in the cytosol is carefully kept in the submicromolar range (100 nM). The calcium ions are actively kept out of the cytosol and stored in the apoplast (0.33-1 mM) or in internal compartments like the vacuole (0.2-80 mM) and the endoplasmatic reticulum (0.05-2 mM). Other cellular organelles that contain calcium are the nucleus (100 nM), mitochondria (200 nM), chloroplasts (150 nM- 15 mM) and perioxomes (150 nM-2 $\mu$ M) (Figure 1) (Stael et al. 2012). The calcium homeostasis in the cytosol is maintained by Ca<sup>2+</sup>- ATPases that actively pump calcium out of the cytosol against the concentration gradient (McAinsh et al. 2009). The significant difference in calcium concentration between the cytosol and the other organelles combined with the existing mechanisms to quickly regulate calcium concentrations in the cytosol create the perfect circumstances to allow dynamic changes in calcium concentrations and to use it as a second messenger. Calcium signaling has been found to be involved in the response to both biotic and abiotic stresses, hormones, plant growth and plays a role in the circadian clock (Dodd et al. 2010; Edel et al. 2017; Tuteja et al. 2007). Plants have a large toolkit of calcium transporters consisting of seven families of calcium permeable channels; cyclic nucleotide gated channels (CNGCs, 20 members), glutamate receptor homologs (GLRs, 20 members), mechanosensitive channel of small conductance-like channels (MSLs, ten members), two-pore channel (TPC, one member), Mid1-complementing activity channels (MCAs, two members), hyperosmolarity-gated calcium permeable channels (OSCA, 15 members) and annexins (ANN, eight members). For active transport there are two classes of Ca<sup>2+</sup>-ATPases and one class of Ca<sup>2+</sup> exchanger; autoinhibited Ca<sup>2+</sup>-

ATPases (ACAs, 11 members), ER-type calcium-ATPases (ECAs, 4 members) and  $\text{Ca}^{2+}/\text{H}^{+}$  exchangers (CAX, six members) (Jammes et al. 2011; Demidchik et al. 2018). During a calcium transient, calcium is released from the apoplast and from internal calcium storages into the cytoplasm (Bush 1995; McAinsh et al. 1995). Afterwards the cytosolic calcium concentration is actively brought back to the resting submicromolar levels (Hirschi 1999). It is assumed that calcium channels are responsible for the influx of calcium into the cytoplasm, that  $\text{Ca}^{2+}/\text{H}^{+}$  antiporters achieve the calcium efflux and that  $\text{Ca}^{2+}$ -ATPases maintain the low resting concentration of calcium in the cytoplasm (Kudla et al. 2010; Moeder et al. 2018).

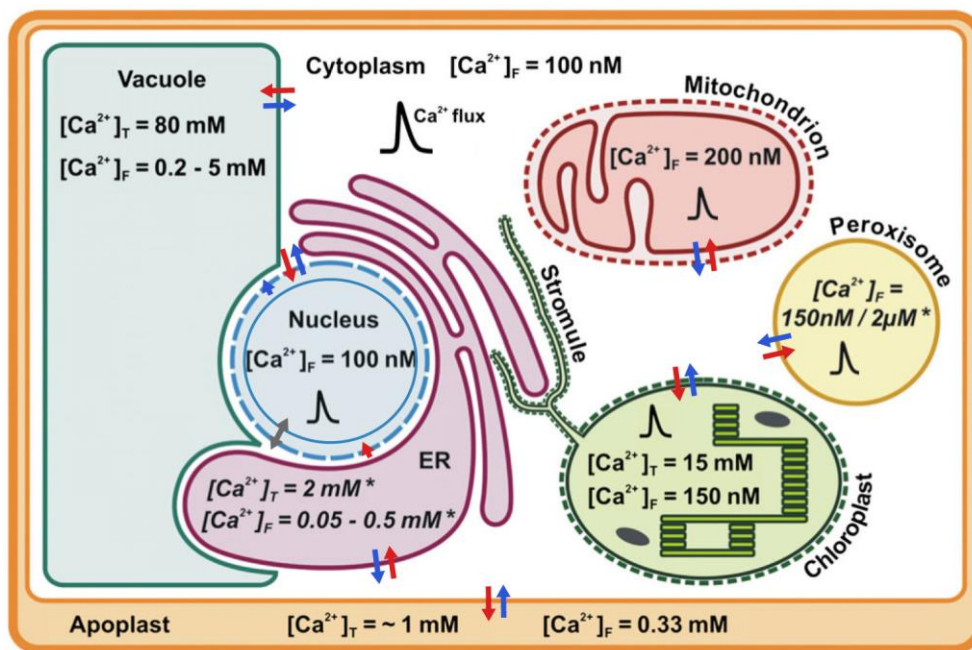


**Figure 1: Overview of the calcium storages of a plant cell.** Values for total ( $[\text{Ca}^{2+}]^T$ ) and free resting ( $[\text{Ca}^{2+}]^F$ ) calcium concentrations of the different organelles. Values are approximate and can vary depending on the tissue or the plant species. Calcium channels are depicted by blue arrows, calcium pumps by red arrows. Gray arrows depict calcium diffusion through the nuclear pores. For ER and peroxisomes no data on calcium concentrations in plants are available. The reported values are taken from the animal field and marked with an (\*). Calcium fluxes are illustrated by a peak-shaped symbol. Figure adapted from Stael et al. 2012.

## 1.2 Calcium signatures

By using the aforementioned calcium concentration modulators plant cells can create a huge variety of calcium signals, ranging from simple transients to traveling waves and oscillations. The calcium signature theory states that for each perceived stress there is a unique calcium transient that starts downstream responses, thus providing signaling specificity. It is thought that the signal information is encoded in the spatio-temporal pattern of cytosolic calcium concentrations (McAinsh et al. 1992; Webb et al. 1996; McAinsh et al. 1998; Sanders et al. 2002). The unique calcium signatures will be decoded by a range of calcium binding proteins such as Calmodulins (CaMs), calcineurin B-like proteins (CBLs), CBL-interacting protein kinases (CIPKs), and calcium dependent protein kinases (CDPKs or CPKs) (Hashimoto et al. 2011). The Arabidopsis genome encodes for at least 250 of these calcium binding EF-hand containing proteins (Day et al. 2002). The binding of calcium to these decoder proteins relays the information from the calcium signature to further downstream targets like transcription factors, protein kinases, transporters or enzymes. In addition to the stimulus-signal specificity a signal-response specificity has been shown where unique calcium signatures were required for changes in the expression of particular genes (W.-G. Choi et al. 2014; Kudla et al. 2010; McAinsh et al. 1998; Ranf et al. 2011; Whalley et al. 2013).

More recently, evidence has been found that in response to salt stress or wounding the transient cytosolic calcium peak in plants can progress successively from cell to cell to communicate with distal tissues (W.-G. Choi et al. 2014; Toyota et al. 2018). It is still unclear how the signal is passed on from cell to cell and whether there is calcium exchanged between neighboring cells. It has however been shown that there is a wave of reactive oxygen species (ROS) accompanying the calcium wave through Arabidopsis roots in response to salt stress and that ROS scavenging by ascorbic acid (Aa) slows down the calcium wave from 400  $\mu\text{m/s}$  to 64  $\mu\text{m/s}$  (Evans et al. 2016). In the most recent model the rise in calcium triggers a wave of reactive oxygen species (ROS) that crosses the cell wall barrier between cells. Upon arriving at the neighboring cell, the ROS wave triggers a calcium increase in the new cell. This rise in cytoplasmic calcium triggers electric signals that mediate the signal from one pole of the cell to the

other. Upon arrival at the opposite polar region the electric signals trigger another calcium increase and the propagation process starts anew (Gilroy et al. 2014).

### **1.3 How are calcium signatures measured?**

Although the definition of a calcium signature is widely accepted as ‘changes in  $[Ca^{2+}]_{cyt}$  that are unique in terms of their spatio-temporal characteristics, in response to an individual stimulus’ (McAinsh et al. 1998), no consensus exists in how to measure or quantify this calcium signature. The most widely used method is to expose whole seedlings expressing the luminescent calcium sensor aequorin to a stress and record the changes in calcium concentration over time (Knight et al. 1991; Kwaaitaal et al. 2011; Tran et al. 2018; Trempel et al. 2016). The resulting graph with its peaks and shoulders is regarded as the calcium signature (Plieth 2010) and can be visually compared to calcium signatures in response to other treatments or mutants. However, the visual characterization is not sufficient to discern subtle differences that might show up in mutants or drug treatments. In addition the shape of the curve of the final calcium signature depends to a large extent on the tissue and cell-type in which the calcium signal has been measured (Marti et al. 2013). This makes it challenging to compare calcium signatures between publications or experiments with even slightly different experimental setups.

The development and introduction into plants of more sensitive fluorescent calcium sensors like yellow cameleon (Krebs et al. 2011) and R-GECO1 (Keinath et al. 2015; Waadt et al. 2017) has allowed calcium imaging with higher resolution in both space and time. This led to the discovery that different tissues and even different cell types respond with their own unique calcium signature (Marti et al. 2013; Walia et al. 2018; Tran et al. 2018). With these new tools it became more apparent that the location of the signal, or the way the signal spreads over a tissue might be parameters of the calcium signature (W.-G. Choi et al. 2014; Behera et al. 2016; Konrad et al. 2018).



## 1.4 Elicitors of calcium signals

Calcium signatures are reported in response to both biotic and abiotic stresses. Biotic stresses are caused by living organisms like bacteria, fungi or insects feeding on plants. Abiotic stresses are negative impacts caused by environmental factors beyond its normal range of variation. Examples are high soil salinity, drought and heat or cold. In this work the following elicitors are used to mimic both biotic and abiotic stresses.

The protein flagellin is the main component of the bacterial flagellum, therefore it is present in all flagellated bacteria. The 22 amino acid consensus motif within the highly conserved N-terminal domain of flagellin, also called flg22, acts as a Microbe-associated molecular pattern (MAMP) to induce the innate immune response. The flg22 peptide is recognized by the leucine-rich repeat (LRR) receptor kinase FLAGELLIN-SENSITIVE 2 (FLS2) (Gómez-Gómez et al. 2000; Chinchilla 2006). Upon binding flg22, FLS2 forms a heterodimer with its co-receptor BRASSINOSTEROID INSENSITIVE 1-associated receptor kinase 1 (BAK1) and later forms a larger complex with another FLS2-BAK1 dimer (Chinchilla et al. 2007; Sun et al. 2013; Somssich et al. 2015). The cytoplasmic receptor-like kinase BOTRYTIS-INDUCED KINASE1 (BIK1) associates with FLS2 and BAK1 and is required for diverse flagellin induced immunity responses (Lu et al. 2010). BIK1 phosphorylates and activates a calcium channel consisting of the two cyclic nucleotide-gated channels CNGC2 and CNGC4 (Tian et al. 2019). In addition BIK1 phosphorylates the calcium-dependent NADPH oxidase respiratory burst oxidase homolog protein D (RbohD) resulting in an enhancement of ROS production (L. Li et al. 2014).

Chitin is a polymer consisting of N-acetylglucosamine chains. C8 is a polymer consisting of eight N-acetylglucosamine units. Chitin is a component of the fungal cell wall and the exoskeleton of arthropods (Tang et al. 2015). In plants it acts as a MAMP in innate immunity (Eckardt 2008). Chitin is recognized by a complex of CHITIN ELICITOR RECEPTOR KINASE 1 (CERK1) (Miya et al. 2007), LysM-containing receptor-like kinase 4 (LYK4), (J. Wan et al. 2012) and LYK5 (Y. Cao et al. 2014). A CERK1 knockout mutant no longer showed a calcium response upon

exposure to chitin while the LYK4 and LYK5 mutants showed only a reduction in calcium concentration of the calcium response.

Elongation factor Tu is the most abundant bacterial protein and is highly conserved among bacteria. It acts as a MAMP in *Arabidopsis* and other *Brassicaceae*. An N- acetylated peptide comprising the first 18 amino acids, named elf18, are sufficient to elicit the full defense response in *Arabidopsis* (Kunze 2004). The receptor for elf 18 has been identified as an LRR receptor kinase called EF-Tu receptor (EFR) (Zipfel et al. 2006). The peptides flg22 and elf18 both activate an overlapping set of signaling events and defense responses, suggesting a common downstream signaling pathway (Navarro 2004; Zipfel et al. 2006).

The MAMP necrosis and ethylene-inducing peptide 1 (NEP1)-like proteins (NLPs) are produced by plant pathogenic bacteria, oomycetes and fungi. A 20 amino acid peptide motif found in these NLPs has been shown to trigger immunity-associated defenses in plants (Böhm et al. 2014). The LRR receptor-like protein 23 (RLP23) binds nlp20 and is required for the activation of the immunity response in response to nlp20 (Albert et al. 2015). Nlp20 and flg22 trigger largely overlapping transcriptional reprogramming (W.-L. Wan et al. 2018) and just like FLS2, RLP23 associates with BAK1.

Endopolygalacturonases (PGs) are a class of pectinases that hydrolyze pectic polysaccharides (van den Brink et al. 2011). They are used by plants to ripen and soften fruits, or by fungi as a virulence factor that helps to get their digestive enzymes into their plant hosts. The MAMP PG3 is an endopolygalacturonase from the grey mold *Botrytis cinerea* that is recognized by the LRR receptor-like protein 42 (RLP42). RLP42 is required for the immune response of the plant and has been shown to interact with the LRR-RLK suppressor of BIR1 (SOBIR1) but not with BAK1 (Zhang et al. 2014).

Cellobiose is a disaccharide consisting of two glucose molecules. It is generated during the degradation of cellulose in the plant cell wall by fungi, and is therefore considered to be a biotic damage-associate molecular pattern (DAMP). It triggers a signaling cascade that shares similarities with chitin and it does not trigger ROS

production or callose deposition (Azevedo Souza et al. 2017). It is currently unknown how the plant senses cellobiose.

D-serine is an amino acid and has been shown to be the main co-agonist of iGLURs in animals (Martineau et al. 2014). In plants D-serine is perceived by GLR1.2 and has been shown to play a key role in signaling between the male gametophyte and pistil tissue (Michard et al. 2011).

Adenosine Triphosphate (ATP) is one of the key components regarding intracellular energy transfer and is used in numerous cellular reactions as energy source. In addition it is an extracellular signaling molecule. In plants extracellular ATP is released after wounding (Song 2006) and in response to several biotic stresses like chitin (S. Y. Kim et al. 2006), yeast extract (Wu et al. 2008) and abscisic acid (Clark et al. 2011). In addition mechanical pressure (Weerasinghe et al. 2009) and hypertonic stress (S.-H. Kim et al. 2014) causes release of extracellular ATP. Extracellular ATP is perceived by the lectin receptor kinase I.9 DORN1 (DOES NOT RESPOND TO NUCLEOTIDES 1). DORN1 was identified in an ethyl methanesulfonate (EMS) mutant screen for mutants with an aberrant calcium response to eATP (J. Choi, Tanaka, Cao, et al. 2014).

In mammals the amino acid glutamate is a key neurotransmitter, mediating calcium fluxes in the synapses of nerve cells (Hayashi 1954; Takeuchi 1987). In plants the glutamate receptor-like genes (GLRs) are homologous to the mammalian ionotropic glutamate receptors (iGLURs) (Lam et al. 1998). Studies have shown that there is an increase in cytosolic calcium upon treatment of *A. thaliana* seedlings with glutamate and that GLRs play a role in this calcium release (Vincill et al. 2012). Recently it has been shown that GLR3.3 and GLR3.6 support the long distance transmission of calcium signals from leaf to leaf upon wounding (Toyota et al. 2018). Leaf wounding can be caused by both biotic (herbivory) and abiotic (mechanical stress) factors. Glutamate has also been implied to play a role in the abiotic heat resistance as Maize seedlings were shown to be more heat resistant after a glutamate treatment (Z.-G. Li et al. 2019).

An abiotic cold shock triggers a rise in the cytosolic calcium concentration of the cell. A drop in temperature is hypothesized to be sensed by changes in the fluidity of the cellular membrane or by the involved calcium channels directly. The calcium-permeable mechano-sensitive channels MCA1 (*mid1*-complementing activity) and MCA2 have been shown to be involved in the calcium burst in response to a cold shock as it lowered the concentration of the resulting calcium response (Mori et al. 2018). In addition to calcium, ROS and nitric oxide (NO) play a role in establishing cold tolerance in plants (Suzuki et al. 2006; Lv et al. 2018).

Abiotic salt stress is caused by high concentration of sodium and chloride ions in the soil (Ismail et al. 2014). Salt stress induces three kinds of stresses in plants: osmotic stress, ionic stress and secondary stress. Osmotic stress is caused by the high concentration of salt in the soil compared to the concentration in the plant cells. This results in reduced water availability for the plant and ultimately to the plant drying up (Hasegawa et al. 2000). In addition salt is reported to induce softening of the cell wall (Feng et al. 2018). Ionic stress is the result of the toxic effect of the salt ions in the plant cells as high concentrations of Na<sup>+</sup> ions in the cytoplasm disrupt the uptake of other ions into the cells (Epstein 1973). These two stresses in turn can cause secondary stresses such as the accumulation of toxic compounds and the disruption of nutrient balances (Yang et al. 2017). It is not known how plants sense an excess of salt. Osmotic stress leads to release of calcium into the cytosol of plant cells, however the salt induced increases in cytosolic calcium occur in the cortical and endodermal cell layers of the root (W.-G. Choi et al. 2014), whereas increases in cytosolic calcium in response to mannitol occur in the epidermis (Kiegle et al. 2000). Nonetheless, salt stress and osmotic stress induced by polyethylene glycol (PEG) or mannitol induced many overlapping genes (Sewelam et al. 2014).

In plants the Salt Overly Sensitive (SOS) signaling pathway acts to protect the cells from damage due to ion accumulation. SOS3 is a calcium sensing protein that detects the calcium increase in response to salt stress (Liu et al. 1998). After binding calcium, SOS3 is able to interact with and activate the protein kinase SOS2 (Halfter et al. 2000). SOS2 phosphorylates SCaBP8, which stabilizes the protein complex (Quan et al. 2007). The SOS3-SOS2 complex (mainly in roots) or the SCaBP8-SOS2 complex (mainly in shoots) is recruited to the plasma

membrane and activates the SOS1 Na<sup>+</sup>/H<sup>+</sup> antiporter that expels excessive Na<sup>+</sup> from the cytosol (Shi et al. 2000; Yang et al. 2018). Recently the putative calcium-permeable transporter ANN4 has been found to be involved in controlling calcium transients in response to salt stress by a negative feedback loop that represses ANN4 activity by phosphorylation by SOS2 (Ma et al. 2019).

There seems to be a link between salt stress tolerance and pathogen defense. It has been shown that the salt and chitin stress responses share a common pathway that both use the CERK1 receptor and the calcium permeable channel annexin D1 (ANN1) (Espinoza et al. 2016). In addition both stresses induce an overlapping set of transcript changes (Espinoza et al. 2016). In the most recent working model ANN1 and CERK1 form a complex that senses both NaCl and chitin and starts a calcium signal in response to these stresses. However, the calcium signals in response to NaCl and chitin have different spatio-temporal properties. Chitin fails to elicit a calcium signal in the *cerk1* knockout mutant, but NaCl does (albeit an attenuated one). In contrast, the ANN1 knockout mutant does still respond with an attenuated calcium release to chitin (Espinoza et al. 2016); the ANN1 knockout mutant has not been tested against NaCl. In addition it has been shown that ANN1 regulates calcium elevations in response to extracellular H<sub>2</sub>O<sub>2</sub> in roots (Laohavisit et al. 2012; Richards et al. 2013). These findings go against the findings that the ANN1-CERK1 complex is responsible for the calcium releases upon chitin or NaCl stress. Rather it points towards the ANN1 channel being responsible for the calcium response upon NaCl stress and the CERK1 receptor as starting the calcium response upon chitin perception.

### **1.5 'Single file' versus 'network' signaling**

The calcium signature hypothesis is based on the 'single-file signaling' view, which posits a single file of events: a unique calcium signature is decoded by calcium dependent proteins that subsequently start the appropriate physiological response. This however is an oversimplified view and does not take into account the complex interwoven mechanisms that have been shown to be involved in some environmental sensing pathways. Christoph Plieth proposes a network-signaling hypothesis with three layers of complexity:

- (1) External, primary stimuli typically have simultaneous effects on diverse cellular actuating variables, and  $[Ca^{2+}]$  is simply one of them. There is a multitude of other variables determining the molecular environment in each cell, for example, the membrane potential, the cellular energy level [ATP], the dissolved oxygen concentration [O], the cellular redox state, antioxidative capacity [GSH], reactive oxygen species [ROS], [NO], or pH.
- (2) The activity of any protein involved in signal transmission depends simultaneously on several such cellular variables. (3) Cellular actuating variables are interdependent. Their interdependence is hard to delineate and may be sequential. (Plieth 2016)

Plieth proposes the simplified “lock-and-key” metaphor to illustrate this network-signaling hypothesis (Figure 2). A similar scale-free signaling network has been proposed in the control of stomatal aperture in guard cells (Hetherington et al. 2003).

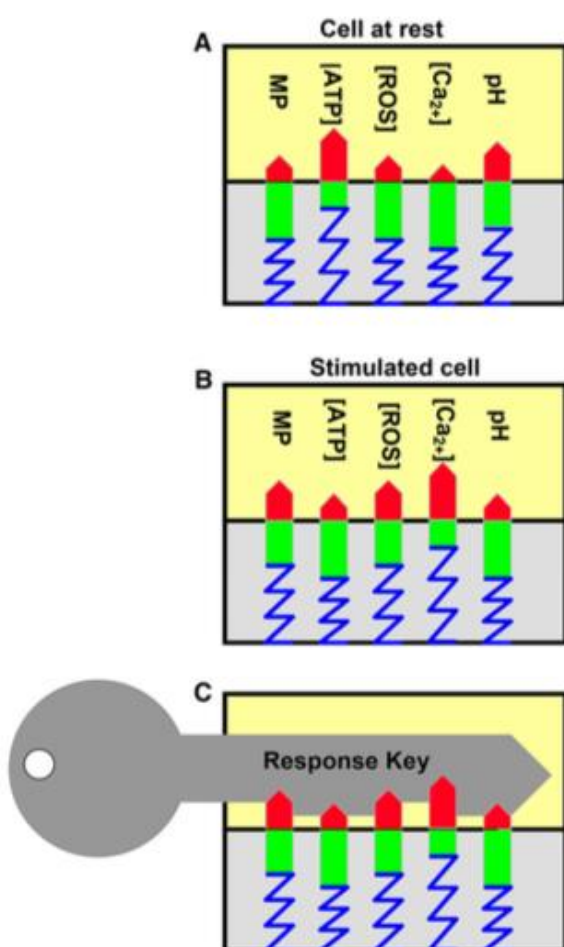


**Figure 2: A cylinder lock as alternative key metaphor for cellular stimulus-response coupling.** (A) An environmental stimulus has effects on diverse cellular actuating variables, such as  $[Ca^{2+}]$ ,  $[H^+]$ , pH, [ATP], and membrane potential. Each variable is reflected here by a red bar. Together they form an amplitude pattern. (B) An environmental stimulus affects some cellular actuating variables, and a new amplitude pattern (cellular state) is established. (C) The new pattern is decoded by a specific key (i.e. cellular receptor proteins with specific sensitivity to the corresponding cellular actuating variables). The key that fits unlocks a gate in the signaling network and provides access to the correct physiological response that the plant species has learned during its evolution (figure adapted from (Plieth 2016)).

## **1.6 The aim of this thesis**

Up until now calcium signatures are mostly quantified by measuring aequorin luminescence over time using whole plants (Ranf et al. 2012). Combining advanced calcium sensors and increased imaging resolution to monitor calcium signaling has led to the discovery of mobile, traveling messenger signals in plants (W.-G. Choi et al. 2014; Toyota et al. 2018). The main goal of this thesis was to develop a novel method to analyze and quantify calcium signatures that includes mobile traveling waves, and subsequently, create a collection of calcium signatures to identify similarities and differences in calcium signatures in response to different stresses, and make predictions about the type of receptors involved. As cross talk between the calcium and ROS signaling pathway has been reported for salt and cold stress (Evans et al. 2016; Guo et al. 2018), another goal was to define the crosstalk between the ROS and calcium signaling pathway for different kinds of stresses, and determine whether ROS is involved in stress prioritization.

## 2 Results:

### 2.1: How to quantify calcium signatures?

#### 2.1.1: A new method for spatio-temporal quantification of calcium signatures in *Arabidopsis* roots

When *Arabidopsis* roots expressing the R-GECO1 calcium sensor (Krebs et al. 2011; Waadt et al. 2017) are exposed to stress, the resulting calcium response spreads over the root resulting in a certain pattern (Figure 3A). If this pattern is unique for each stress it may serve as a readout for stress perception by the plant. However, to find out whether the pattern in which the calcium wave spreads over the root is stress specific, a standardized method to compare these calcium patterns is required.

When roots are globally exposed to flg22, the earliest calcium responses can be observed after a delay of 2 minutes (Figure 3A). This first calcium response takes place in the epidermis of the elongation zone. From the epidermis the calcium wave moves through the underlying cell layers to the vascular tissue. Once the signal arrives at the vasculature it spreads tipwards and shootwards through the vasculature. The calcium wave fades out after traveling approximately half a millimeter away from its starting point (Figure 3A).

By creating a kymograph (a space-time plot, Figure 3B) along the root axis (Figure 3A, dotted line) this specific calcium response can be represented in 2D and can be analyzed and further characterized. The x-axis of the kymograph represents the distance from the root tip, while the y-axis represents the elapsed time. The kymograph is a straightforward way to visualize where and when an increase in calcium concentration occurs along the root. However, there is still interference from background noise, which makes it difficult to detect weak signals.

To make the shape of the wave more visible and to reduce background noise, the Crestline normalization developed by Martin Zauser from the biological information processing group (BioQuant, Heidelberg) was used. In the Crestline normalization



every column of pixels in a picture is scaled between the highest and the lowest pixel value found in that column. As a result, background noise is less visible and the visibility of less pronounced calcium responses is enhanced. However, it makes it impossible to compare intensities between different columns.

The resulting normalized kymograph (Figure 3C) was used to quantify several spatial and temporal aspects of the calcium signature: (a) delay between the application of the stress and the first detected increase in  $[Ca^{2+}]_{cyt}$ , (b) location of the first response measured as the distance from the root tip, (c) duration of the calcium signal defined as the time the signal is above 75% of the maximum signal intensity, (d) distance that the calcium wave travels along the root, (e) velocity with which the calcium wave travels towards the root tip, and (f) velocity with which the calcium wave travels towards the shoot. These parameters serve to describe and quantify most aspects of the calcium signature and enable easier comparison of calcium signatures between used sensors and different setups.

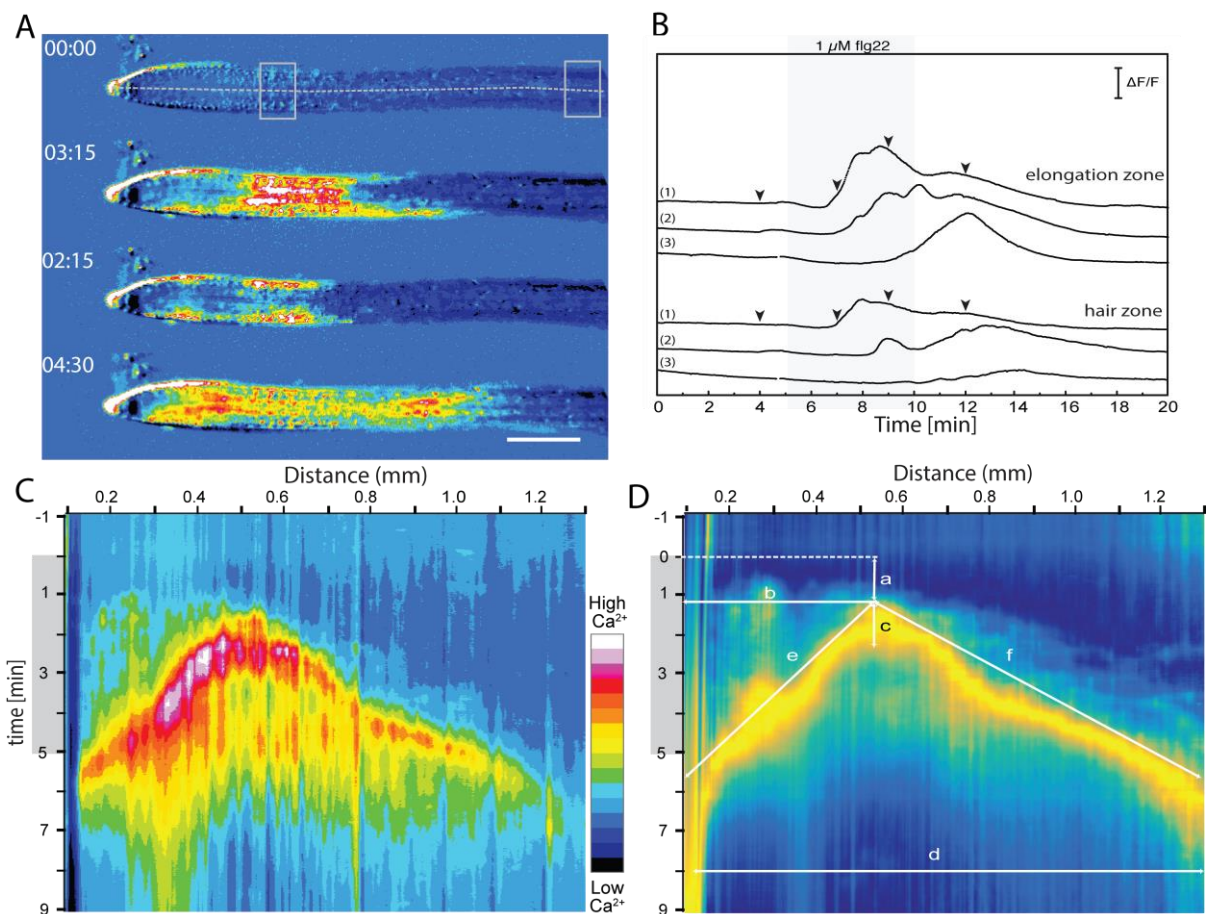


**Figure 3: Calcium signature quantification.** *Arabidopsis* root treated with 1  $\mu\text{M}$  flg22 in the RootChip16 (Jones et al. 2014). **(A)** Time series of normalized R-GECO1 fluorescence images ( $\Delta F/F$ ). Scale bar 200  $\mu\text{m}$ , time format mm:ss. **(B)** Classic calcium signature that measures the intensity changes ( $\Delta F/F$ ) over time. Shown are

measurements from three independent roots from ROIs in the elongation zone and the root hair zone indicated in **(A)**. Arrowheads correspond to the images shown in **(A)**. **(C)** Kymograph produced along a 120  $\mu\text{m}$  wide line (position is indicated by the dotted line in **(A)**). Grey box indicates flg22 treatment (0:00 - 5:00 min). **(C)** Crestline normalized kymograph of **(C)**, intensity of each column is scaled according to the minimum and maximum intensity value in that column. Indicated are the quantified parameters and how they were measured. Parameters are: (a) delay between the application of the stress and the first detected increase in  $[\text{Ca}^{2+}]_{\text{cyt}}$ , (b) location of this first response relative from the root tip, (c) duration of the calcium signal defined as the time the signal is above 75% of the maximum signal intensity, (d) distance the calcium wave covers along the root, (e) velocity with which the calcium wave travels towards the root tip, (f) velocity with which the calcium wave travels towards the shoot. **(A)**, **(B)** and **(C)** of this figure are published in (Keinath et al. 2015).

### **2.1.2: Spatio-temporal quantification of calcium responses in *Arabidopsis* roots reveals stimulus-specific signatures**

Plants respond to a range of external stimuli with an increase of cytosolic calcium (Webb et al. 1996). It has been widely accepted that these releases show unique amplitudes in response to different elicitors. While the amount of calcium released during the response has been quantified, the spatial aspect of the calcium release has never been systematically measured. To quantify the spatio-temporal calcium signatures in *Arabidopsis*, roots were exposed to the biotic stresses flg22 or C8 and to the abiotic stress of NaCl.

As variances between signatures were relatively high and differences between some responses subtle, a higher throughput method was developed in which 30-50 seedlings could be grown and treated simultaneously on a nylon mesh. The roots were grown along the grain of the mesh to avoid overlapping and to enable handling of the mesh without disturbing the roots. The meshes were placed in a chamber mounted on a microscope slide and incubated with medium. A tilting platform, the BalanceSir (Lampou 2015), was used to allow for efficient replacement of medium by treatment solutions, resulting in a simultaneous treatment of all roots. For each individual root a kymograph was created, normalized and analyzed as described above (Figure 4A-C).

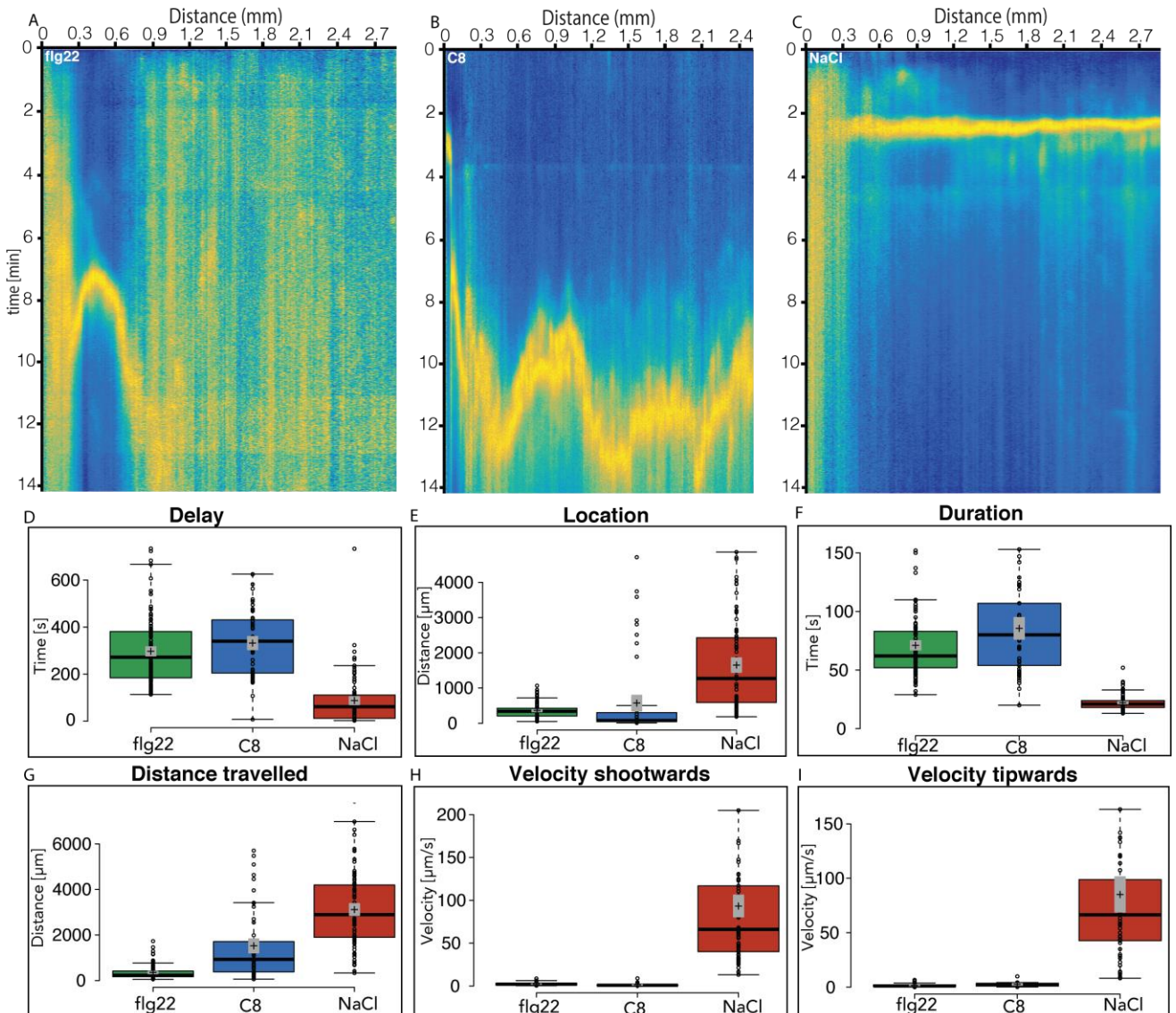


**Figure 4: Calcium signatures of Arabidopsis roots in response to flg22, C8 and NaCl.** Crestline normalized kymographs displaying representative calcium signatures of Arabidopsis roots on meshes treated with (A) 10 $\mu\text{M}$  flg22, (B) 10  $\mu\text{M}$  C8 or (C) 100 mM NaCl. (D) delay between the application of the stress and the first detected increase in  $[\text{Ca}^{2+}]_{\text{cyt}}$ , (E) location of the first response measured as the distance from the root tip, (F) duration of the calcium signal, (G) distance the calcium wave covered along the root, (H) velocity with which the calcium wave traveled towards the shoot and (I) velocity with which the calcium wave traveled towards the root tip. Lines depict sample median. Crosses indicate sample means. Grey boxes define the 83% confidence interval of the mean.  $n=102$  for flg22,  $n=51$  for C8 and  $n=78$  for NaCl.

Comparing the delay of the calcium response between the biotic flg22 and C8 and abiotic NaCl stimuli, it became clear that the roots respond faster to abiotic stress

(Figure 4D). The median delay before the calcium response to NaCl was 61 seconds and the median absolute deviation was 49,5 seconds (from here on indicated with  $61 \pm 49,5$  seconds). The delay before the first calcium signal was longer for C8 ( $340 \pm 128$  seconds) than for flg22 ( $271,5 \pm 91,5$  seconds). The biotic responses started in the elongation zone (flg22:  $338 \pm 113$   $\mu\text{m}$  from the tip, C8:  $78 \pm 44$   $\mu\text{m}$  from the tip) while the location of the NaCl induced calcium wave ( $1256 \pm 758,5$   $\mu\text{m}$  from the tip) did not seem to have a specific starting point, as it varied greatly between measurements (Figure 4E). Calcium signals in response to biotic elicitors (flg22:  $63 \pm 15$  seconds, C8:  $81 \pm 27$  seconds) persisted longer than responses to the abiotic NaCl ( $21 \pm 3$  seconds) (Figure 4F). Calcium releases in response to biotic stresses were restricted to the elongation zone. The flg22 response (spreading  $234 \pm 95,5$   $\mu\text{m}$ ) faded out before leaving the elongation zone while the calcium response to C8 (spreading  $927 \pm 711$   $\mu\text{m}$ ) usually faded out but occasionally was recorded higher up the root. The calcium response to NaCl (spreading  $2890 \pm 1153$   $\mu\text{m}$ ) was recorded all over the root (Figure 4G). The velocity with which the calcium signal in response to NaCl (tipwards:  $66 \pm 29$   $\mu\text{m/s}$ , shootwards:  $66 \pm 35$   $\mu\text{m/s}$ ) spread over the root was significantly faster than both the biotic signals. Comparing the response to biotic elicitors, the calcium signal after flg22 treatment (shoot wards:  $2 \pm 1$   $\mu\text{m/s}$ , tip wards:  $1.1 \pm 0,5$   $\mu\text{m/s}$ ) spread faster towards the shoot than after C8 treatment (shoot wards:  $0,8 \pm 0,3$   $\mu\text{m/s}$ , tip wards:  $2,2 \pm 1,3$   $\mu\text{m/s}$ ) (Figure 4H) but slower towards the root tip (Figure 4I).

It seems that the calcium response does not depend on the concentration of the elicitor but rather on the increase in concentration over time. When the concentration of NaCl is gradually increased over time to the same final concentration over 2:45 minutes, no calcium release could be detected (Suppl. Figure 1). This indicates that there needs to be a minimum amount of elicitor binding and activating its receptor in a certain amount of time to cross an activation threshold that starts the signaling and the calcium release.

To allow for comparison of all the parameters at the same time we performed a principle component analysis (PCA) time in collaboration with Dr. Milan Župunski (University of Novi Sad, Serbia). PCA can be used to show which variables follow the same or a different trend, and to describe a large amount of data using a

smaller number of units (Pearson 1901). For this it takes a number of possibly correlated variables and transforms them into a smaller number of uncorrelated variables called principal components. The first principal component accounts for as much of the variability in the data as possible, each following component in turn accounts for as much of the remaining variability as possible. The PCA method enabled us to group the responses together, to elucidate which parameters make the individual  $\text{Ca}^{2+}$  signature unique and find out how different parameters of the calcium signature influence each other.

Here, the first and second principle component account for 71.1 % and 13 % of the variance, respectively, (x- and y-axis, Figure 5), together they account for the majority of the variance (84.1 %). As the first two principle components account for the majority of the variance we could leave out the other principle components and create a PCA biplot with the first two principle components. The biplot can show us which variables correlate with which component (see suppl. Table 1 for additional eigenvalues and variance percentages). The angle between two arrows indicates how the variables are correlated. A small angle implies positive correlation, closer to a  $90^\circ$  angle indicates no correlation and an angle larger than  $90^\circ$  suggests negative correlation between two characteristics. The intensity of the blue of an arrow represents how much the variable contributes to the principle components. The PCA biplot revealed that from all the variables (blue arrows, Figure 5) the velocities (tip- and shootwards,  $V_t$  and  $V_s$ ) correlated most strongly to the first principle component (x-axis, Figure 5) thus explaining the majority of variance between the treatments. The duration of the signal was negatively correlated to the velocities, meaning that fast traveling signals last only a short time. In addition, the results suggested that the location of the first calcium signal is positively correlated with the velocities. Although velocities and duration (dur) both contribute to the first principle component, comparing arrow intensities revealed that the velocities contributed more than the duration. Other parameters like the distance (d) from the tip, and the delay time (t) also played a role in setting the calcium signatures apart but contributed less to the separation of the groups.

We analyzed the variability of individual calcium signatures represented by single dots in the PCA-biplot. The location of each dot (individual signature) is

determined by the directions of the arrows (how much each variable contributes to each principle component). Dots that cluster together have a similar calcium signature, and the variance of dots within a cluster is represented by the size of its encircling ellipse (see Figure 5). The location of clusters relative to each other represents in which variables the clusters differed from another.

The biplot showed that calcium signatures in response to C8 had a high variance. This was represented by the second principal component (y-axis) where delay time (t) and the distance traveled (l) contributed the most. In other words, there was a high variability among calcium signatures in response to C8 for these two parameters.

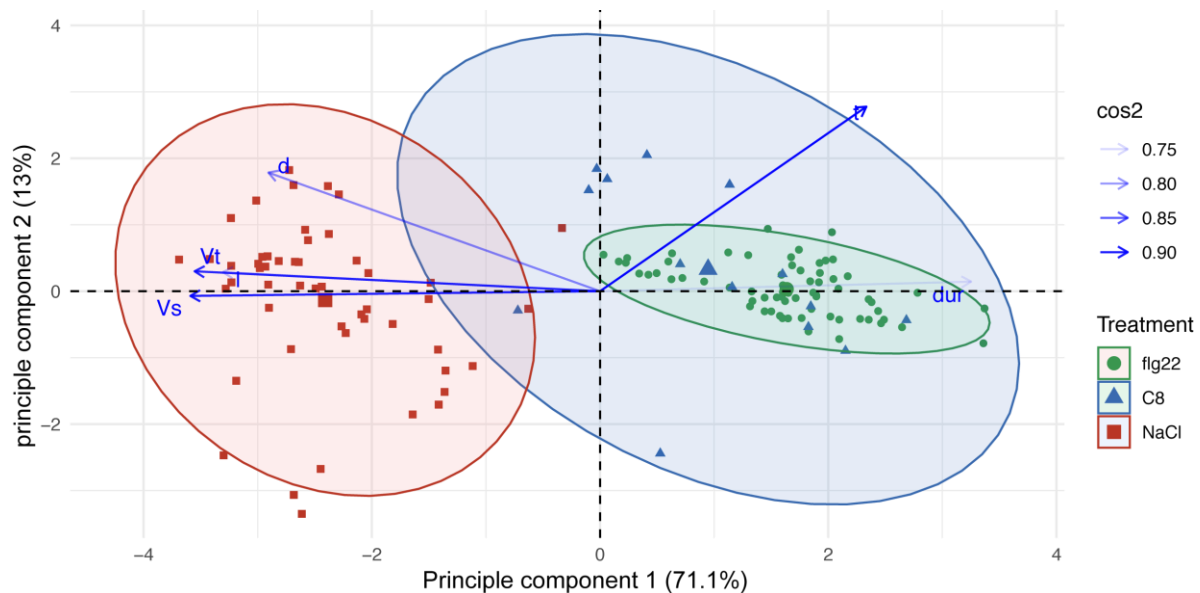


**Figure 5: Principal component analysis (PCA) of calcium signatures for flg22, C8 and NaCl.** The PCA biplot depicts correlation circles for all treatments (flg22, C8 and NaCl). The length of the blue arrows approximates the variance of the parameters. Direction of the arrows shows how strongly each parameter influences a principal component. Angles between the arrows approximate the correlation between the parameters. Intensity of the blue arrow shows which parameters set the responses apart, the darker the arrow the more the parameter contributes to the separation of the responses. Variables depicted are: t: delay, d: distance from tip, dur: duration, l: distance traveled, Vt: velocity tipwards, Vs: velocity shootwards.

The correlation circles were replotted to represent the nature of the treatments (biotic versus abiotic) (Figure 6). This biplot showed that the calcium signatures in



response to biotic (flg22 and C8) and abiotic (NaCl) elicitors were clustered based on their treatment, and that the clusters were distinctly separate from another. Note that the localization of dots is unchanged.

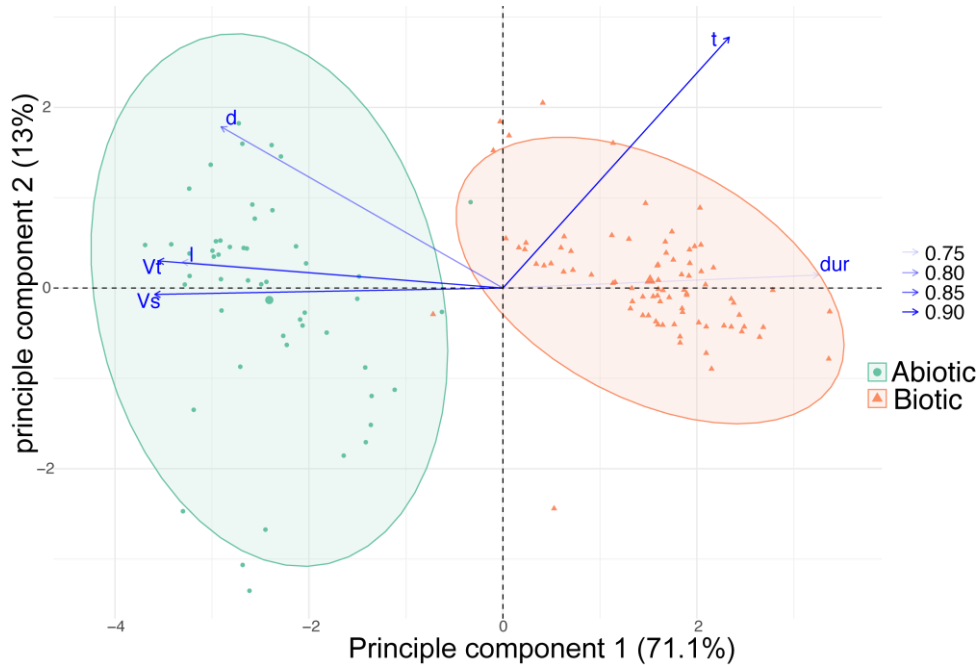


**Figure 6: Principal component analysis (PCA) of calcium signatures for flg22, C8 and NaCl.** This PCA biplot plots the same dataset as figure 5 but shows correlation circles with regard to the nature of treatments (biotic: flg22 and C8) and abiotic (NaCl). The length of the blue arrows approximates the variance of the parameters. Direction of the arrows shows how strongly each parameter influences a principal component. Angles between the arrows approximate the correlation between the parameters. Intensity of the blue arrow shows which parameters set the responses apart, the darker the arrow the more the parameter contributes to the separation of the responses. Variables depicted are: t: delay, d: distance from tip, dur: duration, l: distance traveled, Vt: velocity tipwards, Vs: velocity shootwards.

Taken together, the quantification and the PCA biplot showed that while the parameters for the two biotic stresses are often close together, there is a major difference between the calcium signature between biotic and abiotic stresses. The two biotic stresses (flg22 and C8) only differed by the delay time (t) and the traveled distance (l). In contrast, the response to the abiotic stress (NaCl) was different from the two biotic responses in all measured parameters (Figures 5 and 6). In short, we have established a new way of quantifying calcium signatures that can be used to distinguish between different kinds of stress using the PCA biplot

as a useful tool to visualize these differences. This new method that also analyses the way the calcium response spatially spread over the root allows us to look at calcium signatures from a new angle. The quantification of the six parameters allows for straightforward comparison between experiments and makes it easier to share data. The PCA allows for grouping of signatures by comparing all of the six parameters at the same time and helps in analysis and in making predictions about the used stresses. A drawback of this method is that it does not analyze the amount of calcium that is released. Therefore the outcomes cannot be compared to already published data.

### **2.1.3: The maximum amount of calcium released into the cytoplasm is the same for different stresses**

As depicted in the time series in figure 3A and the kymograph in figure 3B the signal in response to flg22 becomes less intense the further it travels up and down the root. This poses a problem when quantifying the changes in cytoplasmic calcium concentration as the outcome will largely be dependent on the size and placement of the ROI. To be able to still quantify the amount of calcium released into the cytoplasm by the cell, I measured the intensity of the single pixel with the highest fluorescent signal in the kymograph of the calcium signature.

Quantification of the maximum intensity changes in response to flg22 ( $3238 \pm 828$  a.u.), C8 ( $3272 \pm 363$  a.u.), and NaCl ( $3113 \pm 400$  a.u.) (Figure 7) showed that there is no difference in the maximum amount of calcium released in response to the different stresses.



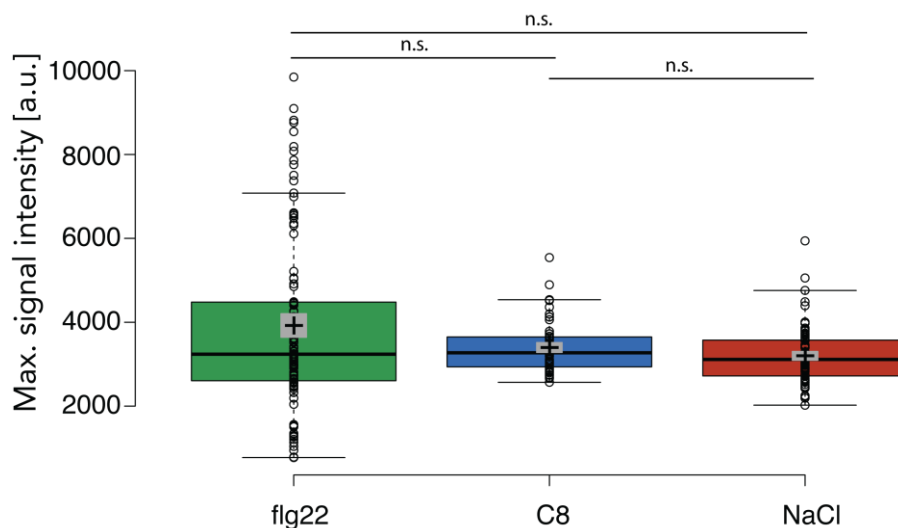


**Figure 7: The maximum amount of calcium released does not differ in response to different stresses (flg22, C8 or NaCl).** Lines depict sample median. Crosses indicate sample means. Grey boxes define the 83% confidence interval of the mean.  $n=116$  for flg22,  $n=52$  for C8 and  $n=76$  for NaCl. n.s. =  $p \geq 0.05$  in Student's t-test

## 2.2: Differences in calcium signatures of biotic and abiotic stresses

With this new way of quantifying and visualizing calcium signatures established, we applied a range of stresses to roots in order to investigate whether similar stresses result in similar calcium signatures. In this chapter, we investigate whether we can distinguish between calcium signatures in response to biotic and abiotic stresses. In addition we use the collected data to make predictions about receptor types involved in currently unknown stress sensing pathways.

### 2.2.1: There are distinct biotic and abiotic features in calcium signatures

We showed that two biotic elicitors (flg22 and C8) resulted in similar calcium signatures, which were both distinctly different from the calcium signature in response to the abiotic elicitor NaCl. This led to the hypothesis that biotic and abiotic calcium signatures have distinct characteristics that are reflected in the measured parameters and can therefore be used to investigate how plants respond differentially to distinct stresses. To this end, we exposed *Arabidopsis* roots to the biotic stresses nlp20, C8, flg22, PG3, D-serine and elf18, to the abiotic

stresses cold and salt, as well as to cellobiose, ATP and glutamate which are signaling molecules that may play roles in responses to both biotic and abiotic stresses (Table 1).

**Table 1: Used elicitors and their receptors**

Elicitor	Stress	Receptor	Receptor type	Conc.	Reference
nlp20	Biotic	RLP23	LRR-receptor protein	10 $\mu$ M	(Albert et al. 2015)
C8	Biotic	CERK1	Lysm-receptor like kinase	10 $\mu$ M	(Miya et al. 2007)
flg22	Biotic	FLS2	LRR-receptor kinase	10 $\mu$ M	(Felix et al. 1999)
PG3	Biotic	RLP42	LRR-receptor protein	5 $\mu$ M	(Zhang et al. 2014)
elf18	Biotic	EFR	Receptor kinase	10 $\mu$ M	(Zipfel et al. 2006)
Cellobiose	Biotic	Unknown	Unknown	100 $\mu$ M	-
D-Serine	Biotic	GLRs	Ligand gated ion channel	1 mM	(Michard et al. 2011)
ATP	Biotic/Abiotic	DORN1	Lectin-receptor kinase	150 $\mu$ M	(J. Choi, Tanaka, Liang, et al. 2014)
Glutamate	Biotic/Abiotic	GLRs	Ligand gated ion channel	1 mM	(Toyota et al. 2018)
NaCl	Abiotic	Unknown	Unknown	100 mM	-
Cold	Abiotic	Unknown	Membrane fluidity	0°C	(Miura et al. 2013)

Quantification of calcium signatures elicited by nlp20, C8, flg22, PG3, cellobiose, ATP, glutamate, NaCl or cold revealed that responses to biotic and abiotic stresses were distinctly different (Figure 8). The responses to biotic elicitors started later than responses to abiotic elicitors (nlp20: 374  $\pm$ 35 seconds, C8: 340  $\pm$ 128 seconds, flg22: 271,5  $\pm$ 91,5 seconds, PG3: 137  $\pm$ 31 seconds, cellobiose: 104  $\pm$ 8 seconds, ATP: 4  $\pm$ 1 seconds, glutamate: 2,5  $\pm$ 1 seconds, NaCl: 61  $\pm$ 49,5 seconds, cold: 1,9  $\pm$ 1,6 seconds) (Figure 9A). Considering the localization of calcium signatures, biotic stress responses started in the elongation zone, with the exception of cellobiose, while abiotic stress responses did not seem to have a preferred starting point (nlp20: 95  $\pm$ 17  $\mu$ m, C8: 78  $\pm$ 44  $\mu$ m, flg22: 338  $\pm$ 113  $\mu$ m, PG3: 452,5  $\pm$ 91  $\mu$ m, cellobiose: 4038  $\pm$ 1075  $\mu$ m, ATP: 121  $\pm$ 9  $\mu$ m, glutamate: 1031  $\pm$ 546  $\mu$ m, NaCl: 1274  $\pm$ 759  $\mu$ m, cold: 1846  $\pm$ 910  $\mu$ m from the tip) (Figure 9B). Calcium responses to biotic stresses persisted longer than those to abiotic stresses, with the duration of the responses to cellobiose and ATP lying between the two groups (nlp20: 64  $\pm$ 12 seconds, C8: 80  $\pm$ 27 seconds, flg22: 62  $\pm$ 15 seconds, PG3: 50  $\pm$ 7 seconds, cellobiose: 34  $\pm$ 8 seconds, ATP: 37  $\pm$ 7 seconds, glutamate: 12,5  $\pm$ 2,5 seconds, NaCl: 21  $\pm$ 3 seconds, cold: 13,2  $\pm$ 1.9 seconds) (Figure 9C). How much of the root was covered by the calcium response was not distinctly different between biotic and abiotic elicitors. Responses to the biotic

elicitors nlp20, C8 and nlp20 were restricted to the elongation zone, with responses to C8 occasionally spreading further up the root, while calcium responses to PG3 and cellobiose covered a larger portion of the root. Calcium responses to abiotic stresses covered a large area of the root, except ATP, for which the calcium signal seemed to be restricted (nlp20:  $266 \pm 45 \mu\text{m}$ , C8:  $927 \pm 711 \mu\text{m}$ , flg22:  $234 \pm 96 \mu\text{m}$ , PG3:  $2806 \pm 1090 \mu\text{m}$ , cellobiose:  $4836 \pm 1110 \mu\text{m}$ , ATP:  $979 \pm 321 \mu\text{m}$ , glutamate:  $1568 \pm 871 \mu\text{m}$ , NaCl:  $2890 \pm 1153 \mu\text{m}$ , cold:  $5607 \pm 1967 \mu\text{m}$ ) (Figure 9D). The velocities with which the calcium signatures spread through the root proved most informative to distinguish biotic and abiotic responses. Both, the velocity shootwards ( $V_s$ ) (nlp20:  $0,8 \pm 0,2 \mu\text{m/s}$ , C8:  $0,8 \pm 0,3 \mu\text{m/s}$ , flg22:  $2,0 \pm 1,1 \mu\text{m/s}$ , PG3:  $4,0 \pm 1,0 \mu\text{m/s}$ , cellobiose:  $10,7 \pm 5,4 \mu\text{m/s}$ , ATP:  $19,1 \pm 9,0 \mu\text{m/s}$ , glutamate:  $47,6 \pm 21,0 \mu\text{m/s}$ , NaCl:  $66 \pm 35,5 \mu\text{m/s}$ , cold:  $107,4 \pm 62,0 \mu\text{m/s}$ ) (Figure 9E), as the velocity tipwards ( $V_t$ ) (nlp20:  $0,74 \pm 0,32 \mu\text{m/s}$ , C8:  $2,2 \pm 1,4 \mu\text{m/s}$ , flg22:  $1,1 \pm 0,5 \mu\text{m/s}$ , PG3:  $1,8 \pm 0,5 \mu\text{m/s}$ , cellobiose:  $9,2 \pm 3,3 \mu\text{m/s}$ , ATP:  $20,6 \pm 8,6 \mu\text{m/s}$ , glutamate:  $46,7 \pm 21,7 \mu\text{m/s}$ , NaCl:  $66,3 \pm 29 \mu\text{m/s}$ , cold:  $115,6 \pm 45,4 \mu\text{m/s}$ ) (Figure 9F) showed a gradient with calcium responses to biotic stresses spreading slower, and those to the abiotic stresses spreading faster. See suppl. Table 2-7 for Student t-test p-values.

Out of eleven elicitors tested, (Table 1), only elf18 and D-serine did not elicit a calcium response under the tested conditions. Elf18 is reported to elicit a calcium response in whole seedlings of the same age, but not in roots (Ranf et al. 2011). D-serine has not been tested in roots previously but is only reported to play a role in the signaling between the male gametophyte and the pistil (Michard et al. 2011).

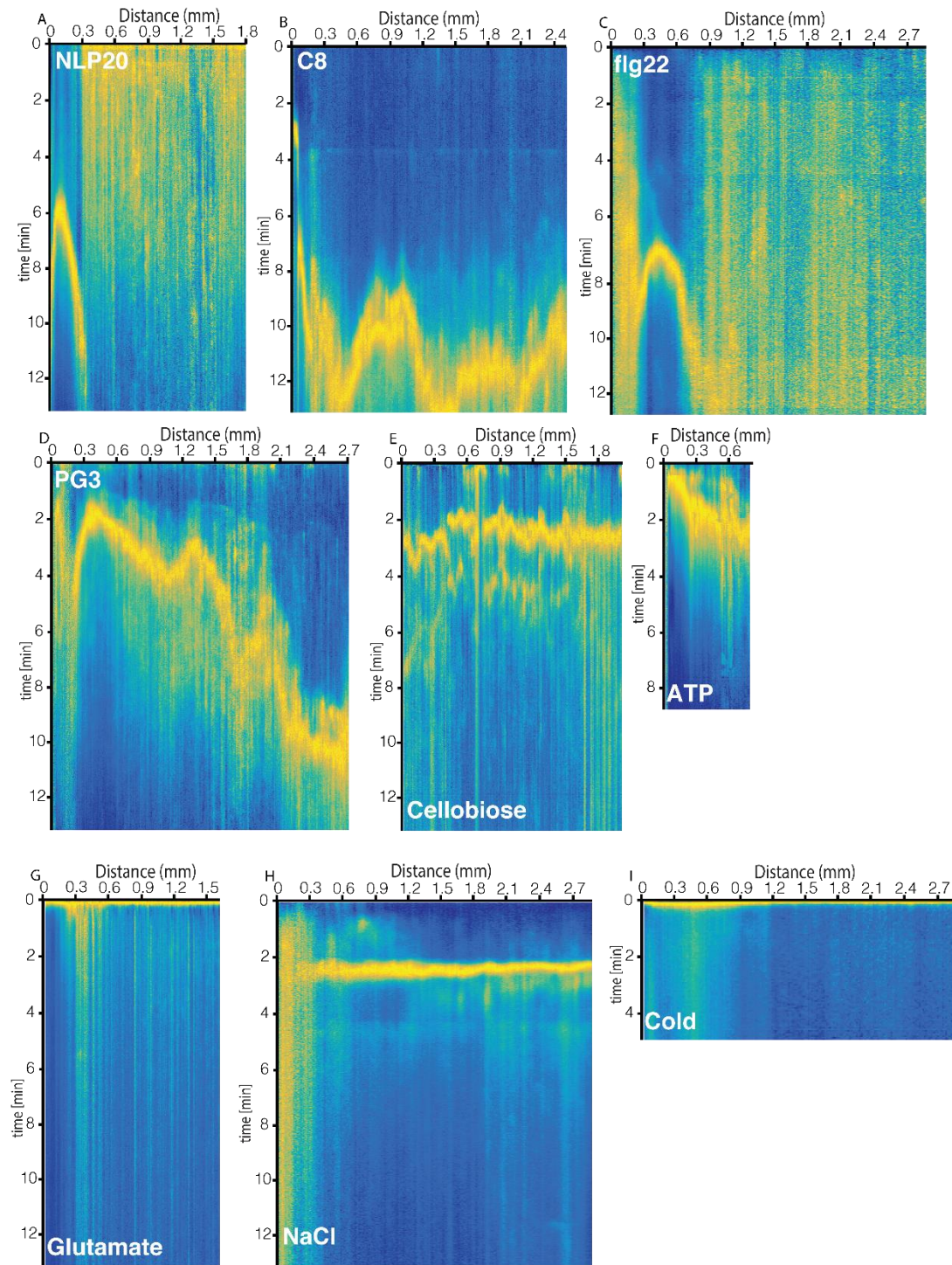


**Figure 8: Representative calcium signatures of single roots in response to treatment with different elicitors.** Crestline normalized kymographs displaying calcium signatures of *Arabidopsis* roots on meshes treated elicited by (A) nlp20, (B) C8, (C) flg22, (D) PG3, (E) cellobiose, (F) ATP, (G) glutamate, (H) NaCl or (I) cold.

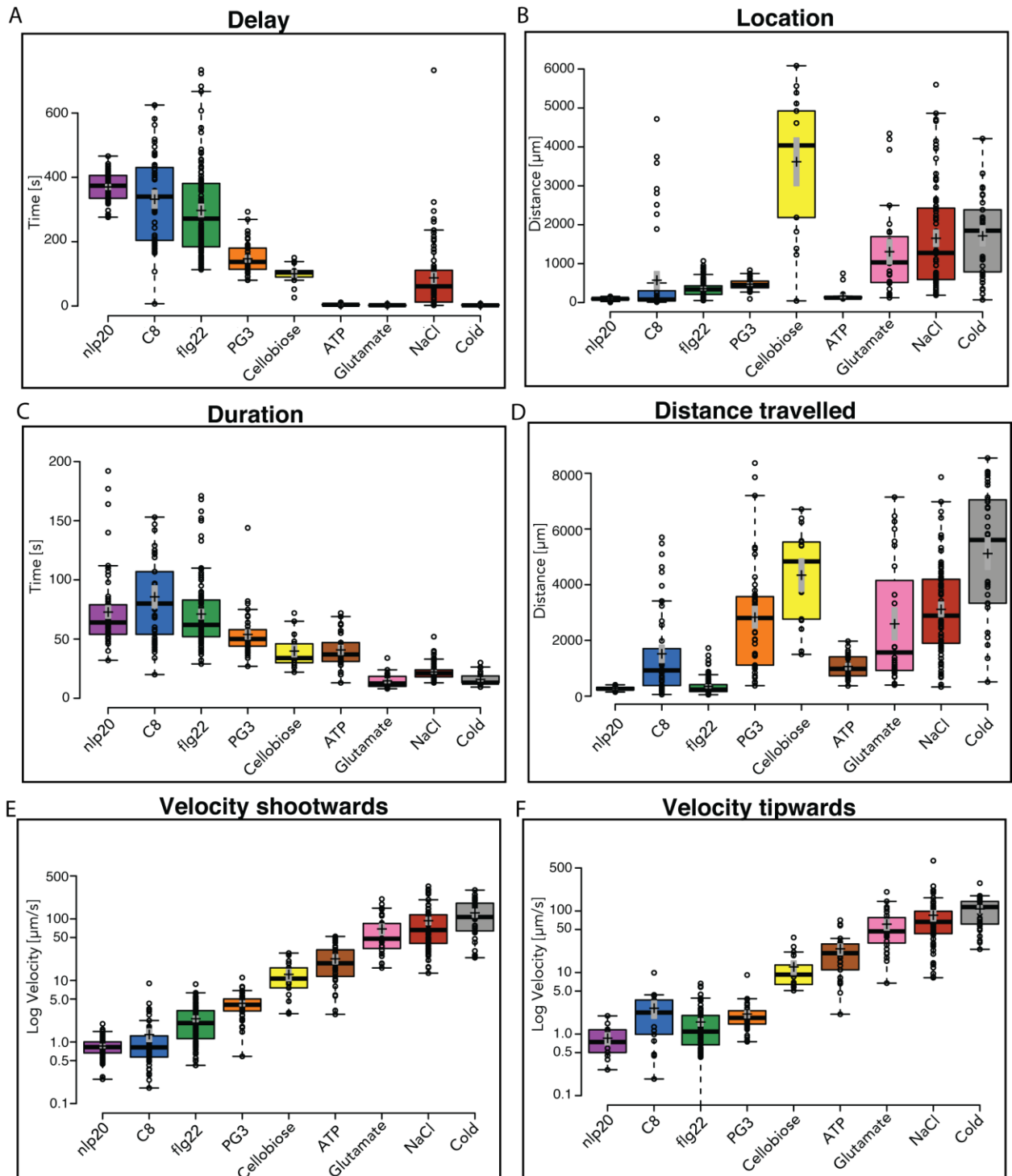


**Figure 9: Quantification of calcium signature characteristics elicited by nlp20, C8, fig22, PG3, cellobiose, ATP, glutamate, NaCl or cold sorted by velocity shootwards. (A)** Delay between the application of the stress and the first detected increase in  $[Ca^{2+}]_{cyt}$ , **(B)** location of the first response measured as the distance from the root tip, **(C)** duration of the calcium signal, **(D)** distance the calcium wave covered along the root, **(E)** velocity with which the calcium wave traveled towards the shoot and **(F)** velocity with which the calcium wave traveled towards the root tip.

Lines depict sample median. Crosses indicate sample means. Grey boxes define the 83% confidence interval of the mean. n=66 for nlp20, n=51 for C8, n=102 for flg22, n=46 for PG3, n=16 for cellobiose, n=47 for ATP, n=27 for glutamate, n=78 for NaCl and n=32 for cold. See suppl. table 2-7 for Student t-test p-values.

The PCA biplot revealed that the calcium signature of cellobiose had both biotic and abiotic characteristics as it overlapped with stresses from both groups (Figure 10). The calcium signature in response to cellobiose started in the differentiation zone, about 4 mm away from the tip, and spread over the root for about 5 mm, similar to abiotic responses. The first calcium signal could be identified at around 100 seconds after treatment. This is later than abiotic stress responses, but sooner than any other of the measured biotic stress responses. The calcium wave spread over the root with about 9  $\mu\text{m/s}$  towards the tip and with 10  $\mu\text{m/s}$  towards the shoot. This was again slower than an abiotic stress but faster than any biotic stress. The duration (dur) also ranged between that of abiotic and biotic stress responses, lasting about 30 seconds.

Overall, Delay times (t), duration of the signal (dur) and the velocities (V) of the responses of all the tested elicitors showed a gradient from biotic to abiotic stress responses. Therefore, it was challenging to determine the border between a biotic and an abiotic stress response for these parameters. The combination of the signal starting in the elongation zone or being restricted to it, however, appeared to be typical for all the tested biotic stresses, with the exception of cellobiose (Figure 10).



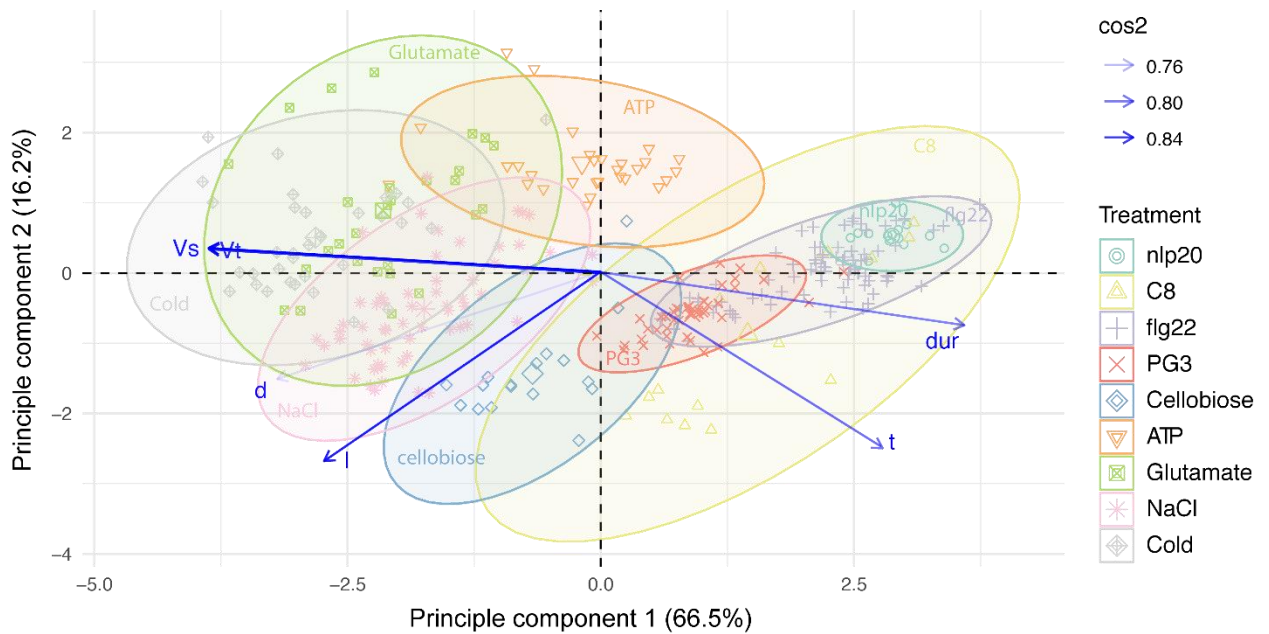


**Figure 10: Principal component analysis (PCA) of calcium signatures for all elicitors clustered by the biotic (nlp20, C8, flg22, PG3) and abiotic (NaCl and cold) stresses, and those of unknown nature (glutamate and ATP).** The PCA biplot shows correlation circles for the biotic elicitors nlp20, C8, flg22, PG3 and cellobiose, and the abiotic elicitors NaCl and cold stress. In addition the stresses of unknown origin, glutamate and ATP, are plotted. The length of the blue arrows approximates the variance of the parameters. Direction of the arrows shows how strongly each parameter influences a principal component. Angles between the arrows approximate the correlation between the parameters. Intensity of the blue arrow shows which parameters distinguish responses, the darker the arrow the more the parameter contributes to the separation of the responses. Variables depicted are: t: delay, d: distance from tip, dur: duration, I: distance traveled, Vt: velocity tipwards, Vs: velocity shootwards.

Extracellular ATP and glutamate are messenger molecules that are involved in both biotic and abiotic stresses. By plotting the ATP and glutamate stress responses together with clustered biotic and abiotic stress responses on the same PCA biplot, I analyzed whether the plant might perceive extracellular ATP and glutamate as a biotic or abiotic stress (Figure 11) (see suppl. Table 8 for the eigenvalues of all the principle components).

The calcium response to ATP displayed typically biotic characteristics, starting in the elongation zone around 120  $\mu\text{m}$  from the root tip and spreading about one mm over the elongation zone. However, the delay (t) before the first signal, the velocities (V) and the duration (dur) of the signal displayed more abiotic characteristics by appearing after only a few seconds and lasting for about 30

seconds. The signal traveled both tip- and shootwards with about 20  $\mu\text{m/s}$ . In short, ATP displayed characteristics of both biotic and abiotic calcium signatures as starting point and restriction to the elongation zone indicated biotic stress, and delay, velocity and duration pointed to abiotic stress. The biplot shows that the ATP-elicited calcium signature hardly overlapped with either of the correlation circles (Figure 11). This non-standard response might be due to the role of ATP as a second messenger molecule involved in both biotic and abiotic stress responses rather than as a first messenger-signaling molecule.

Similar to ATP, glutamate is a signaling molecule used in both biotic and abiotic stress responses. Characterization of the calcium signature upon exposure to glutamate revealed that it exhibited abiotic characteristics for all the measured parameters (Figure 9). Its response displayed a large range of starting locations and spread far over the root. It starts soon after exposure, propagates fast and the calcium release only lasts for about 10 seconds. Based on the PCA biplot analysis, the glutamate calcium signature falls in the abiotic response and does not overlap with the biotic response at all (Figure 11). This suggests that the so far unknown nature of glutamate as an elicitor is that of an abiotic stressor and/or is only involved in abiotic responses as a second messenger.



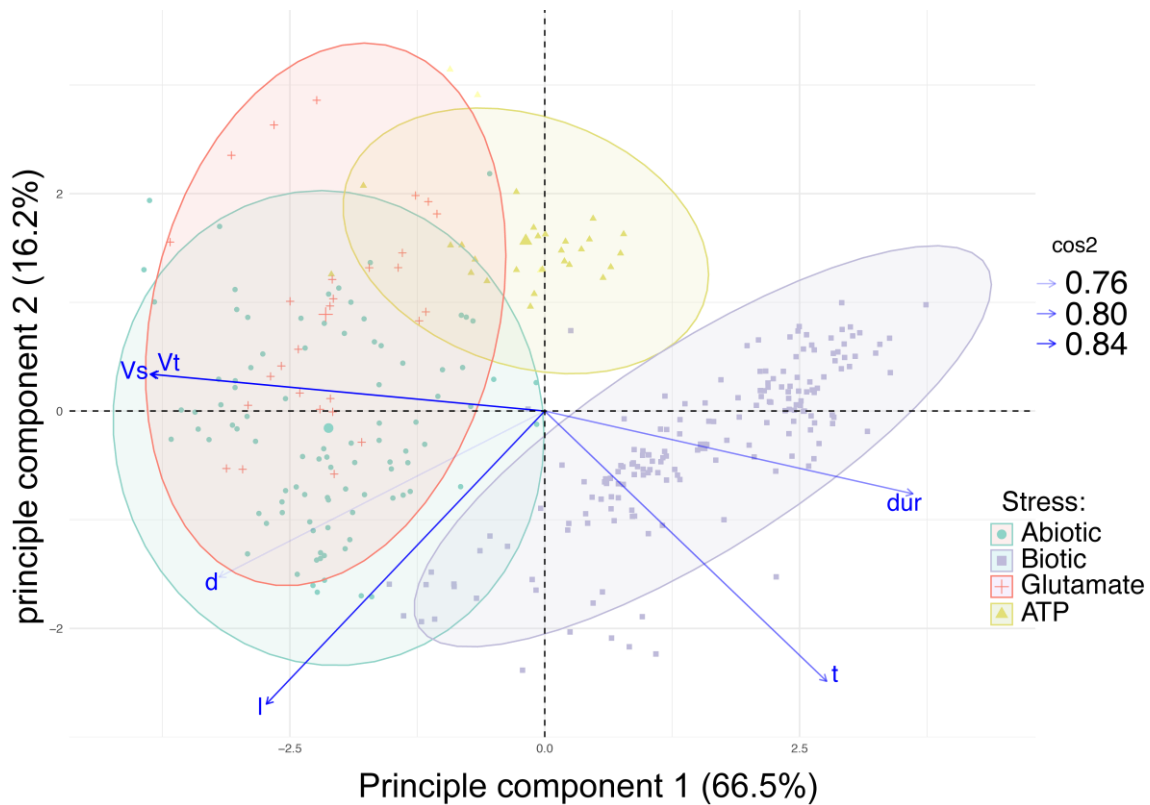


**Figure 11: Principal component analysis (PCA) of calcium signatures for all elicitors clustered by the nature of the induced stress.** The PCA biplot shows correlation circles for biotic stress, abiotic stress and ATP and glutamate. The length of the blue arrows approximates the variance of the parameters. Direction of the arrows shows how strongly each parameter influences a principal component. Angles between the arrows approximate the correlation between the parameters. Intensity of the blue arrow shows which parameters distinguish responses, the darker the arrow the more the parameter contributes to the separation of the responses. Variables depicted are: t: delay, d: distance from tip, dur: duration, l: distance traveled, Vt: velocity tipwards, Vs: velocity shootwards.

### 2.2.2: The calcium signature can be used to make predictions about the nature of sensing mechanisms

For most of the tested biotic elicitors their receptors are known (Table 1). However, it is still unknown which calcium channels are involved in the calcium release and how exactly these calcium channels are activated. It is known that the membrane localized kinase Brassinosteroid Insensitive1-associated receptor kinase 1 (BAK1), the cytoplasmic receptor-like kinases Botrytis-induced kinase 1 (BIK1), and avrPphB sensitive 1-like 1 (PBL1) are required for flg22 and elf18

induced calcium elevations (Jeworutzki et al. 2010; Ranf et al. 2014). By quantifying the location and the delay of the first calcium response to flg22 and nlp20 (Figure 9), I have shown that there actually is a difference in timing of early immune responses between the Leucine-rich repeat receptor kinase (LLR-RK) FLS2 and LRR receptor protein (LRR-RP) RLK23, with the early immune responses of the LRR-RP typically being slower and more prolonged than that of the LRR-RK (W.-L. Wan et al. 2018). This led to the hypothesis that during stress responses the type of receptor influences the timing of the calcium signature.

Comparison of delay times of elicitors using different pattern recognition receptors revealed that the kind of receptor does not influence the delay time (Table 1 and Figure 9). In addition, the PCA biplot indicated that the delay time does not contribute much to explaining the difference between the responses (Figure 10). Velocities and duration contributed more to distinguishing calcium responses. Therefore, I re-plotted the correlation circles based on receptor types to get an indication of the receptor type used for stresses with yet unknown receptors. The PCA biplot showed overlap between all different types of receptors (Figure 12). Most notably the LRR-RP and LRR-RK receptors overlapped almost completely, indicating that calcium responses to the stresses they recognize are similar. The similar calcium responses might be the result of the receptors having the same calcium channel targets. The correlation circles of the two stresses with unknown receptors did not clearly overlap with one or the other receptor type. The correlation circle of the receptor of NaCl partially overlapped with that of the ligand-gated ion channel, lectin receptor kinase, membrane fluidity, and that of cellobiose. This indicates that the receptor that recognizes NaCl might be of one of those receptor types and most likely not a LRR-RK, LRR-RP, or a LysM-RLK. The correlation circle of cellobiose overlapped with that of LysM-RLKL, RR-RP, LRR-RK and NaCl, possibly indicating that the receptor of cellobiose is most likely a receptor kinase or receptor protein.

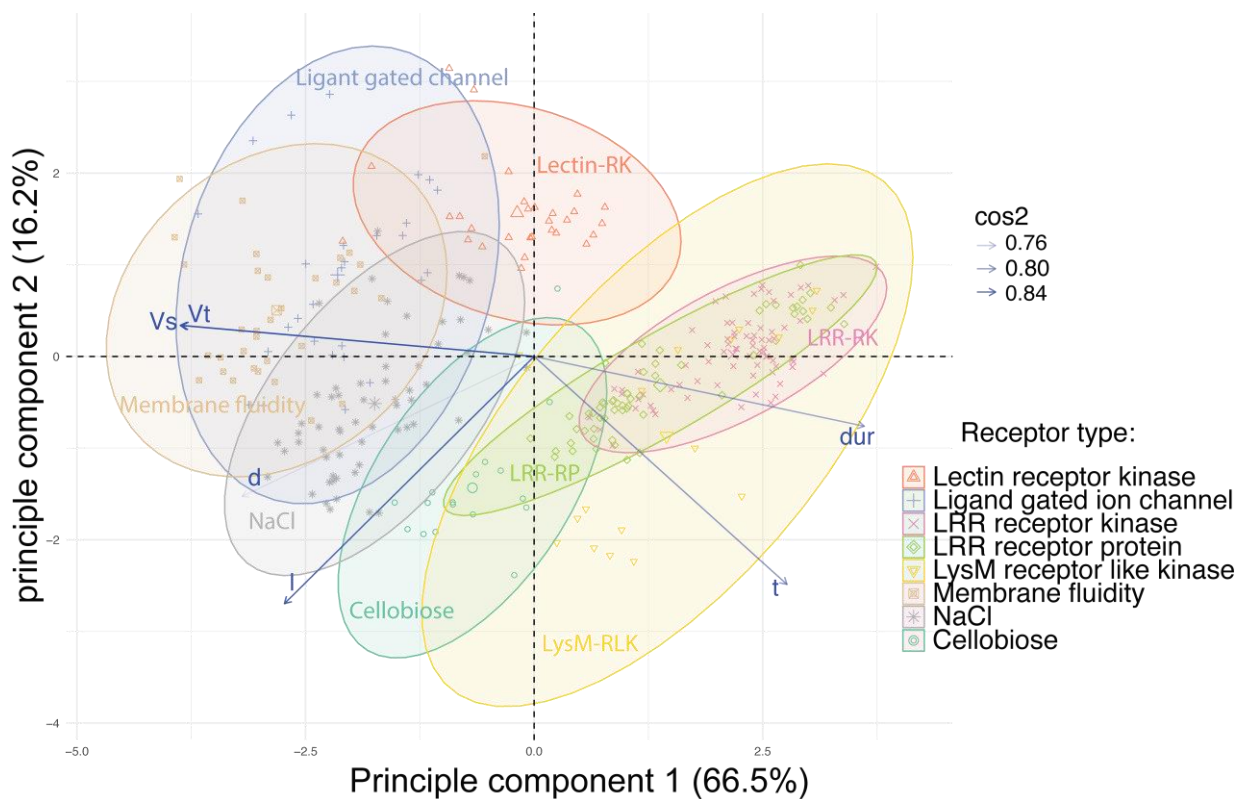


**Figure 12: Principal component analysis (PCA) of calcium signatures clustered by receptor types involved in the recognition of the elicitors.** The PCA biplot shows correlation circles for receptor proteins used in the recognition of nlp20 and PG3. Receptor kinases are used in the recognition of C8, flg22 and ATP. Ligand gated ion channels are used for the recognition of glutamate. NaCl and cold are depicted separately as their receptors are unknown. The length of the blue arrows approximates the variance of the parameters. Direction of the arrows shows how strongly each parameter influences a principal component. Angles between the arrows approximate the correlation between the parameters. Intensity of the blue arrow shows which parameters set the responses apart, the darker the arrow the more the parameter contributes to the separation of the responses. Variables depicted are: t:delay, d:distance from tip, dur:duration, l: distance traveled, Vt:velocity tipwards, Vs:velocity shootwards.

### 2.2.3: The calcium response to biotic stresses is not propagated through the root

To find out whether the restriction of the biotic signals to the elongation zone is caused by the signal not being propagated from the starting point or because other tissues are insensitive to the elicitor, I locally applied elicitors to roots and monitored the spread of the calcium signature throughout the root.

I used the dual-flow-Rootchip (Stanley et al. 2017; Stanley et al. 2018) to expose one side of the root to an elicitor while the other side stayed naïve. For flg22 the

calcium response of the root started in the elongation zone on the treated side of the root. From there the signal moved over the root, but nontreated cells never responded with a calcium signal. When treated with salt, however, the calcium signal spread all the way to the other side of the root as well as spreading shootwards (Figure 13). This data indicates that in contrast to salt-induced calcium response, flg22 only triggered a calcium response in cells that were in direct contact with the elicitor. The results of this experiment have also been published in (Stanley et al. 2017) and have been confirmed using two additional methods of local application (Löffler 2018).

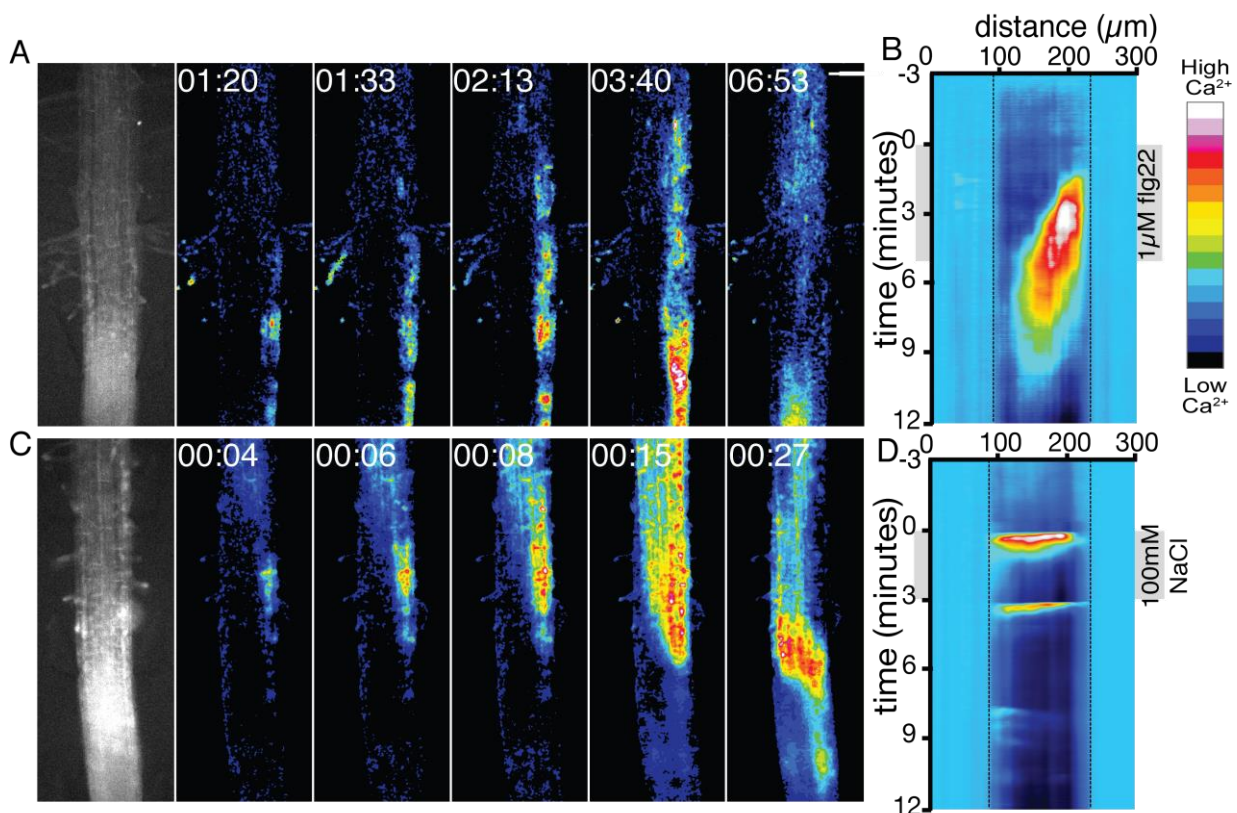


**Figure 13: Local application of elicitors using the Dual-flow RootChip.** Time series of changes in  $[Ca^{2+}]_{cyt}$  upon asymmetric stimulation with 1  $\mu$ M flg22 (**A, B**) and 100 mM NaCl (**C, D**). **A** and **C** depict time series of normalized R-GECO1 fluorescence images with on the left an epifluorescent image to depict the root outline. **B** and **D** depict kymographs generated from left to right over the whole height of the image sequences represented in **A** and **C** respectively, averaging the intensity over the whole height of the image. Scale bar represents 100  $\mu$ m. This figure has been published in (Stanley et al. 2017).

### **2.3: Different stress responses use overlapping signaling pathways**

In nature, plants are constantly exposed to multiple stresses in parallel and have to respond and recognize them all at the same time. This could cause problems if the pathways overlap and use the same signaling molecules. Solutions for this could be to keep the signals spatially separated by restricting them to different organelles, or to be able to filter out the correct information from mixed signals from the dynamics of the calcium releases. Many calcium-binding molecules have been found in plants (Edel et al. 2015), but for most the location in the cell and the responsiveness to specific calcium kinetics are still to be determined.

To find out whether stresses use the same pathways, roots were treated with combinations of flg22, C8 and NaCl at the same time to find out what the resulting calcium signature would look like. If the used elicitors share a pathway in the signal initiation phase, only one calcium signature of the stress that triggers the earliest response is expected. If there are no overlapping pathways, two overlapping calcium bursts at the previously determined location after the appropriate delay time for the two elicitors are expected. How these signals spread depends on whether there is overlap in the signal propagation mechanisms. Since calcium is being used as a readout, only responses that use calcium can be tested. However, it is unclear whether calcium is involved in the signal recognition, the signal propagation or the response to the signal. If there is overlap in the mechanisms of signal propagation, I expect that only one message can be propagated at the time. However, the second message might still be propagated after a refractory period, resulting in a second calcium propagation. If there is no overlap in the propagation mechanisms, two signals can be propagated simultaneously resulting in two overlapping signatures.



### 2.3.1: Simultaneous exposure to flg22 and C8 results in one unique calcium response

To investigate whether biotic responses share signaling components, *Arabidopsis* roots were exposed to a mix containing both flg22 and C8 (Figure 14A). The delay of the combination was shorter ( $180 \pm 27$  seconds) than for flg22 ( $272 \pm 92$  seconds) or C8 ( $340 \pm 128$  seconds) (Figure 15A). The location of the first calcium response moved higher up the root for the combination of the elicitors ( $450 \pm 65$   $\mu\text{m}$  from the tip) than for the single flg22 ( $338 \pm 113$   $\mu\text{m}$  from the tip) or C8 ( $78 \pm 44$   $\mu\text{m}$  from the tip) (Figure 15B). The signal persisted for a shorter time for the combination ( $50 \pm 6,5$  seconds) than for the single flg22 ( $63 \pm 15$  seconds) or C8 ( $81 \pm 270$  seconds) elicitor (Figure 15C). The signal traveled further up the root ( $4056 \pm 2360$   $\mu\text{m}$ ) than in response to flg22 ( $234 \pm 96$   $\mu\text{m}$ ) or C8 ( $927 \pm 711$   $\mu\text{m}$ ) (Figure 15D). In addition, the velocity shoot wards was faster ( $4,8 \pm 2,7$   $\mu\text{m/s}$ ) than for flg22 ( $2 \pm 1,1$   $\mu\text{m/s}$ ) or C8 ( $0,8 \pm 0,3$   $\mu\text{m/s}$ ) (Figure 15E). The velocity tip wards ( $1 \pm 0,3$   $\mu\text{m/s}$ ) was similar to that of flg22 ( $1,1 \pm 0,5$   $\mu\text{m/s}$ ), and therefore slower than C8 ( $2,2 \pm 1,3$   $\mu\text{m/s}$ ) (Figure 15F). These results showed that there is only one response to the combined stresses and that this single calcium response to this combined stress is different from the responses to the single stresses. These outcomes indicated that there is crosstalk between the two stress response pathways upstream of the calcium releases.

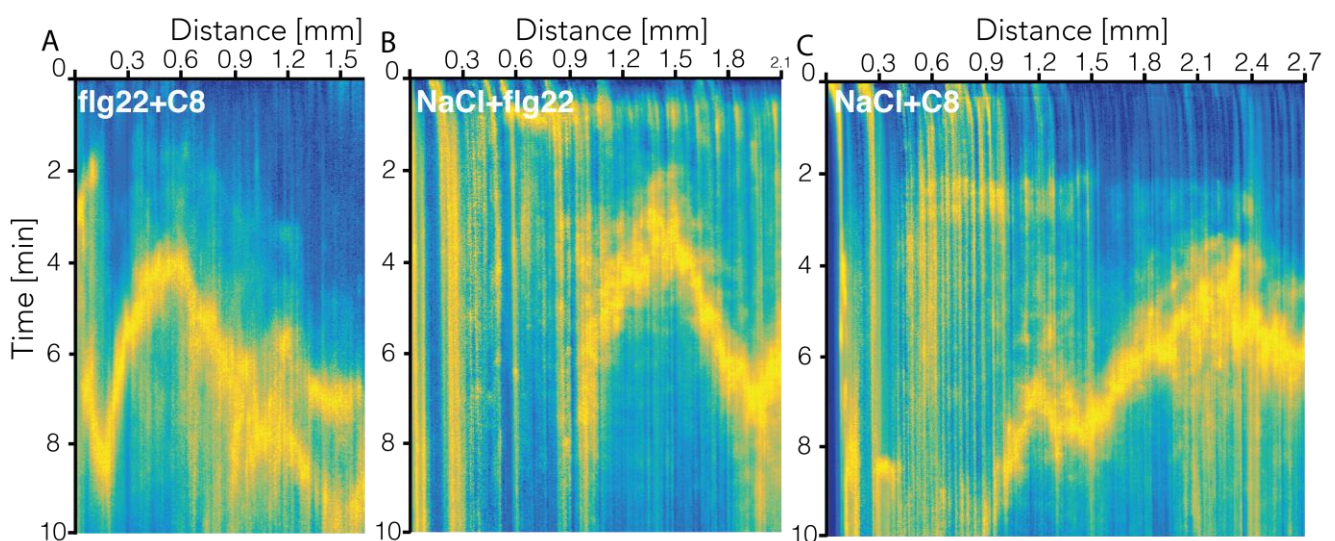


**Figure 14: Representative calcium signatures of single roots in response to treatment with combinations of elicitors.** Crestline normalized kymographs

displaying calcium signatures of *Arabidopsis* roots on meshes treated with **(A)** 10  $\mu$ M flg22+10  $\mu$ M C8, **(B)** 100 mM NaCl+10  $\mu$ M flg22 or **(C)** 100 mM NaCl+10  $\mu$ M C8.

### 2.3.2: Exposure to NaCl and flg22 simultaneously results in an intermediate calcium signature

To investigate whether biotic and abiotic response pathways show similar overlap, *Arabidopsis* roots were exposed to a mix containing both NaCl and flg22 and the resulting calcium signature was characterized (Figure 14B). This resulted in intermediate numbers for the delay (combination: 163  $\pm$ 54 seconds, flg22: 272  $\pm$ 92 seconds, NaCl 61  $\pm$ 50 seconds) (Figure 15A), the duration (combination: 45  $\pm$ 20 seconds, flg22: 63  $\pm$ 15 seconds, NaCl: 21  $\pm$ 3 seconds) (Figure 15C) and the velocities (Shoot wards: combination: 12,5  $\pm$ 10,7  $\mu$ m/s, flg22: 2  $\pm$ 1,1  $\mu$ m/s, NaCl: 66  $\pm$ 35,5  $\mu$ m/s. Tip wards: combination: 13  $\pm$ 10,1  $\mu$ m/s, flg22: 1,1  $\pm$ 0,5  $\mu$ m/s, NaCl: 66,3  $\pm$ 29  $\mu$ m/s) (Figure 15,F), the signal started higher up the root (combination: 2886  $\pm$ 429  $\mu$ m from the tip, flg22: 338  $\pm$ 113  $\mu$ m from the tip, NaCl: 1256  $\pm$ 759  $\mu$ m from the tip) (Figure 15B) and spread further over the root (combination: 4225  $\pm$ 2300  $\mu$ m, flg22: 234  $\pm$ 96  $\mu$ m, NaCl: 2890  $\pm$ 1153  $\mu$ m) (Figure 15D) than for either of the single elicitors. Interestingly, in 35% of the cases a second calcium wave with the same pattern as the first wave could be discerned (Figure 16). The second wave followed the first with an average delay of 52 seconds. In the cases where two waves were present the wave parameters have been measured using the first wave.

The altered delay time and location of the first calcium response indicate that there was feedback between the two signaling responses as the fast and early NaCl signal was affected by the addition of flg22. In the single stress treatment the calcium signal in response to NaCl was already over before the flg22 signal started. However, in combination with flg22 the calcium response was delayed. This shows that the recognition of flg22 starts as early as that of salt, but that it takes longer before there is a calcium release. The intermediate velocities indicated that the method of signal propagation that is used is different from either of the responses to the single elicitors, or that other sensors are used in the perception of combined NaCl and flg22 stress. See suppl. Table 9-14 for Student t-test p-values.

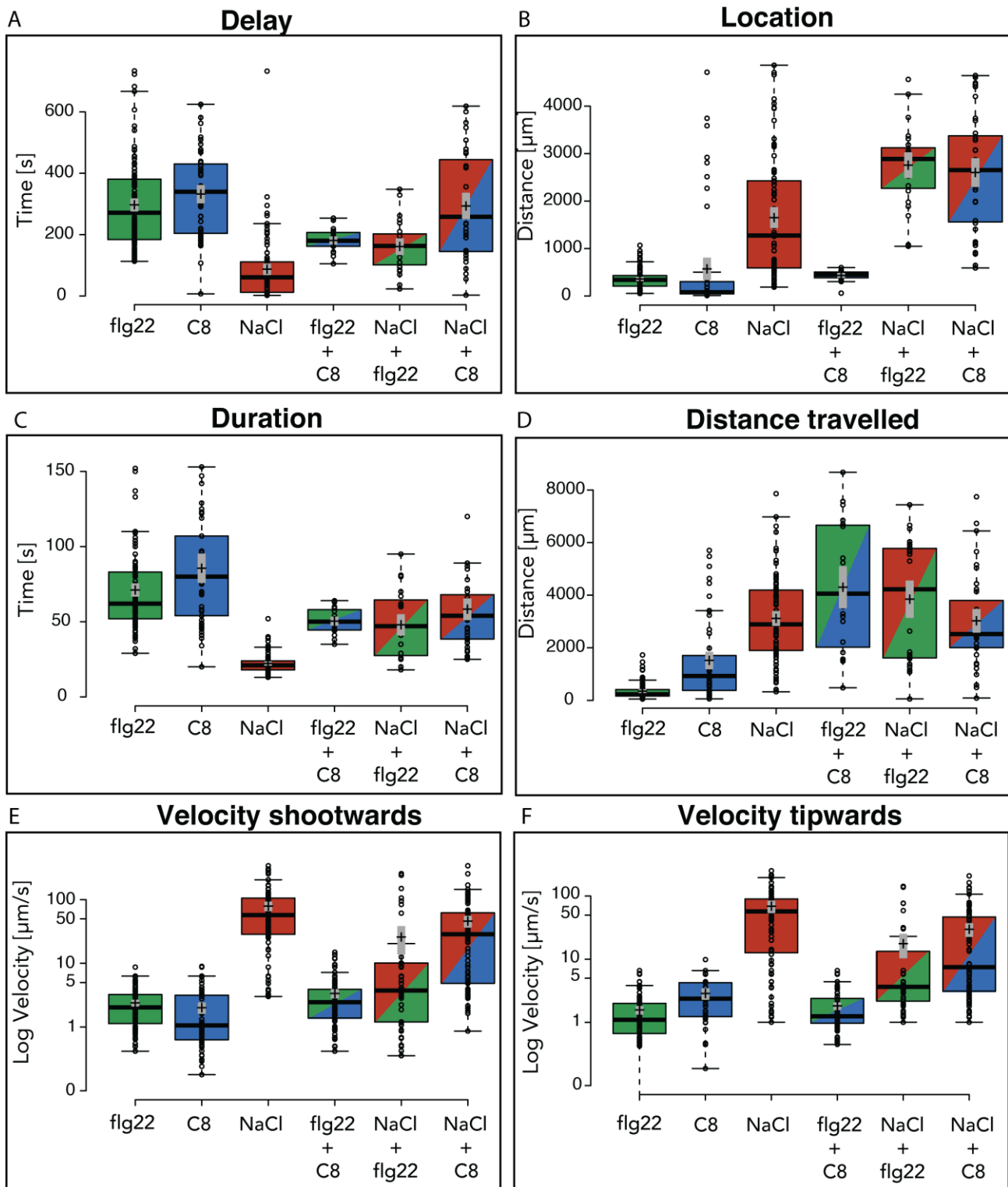


**Figure 15: Quantification of calcium signature characteristics elicited by combinations of elicitors. (A)** Delay between the application of the stress and the first detected increase in  $[Ca^{2+}]_{cyt}$ , **(B)** location of the first response measured as the distance from the root tip, **(C)** duration of the calcium signal, **(D)** distance the calcium wave covered along the root, **(E)** velocity with which the calcium wave traveled towards the shoot and **(F)** velocity with which the calcium wave traveled towards the root tip.



Lines depict sample median. Crosses indicate sample means. Grey boxes define the 83% confidence interval of the mean. n=102 for flg22, n=51 for C8, n=78 for NaCl, n=21 for flg22+C8, n=23 for NaCl+flg22, and n=35 for NaCl+C8. See suppl. table 9-14 for Student t-test p-values.

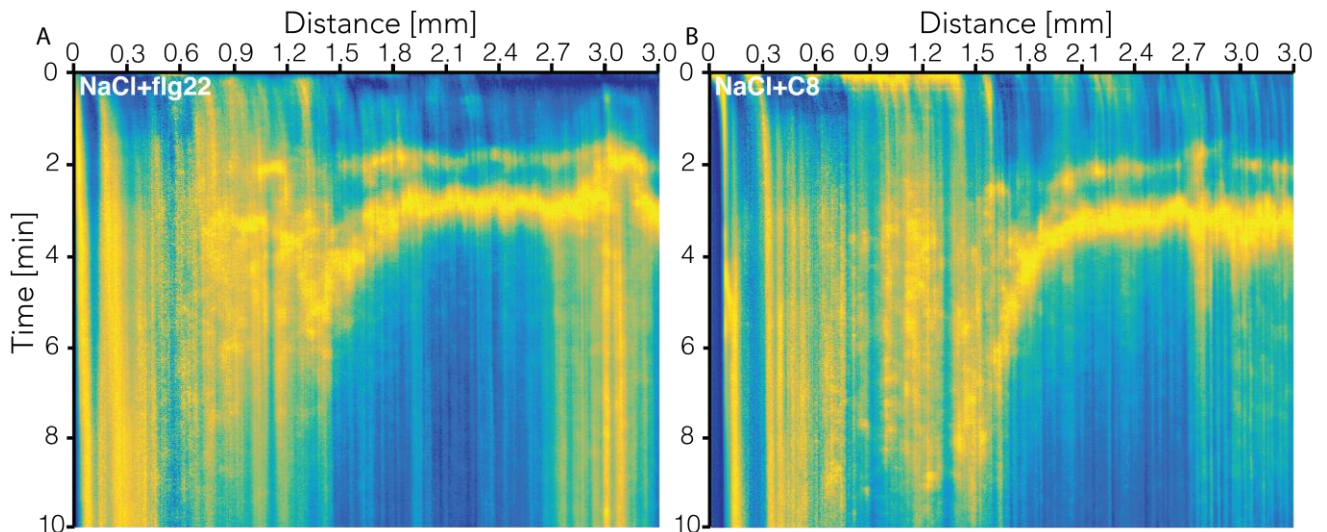


**Figure 16: Representative double calcium signatures of single roots in response to NaCl and flg22 or C8.** Crestline normalized kymographs displaying calcium signatures of *Arabidopsis* roots on meshes treated with (A) 100 mM NaCl+10  $\mu$ M flg22 or (B) 100 mM NaCl+10  $\mu$ M C8.

### 2.3.3: Calcium signatures in response to simultaneous NaCl and C8 exposure exhibit parameters from both single elicitors

To test whether all biotic and abiotic stresses interact in the same manner, *Arabidopsis* roots were treated with a mix containing both C8 and NaCl and the resulting calcium signature was characterized. Interestingly, the response to the biotic C8 and the abiotic NaCl was different in some parameters to the response to the flg22+NaCl combination (Figure 14C). The delay (combination: 258  $\pm$ 136 seconds, C8: 340  $\pm$ 128 seconds, NaCl: 61  $\pm$ 50 seconds) (Figure 15A) and the velocities (shoot wards: combination: 6  $\pm$ 3,8  $\mu$ m/s, C8 0,8  $\pm$ 0,3  $\mu$ m/s, NaCl: 66  $\pm$ 35,5  $\mu$ m/s, tip wards: combination: 5  $\pm$ 2,6  $\mu$ m/s, C8: 2,2  $\pm$ 1,3  $\mu$ m/s, NaCl: 66  $\pm$ 29  $\mu$ m/s) (Figure 15E,F) parameters were similar to that of a regular C8 response, while the distance traveled was more in the NaCl range (combination: 2522  $\pm$ 845  $\mu$ m, C8: 927  $\pm$ 711  $\mu$ m, NaCl: 2890  $\pm$ 1153  $\mu$ m) (Figure 15D). The location of the first signal (combination: 2685  $\pm$ 1044  $\mu$ m from the tip, C8: 78  $\pm$ 44  $\mu$ m from the tip,

NaCl:  $1256 \pm 759$   $\mu\text{m}$  from the tip) (Figure 15B) and the duration of the signal (combination:  $54 \pm 16$  seconds, C8:  $81 \pm 27$  seconds, NaCl:  $21 \pm 3$  seconds) (Figure 15C) were not similar to a calcium response to either single elicitor but were somewhere in-between (Figure 15). Just like the combined NaCl and flg22 stress, sometimes a second wave appeared after the first response. However, for salt and C8 this only occurred in 16% of the cases and the second wave started 47 seconds after the initial wave (Figure 16).

That the roots respond with only one calcium signal that is different from the signals in response to the single elicitors indicates that there is crosstalk between the two signaling responses. However, the result that the calcium signature shows characteristics of the two different single responses simultaneously indicates that there is overlap in the signaling mechanisms used in the response to NaCl and C8. This means that the parameters do not group together in a signal perception group and a signal propagation group as hypothesized before, since the delay parameter is similar to a C8 response while the location of the first response and the distance traveled parameters are similar to a NaCl response.

#### **2.4: ROS plays a role in both biotic and abiotic signaling responses**

The difference between the velocity of calcium wave propagation for biotic and abiotic stresses (see Figure 4H, I) could be explained by different underlying mechanisms of signal propagation. It has been shown that ROS play a role in the propagation of salt stress information (Evans et al. 2016). To test whether a system that uses global treatment can be used to test for factors involved in signal propagation, the velocity and other parameters of the calcium wave in response to salt treatment after ROS scavenging with ascorbic acid (Aa) were quantified. Aa is a non-enzymatic ROS scavenger that can be used to scavenge extracellular ROS (Monshausen et al. 2007; Monshausen et al. 2009; Jiang et al. 2013; Evans et al. 2016). Additionally, the ROS scavenging properties of Aa were used to test whether ROS play a role in the signal propagation in response to biotic stresses.

### 2.4.1: ROS play a role in both the initiation and the propagation of calcium signals in response to salt stress

*Arabidopsis* roots were pre-treated with 100  $\mu$ M Aa for 10 minutes before treating them with 100 mM NaCl (Figure 17C). After global treatment the first calcium signal in response to salt could be detected sooner (after  $61 \pm 49,5$  seconds in the control,  $10 \pm 6$  seconds with ROS scavenging by Aa) (Figure 18A) and the location of this first signal was shifted rootwards, although the variance was high (control:  $1256 \pm 758,5$   $\mu$ m from the tip, Aa:  $511 \pm 161$   $\mu$ m from the tip) (Figure 18B). The calcium signal persisted only slightly longer (control:  $21 \pm 3$  seconds, Aa:  $25 \pm 6$  seconds) (Figure 18C) but covered a smaller portion of the root after ROS scavenging (control:  $2890 \pm 1153$   $\mu$ m, Aa:  $2062 \pm 689$   $\mu$ m) (Figure 18D). After global treatment both the velocity shootwards (control:  $66,0 \pm 35,5$   $\mu$ m/s, Aa:  $31,7 \pm 21,3$   $\mu$ m/s) and tipwards (control:  $66,3 \pm 29,0$   $\mu$ m/s, Aa:  $28,4 \pm 17,4$   $\mu$ m/s) were reduced (Figure 18E, F). These findings point towards an additional role for ROS in the initiation of the salt signaling response in addition to its already postulated role in signal propagation.

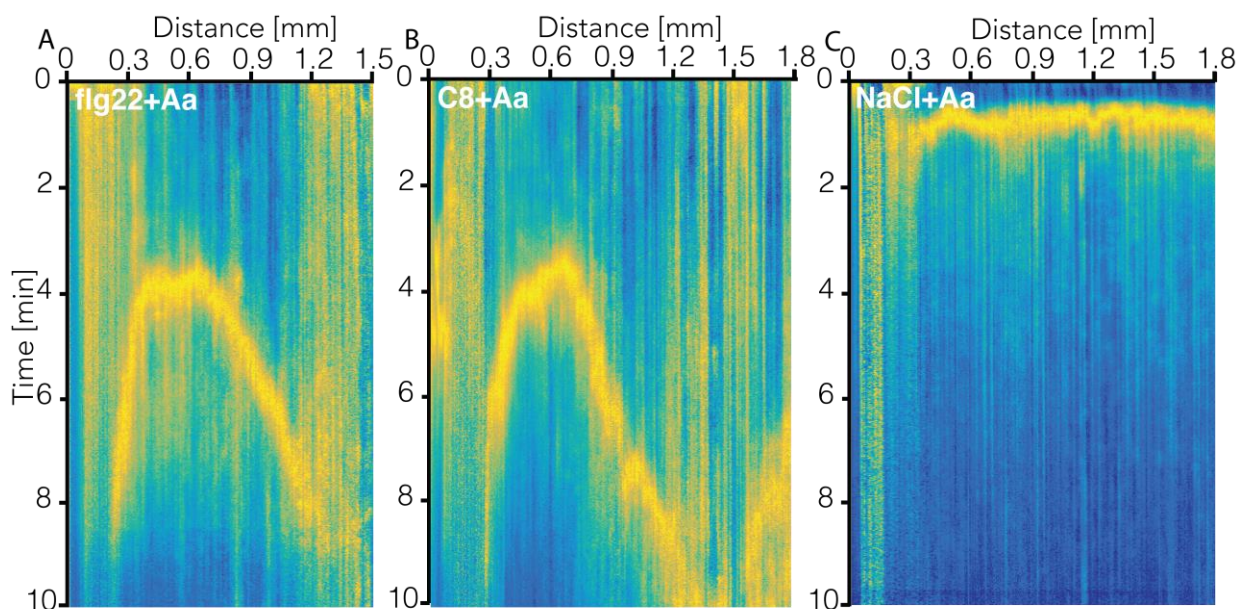


**Figure 17: Representative calcium signatures of single roots in response to flg22, C8 and NaCl after ROS scavenging using Ascorbic acid (Aa).** Crestline normalized kymographs displaying calcium signatures of *Arabidopsis* roots on meshes treated with (A) 10  $\mu$ M flg22, (B) 10  $\mu$ M C8 or (C) 100 mM NaCl after 30 minute pre-treatment with 100  $\mu$ M Aa.

### **2.4.2: ROS targets and restricts the biotic calcium response to the elongation zone**

To test whether ROS might also be involved in the initiation or propagation of the biotic stress signal, *Arabidopsis* roots were pre-treated with 100  $\mu$ M Ascorbic acid (Aa) for 10 minutes to scavenge apoplastic ROS before treating them with 10  $\mu$ M of flg22 or C8 (Figure 17 A, B). After ROS scavenging the calcium response to both flg22 (control: 272  $\pm$ 92 seconds, Aa: 202  $\pm$ 19 seconds) and to C8 (control: 340  $\pm$ 128 seconds, Aa: 208  $\pm$ 30 seconds) appeared earlier (Figure 18A). The location of the first calcium signal had moved higher up the root for both flg22 (control: 338  $\pm$ 113  $\mu$ m from the tip, Aa: 550  $\pm$ 87  $\mu$ m from the tip) and C8 (control: 78  $\pm$ 44  $\mu$ m from the tip, Aa: 533  $\pm$ 109  $\mu$ m from the tip) (Figure 18B). The calcium signals in response to both biotic elicitors lasted about the same time (flg22: control: 63  $\pm$ 15 seconds, Aa: 54  $\pm$ 9 seconds and C8: control: 81  $\pm$ 27 seconds, Aa: 62  $\pm$ 12 seconds) (Figure 18C). The signal spread further over the root for both flg22 and for C8 (flg22: control: 234  $\pm$ 96  $\mu$ m, Aa: 936  $\pm$ 304  $\mu$ m and C8: control: 927  $\pm$ 711  $\mu$ m Aa: 1581  $\pm$ 606  $\mu$ m) (Figure 18D). The signals spread faster shoot wards (flg22: control: 2  $\pm$ 1  $\mu$ m/s, Aa: 2,5  $\pm$ 0,7  $\mu$ m/s and C8: control: 0,8  $\pm$ 0,3  $\mu$ m/s, Aa: 2,7  $\pm$ 0,8  $\mu$ m/s) (Figure 18E), but stayed the same spreading tip wards (flg22: control: 1,1  $\pm$ 0,5  $\mu$ m/s, Aa: 1,4  $\pm$ 0,5  $\mu$ m/s and C8: control: 2,2  $\pm$ 1,3  $\mu$ m/s, Aa: 3,0  $\pm$ 1 $\mu$ m/s) (Figure 18F). These results point toward ROS playing a role in the initial perception of biotic signals rather than in the propagation of the signal to other parts of the root. It seems that ROS restrict the MAMP response to the elongation zone of the root as the calcium signals appear outside of the elongation zone and spread further after ROS scavenging. The effects of Aa on the calcium signature was not due to a change in pH of the application medium as the addition of Aa to the medium did not significantly affect the pH (<0.1 unit, data not shown).

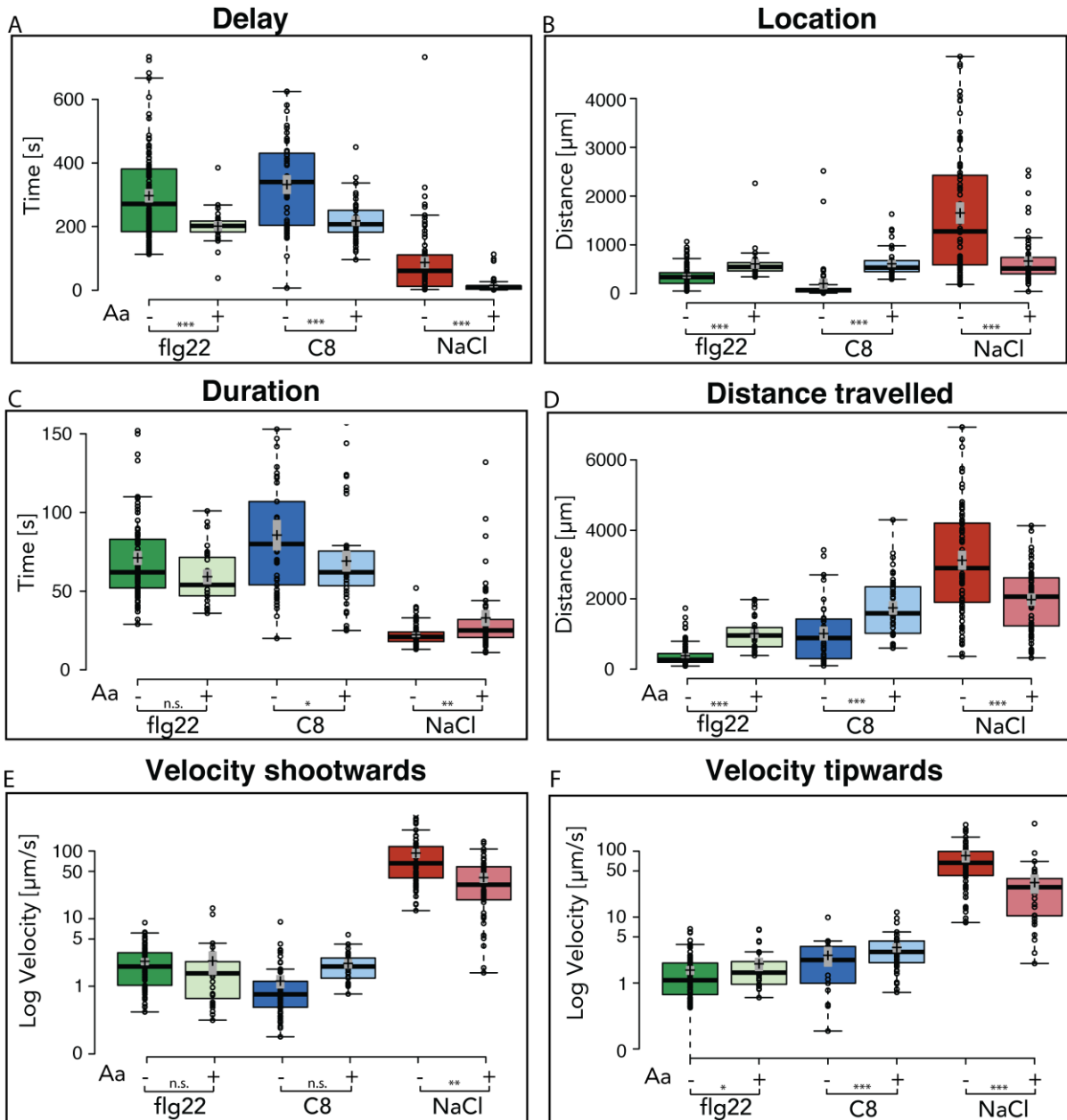


**Figure 18: Quantification of calcium signature characteristics elicited by flg22, C8 and NaCl after ROS scavenging using Ascorbic acid (Aa).** (A) Delay between the application of the stress and the first detected increase in  $[Ca^{2+}]_{cyt}$ , (B) location of the first response measured as the distance from the root tip, (C) duration of the calcium signal, (D) distance the calcium wave covered along the root, (E) velocity with which the calcium wave traveled towards the shoot and (F) velocity with which the calcium wave traveled towards the root tip. Lines depict sample median. Crosses indicate sample means. Grey boxes define the 83% confidence interval of the mean. n=102 for flg22, n=31 for flg22+Aa, n=51 for C8, n=44 for C8+Aa, n=78 for NaCl and n=67 for NaCl+Aa. Asterisks indicate p-values with \* =  $p < 0,05$ ; \*\* =  $p < 0,01$ ; \*\*\* =  $p < 0,001$  or n.s. =  $p \geq 0,05$  in Student's t-test.

### 2.4.3: ROS scavenging results in a higher maximum calcium release for C8

Scavenging ROS results in calcium signals showing up in root regions where they normally do not occur for biotic stresses. This points towards ROS suppressing the release of calcium in biotic stress signaling. In contrast, ROS induced calcium releases are hypothesized to play a role in the propagation of the calcium signal in response to the abiotic NaCl (Gilroy et al. 2016). To figure out whether ROS inhibit or stimulate the release of calcium, the maximum intensity change during the calcium signature (Figure 19) in response to flg22, C8 or NaCl with and without ROS scavenging by Aa was measured.

For flg22 (control:  $3238 \pm 828$  a.u., Aa:  $3867 \pm 691$  a.u.) and NaCl (control:  $3113 \pm 400$  a.u., Aa:  $3360 \pm 614$  a.u.) the maximum intensity was in the same range before and after ROS scavenging. For NaCl this is in line with published data that found that ROS scavenging does not have a significant effect on the amount of calcium released in response to NaCl (Jiang et al. 2013). For C8 (control:  $3272 \pm 363$  a.u., Aa:  $4931 \pm 1096$  a.u.) the maximum intensity was higher after ROS scavenging. This indicates that for the C8, ROS normally represses the release of calcium. This points towards a role for ROS in keeping the calcium response restricted to the elongation zone by repressing the release of calcium in the other tissues.

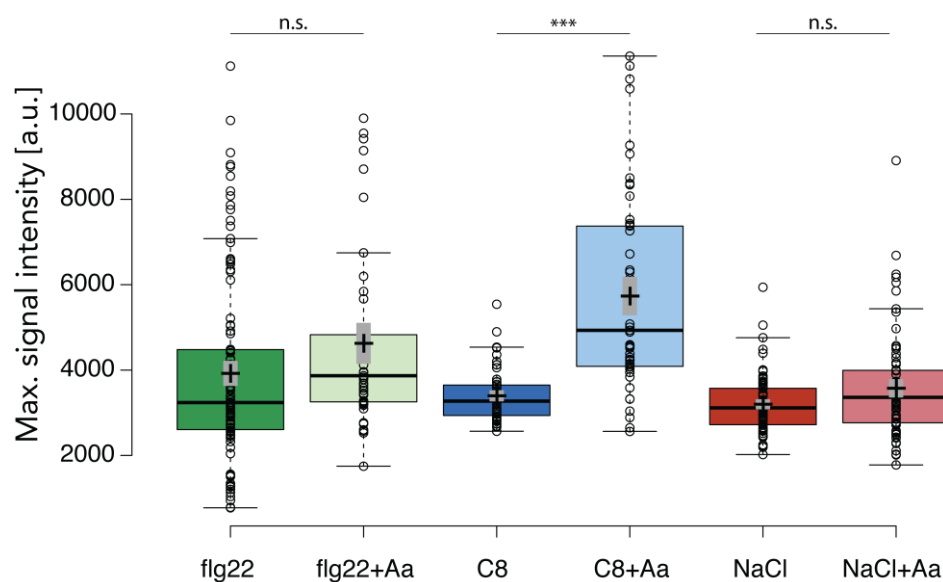


**Figure 19: Maximum signal intensity measured during the calcium signature in response to flg22, C8 or NaCl with and without ROS scavenging using Ascorbic acid (Aa). Lines depict sample median. Crosses indicate sample means.**

Grey boxes define the 83% confidence interval of the mean. n=116 for flg22, n=41 for flg22+Aa n=52 for C8, n=53 for C8+Aa, n=76 for NaCl and n= 72 for NaCl+Aa. Asterisks indicate p-values with \*= p<0,05; \*\*= p<0,01; \*\*\*= p<0,001 or n.s.= p≥ 0,05 in Student's t-test.

#### **2.4.4: ROS is produced during salt signaling responses, but not during flg22 or C8 signaling responses**

To check for additional ROS production in response to the tested stresses, the fluorescent ROS reporter OxyBurst Green HHFF conjugated to bovine serum albumin (BSA) to prevent it from being taken up into the cells was used. OxyBurst Green becomes irreversibly fluorescent upon oxidation and therefore can give us a measure of ROS production in the root upon treatments (Monshausen et al. 2009; Evans et al. 2016). Treatments were done in the Rootchip16 where the medium could be rapidly exchanged without perturbing the root (Figure 20A). Each treatment started with a control of OxyBurst Green dissolved in regular ½ HM medium to record the baseline of ROS production in the root. The slopes after treatment with flg22 and C8 were similar to the slopes of the baseline with a ratio of 0.99 for flg22 and 0.85 for C8 (Figure 20B, C, E). However, after treatment with NaCl a 1.8 fold increase in ROS production could be observed. (Figure 20D, E). This means that there was no increase in ROS production in response to biotic stresses, but there was an almost two-fold increase in ROS production in response to NaCl stress.



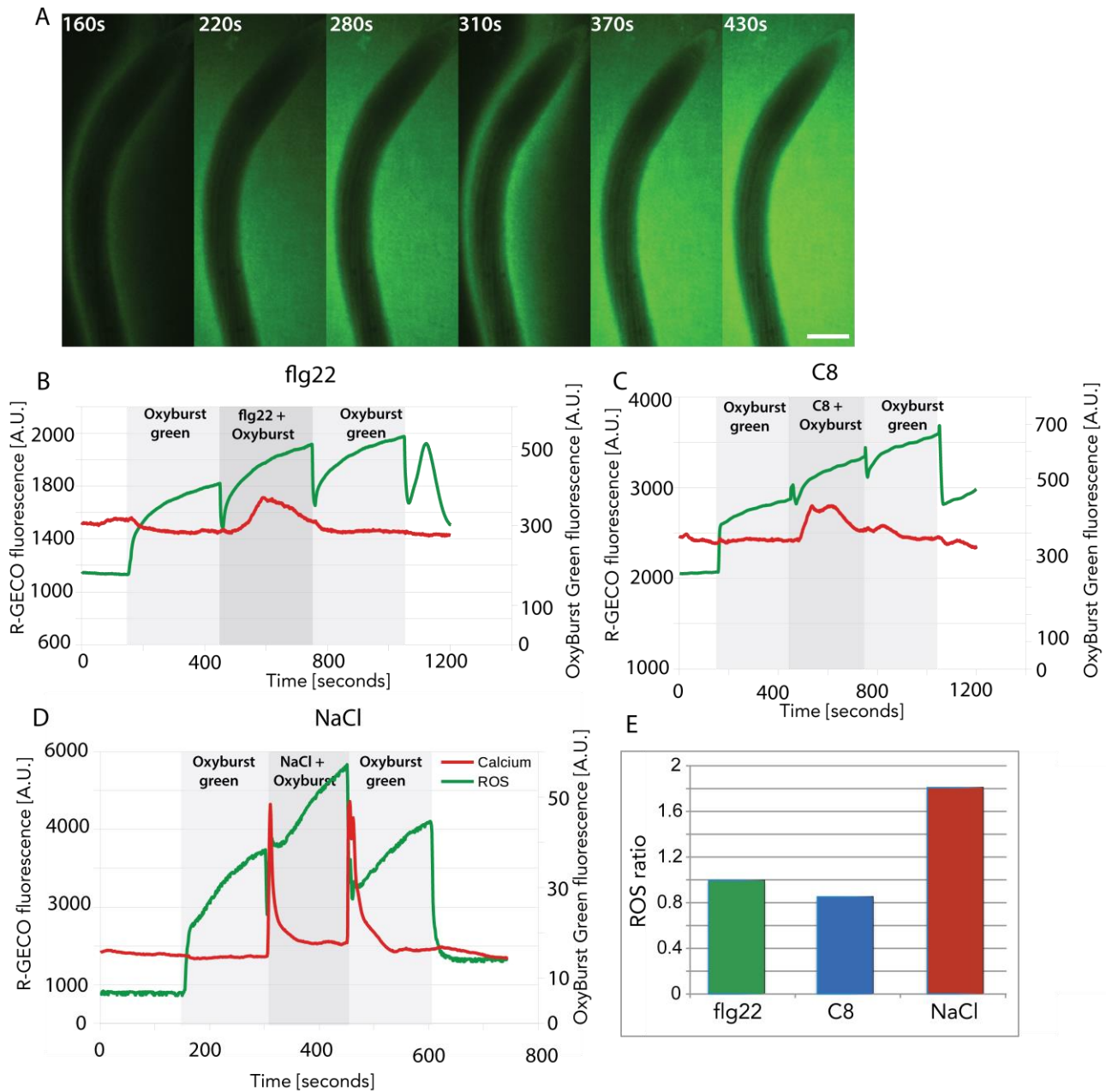


**Figure 20: Measurements of ROS production during the calcium signaling response. (A)** Time series of *Arabidopsis* roots treated with 100 mM NaCl and the fluorescent ROS reporter OxyBurst Green. Scale bar 100  $\mu$ m. **(B,C,D)** Time-dependent fluorescent intensities of R-GECO1 and OxyBurst Green measured over the whole root. Light grey areas indicate treatment with fresh OxyBurst Green, dark grey area indicates treatment with fresh OxyBurst green supplemented with **(B)** 1  $\mu$ M flg22, **(C)** 1  $\mu$ M C8 or **(D)** 100 mM NaCl. **(E)** Ratio between control treatment with OxyBurst green (first light grey box) and the treatment (dark grey box).



These results indicate that ROS is not involved in the signal propagation of the biotic flg22 or C8 stimuli. Instead, the tightly regulated ROS homeostasis might help restricting the responses to biotic stress to the elongation zone as calcium spreads into other root zones after ROS scavenging. In addition, as the calcium response to NaCl appears sooner after ROS scavenging ROS does not only play a role in the signal propagation of the abiotic NaCl stress, but also in the signal initiation.

## **2.5: Different signaling pathways start their own set of downstream responses**

### **2.5.1: ROS targets the calcium response to a combination of flg22 and C8 to the elongation zone**

To test whether the calcium signature in response to combinations of two biotic elicitors is using the same pathways as the single elicitors or whether a different, new pathway is utilized, I tested whether ROS plays a role in the response to the combined biotic elicitors. The calcium signature in response to the flg22+C8 combination with ROS scavenging was roughly the same as without the ROS scavenging (Figure 21). The delay before the first calcium signal (control:  $180 \pm 27$  seconds, Aa:  $193 \pm 13$  seconds) (Figure 22A) and the location of first signal (control  $450 \pm 65$   $\mu\text{m}$  from the tip, Aa:  $472 \pm 130$   $\mu\text{m}$  from the tip) (Figure 22B) were in the same range with and without ROS scavenging. The signal faded away faster after ROS scavenging (control:  $50 \pm 6.5$  seconds, Aa:  $39 \pm 7.5$  seconds) (Figure 22C) and did not travel as far anymore (control:  $4056 \pm 2360$   $\mu\text{m}$ , Aa:  $3036 \pm 1003$   $\mu\text{m}$ ) (Figure 22D) but spread faster over the root (tip wards: control:  $1 \pm 0.3$   $\mu\text{m/s}$ , Aa:  $1.7 \pm 0.8$   $\mu\text{m/s}$ , shoot wards: control:  $4.8 \pm 2.7$   $\mu\text{m/s}$ , Aa:  $6.2 \pm 1.2$   $\mu\text{m/s}$ ) (Figure 22E, F).

The calcium signature in response to the combination of flg22 and C8 after ROS scavenging showed the same trend as the responses to the single elicitors after ROS scavenging. This indicated that ROS also restricted the calcium response of the combined stresses to the elongation zone.

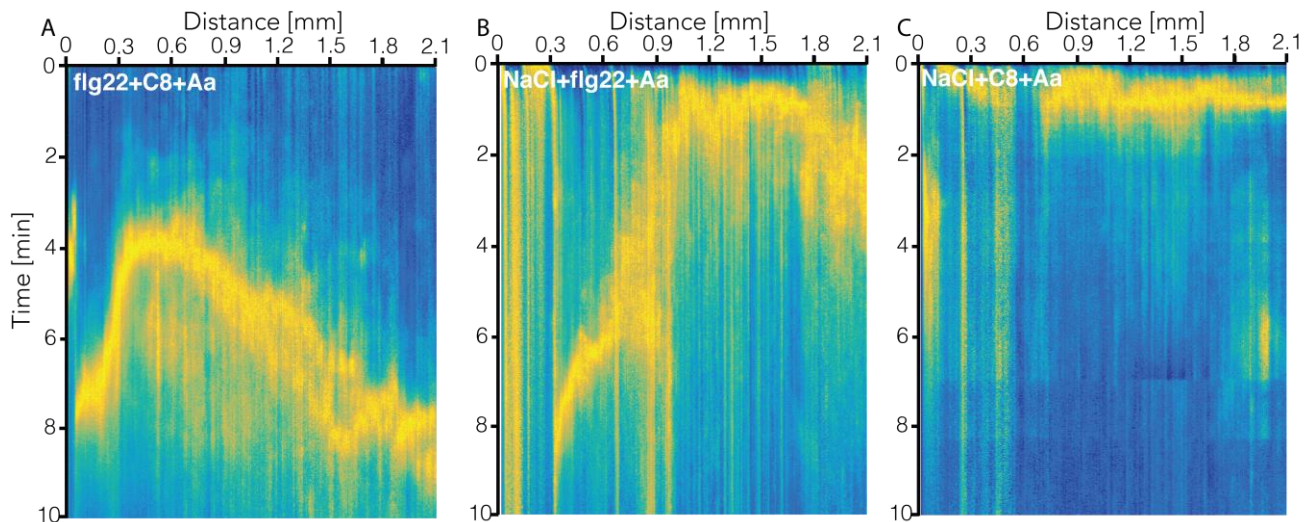


**Figure 21: Representative calcium signatures of single roots in response to treatment with combinations of elicitors after ROS scavenging using Ascorbic acid.** Crestline normalized kymographs displaying calcium signatures of *Arabidopsis* roots on meshes treated with **(A)** 10  $\mu$ M flg22+10  $\mu$ M C8, **(B)** 100 mM NaCl+10  $\mu$ M flg22 or **(C)** 100 mM NaCl+10  $\mu$ M C8 after 30 minutes pre-treatment with Aa.

### 2.5.2: ROS plays a role in the signal initiation and propagation response to combined NaCl and flg22 stress

To find out whether the signaling in response to a combination of NaCl and flg22 use the relatively well known signaling pathway of flg22 or the unknown pathway of NaCl Aa was used to test whether the calcium signature in response to NaCl+flg22 would follow the same trend as the signal in response to NaCl or flg22 after ROS scavenging. The calcium signature elicited by NaCl+flg22 after ROS scavenging followed the trend of NaCl after ROS scavenging (Figure 21). The median first calcium response showed up sooner (control:  $163 \pm 54$  seconds, Aa:  $23 \pm 13$  seconds), but not significantly so (Figure 22A). Like a calcium response to NaCl after ROS scavenging, the first calcium signal started closer to the root tip (control:  $2886 \pm 429 \mu$ m, Aa:  $1070 \pm 456 \mu$ m) (Figure 22B). The signal persisted for a similar period of time (control:  $45 \pm 20$  seconds, Aa:  $34 \pm 10$  seconds) (Figure 22C), but traveled less over the root (control:  $4225 \pm 2300 \mu$ m, Aa:  $2104 \pm 1200 \mu$ m) (Figure 22D). The velocity with which the signal spread over the root after ROS scavenging was unaffected in the direction of the shoot (control:  $12,5 \pm 10,6$

$\mu\text{m/s}$ , Aa:  $16,4 \pm 13,1 \mu\text{m/s}$ ) (Figure 22E), but slowed down towards the shoot (control:  $13 \pm 10,1 \mu\text{m/s}$ , Aa:  $2,3 \pm 1 \mu\text{m/s}$ ) (Figure 22F), although again not significantly. A second calcium wave was now only reported in 20% of the responses and started 41 seconds after the first wave. All the parameters that were affected followed the same trend as the response to NaCl after ROS scavenging. This indicates that ROS plays the same role in the signaling response to the combined stresses as plays in the response to the single NaCl stress and points towards the signaling pathways using similar components.

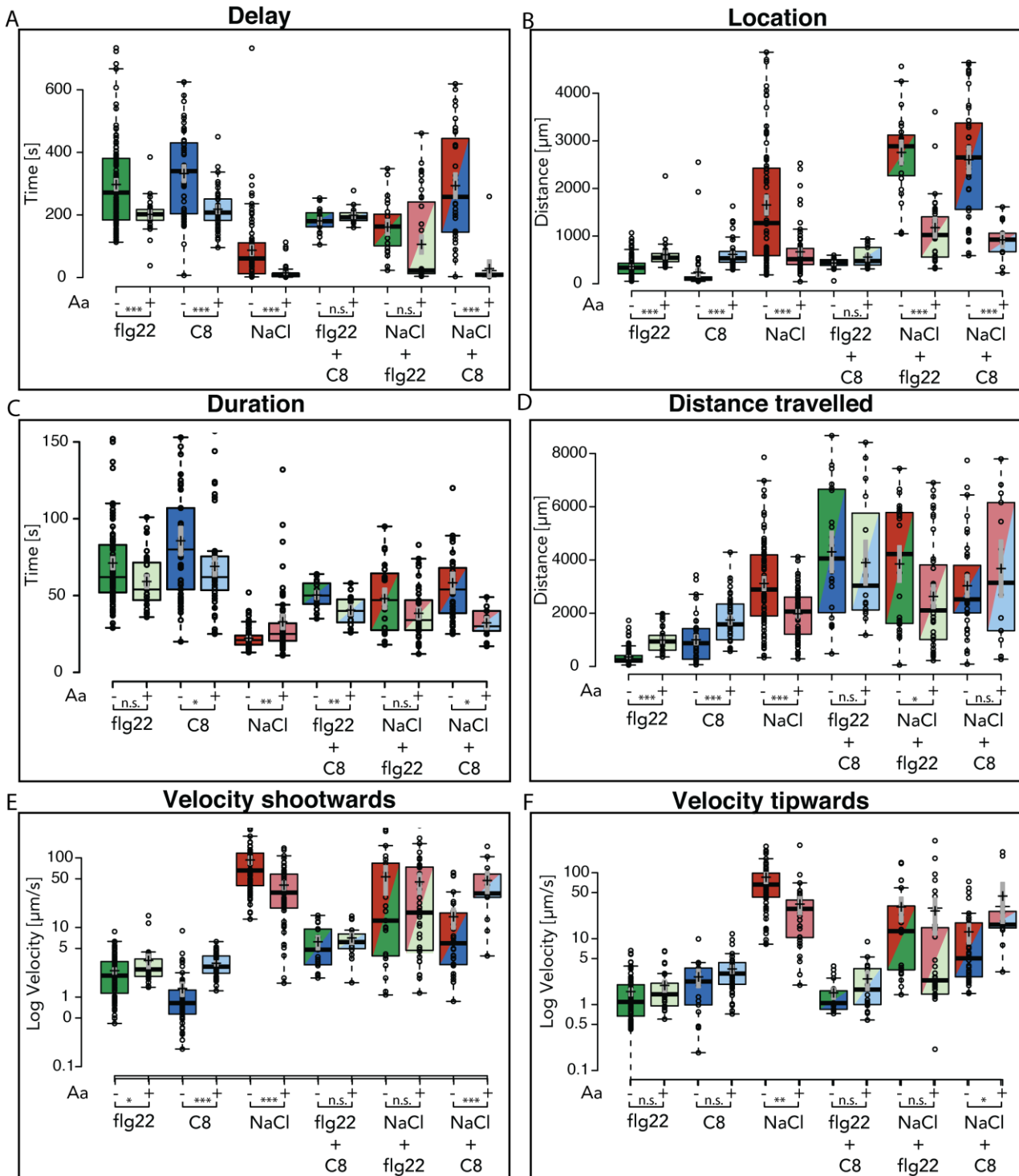


**Figure 22: Quantification of calcium signature characteristics elicited by combinations of elicitors after scavenging using Ascorbic acid.** Delay between the application of the stress and the first detected increase in  $[Ca^{2+}]_{\text{cyt}}$ , **(B)** location of the first response measured as the distance from the root tip, **(C)** duration of the calcium signal, **(D)** distance the calcium wave covered along the root, **(E)** velocity with which the calcium wave traveled towards the shoot and **(F)** velocity with which the calcium wave traveled towards the root tip. Lines depict sample median.

Crosses indicate sample means. Grey boxes define the 83% confidence interval of the mean. n=102 for flg22, n=31 for flg22+Aa, n=51 for C8, n=44 for C8+Aa, n=78 for NaCl, n=67 for NaCl+Aa, n=21 for flg22+C8, n=16 for flg22+C8+Aa, n=23 for NaCl+flg22, n=40 for NaCl+flg22+Aa, n=35 for NaCl+C8 and n=13 for NaCl+C8+Aa. Asterisks indicate p-values with \*= p<0,05; \*\*= p<0,01; \*\*\*= p<0,001 or n.s.= p≥ 0,05 in Student's t-test. suppl. table 9-14 for additional Student t-test p-values

### 2.5.3: ROS plays a role in prioritization between NaCl and C8 stress

The calcium signature in response to the combined treatment of NaCl+C8 showed characteristics of the two different single responses simultaneously. This raised the hypothesis that we could shift this to a complete C8 response by interfering with the response to NaCl by scavenging of ROS. To test this hypothesis roots were treated with 100  $\mu$ M Aa and exposed to double treatments of NaCl and C8 (Figure 21). After ROS scavenging the delay before the first calcium signal in response to NaCl+C8+Aa treated roots (control: 258  $\pm$ 136 seconds, Aa: 9  $\pm$ 5 seconds) (Figure 22A) showed similar values as the single NaCl+Aa treatment. The location of the first calcium response was closer to the root tip compared to the untreated control (control: 2685  $\pm$ 1044  $\mu$ m from the tip, Aa: 919  $\pm$ 256  $\mu$ m from the tip) (Figure 22B), but not in the elongation zone. The calcium signal was over sooner (control: 54  $\pm$ 16 seconds, Aa: 32  $\pm$ 6 seconds) (Figure 22C) and spread a similar distance over the root (control: 2522  $\pm$ 845  $\mu$ m, Aa: 3141  $\pm$ 2301  $\mu$ m) (Figure 22D). The calcium response spread faster over the root compared to the response without ROS scavenging (shoot wards: control: 6  $\pm$ 3,8  $\mu$ m/s, Aa: 30,8  $\pm$ 19,5  $\mu$ m/s, tip wards: control: 5  $\pm$ 2,6  $\mu$ m/s, Aa: 16,3  $\pm$ 8,3  $\mu$ m/s) (Figure 22E, F) and was now more similar to the values of the response to NaCl after ROS scavenging. In addition, 61% of the responses now had a second calcium response following the first with a delay of 38 second. The delay and velocity changing from values in the range of a chitin response after NaCl+C8 treatment to values in the range of a NaCl response after ROS scavenging resulted in a calcium signature that was similar to a NaCl calcium signature after ROS scavenging. This points towards a role for ROS in the prioritization of fungal stress over salt stress.

## 2.6: Crestline: An automated image analysis pipeline for calcium signature analysis

A drawback of measuring all the parameters by hand is that this could introduce an experimenter bias. To counter this problem a collaboration with Jurgen Pahle and Martin Zauser from the Biological Information Processing Group at the Center for Quantitative Analysis of Molecular and Cellular Biosystems (BioQuant) in Heidelberg was initiated. In an effort to automate the quantification of the calcium signature parameters we created the “AutoCrestline” algorithm. The AutoCrestline algorithm is an image analysis pipeline written in the open source software R (Team 2018). It uses time-lapse movies of roots expressing fluorescent sensors (Figure 23A). The algorithm automatically finds the root outline (Figure 23B), midline and root width (Figure 23C). It uses this to create a kymograph of the response (Figure 23D). The kymograph is normalized using Crestline normalization and the algorithm traces the calcium wave and quantifies the delay between the application of the stress, the first detected increase in  $[Ca^{2+}]_{cyt}$ , the location of the first response, measured as the distance from the root tip, the velocity with which the calcium wave travels towards the root tip and the velocity with which the calcium wave travels towards the shoot (Figure 23E).

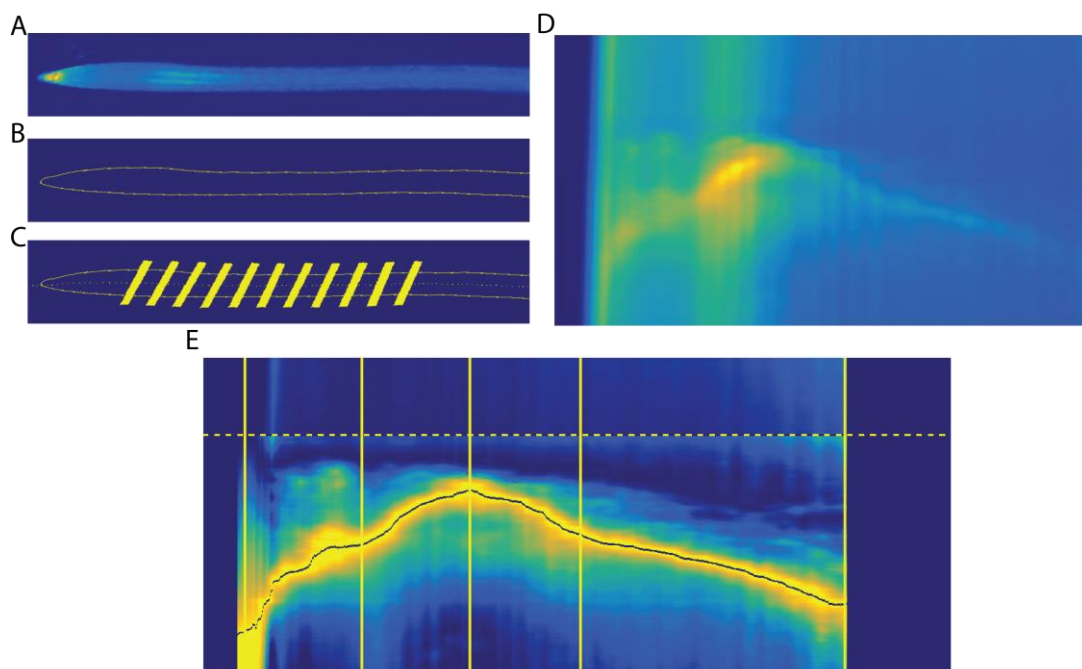


**Figure 23: AutoCrestline algorithm image analysis pipeline.** The algorithm uses raw time-lapse data of roots expressing a fluorescent reporter. In this case, a time-lapse movie of an *Arabidopsis* root expressing R-GECO1 treated with 1  $\mu$ M

flg22 **(A)**. The root outline **(B)** and thickness of the root **(C)** are determined by the algorithm. A raw kymograph is generated **(D)** and subsequently normalized by scaling each column between its minimum and maximum value according to Crestline normalization **(E)**. Finally, the wave of fluorescence moving over the root is tracked and the parameters are quantified **(E)**.

To test whether the algorithm is functioning properly a set of calcium signatures was analyzed by hand and by the algorithm to characterize the same set of calcium signatures. The outcome showed that only the delay time differs between the hand analyzed and computer analyzed, however, the trend between flg22 and C8 is the same (Figure 24). Currently the algorithm only quantifies 4 of the 6 parameters that have been measured. The algorithm is susceptible to noise in the images; therefore it does not work for the lower resolution data produced by the higher throughput method using multiple roots grown on meshes. In addition, the algorithm failed to characterize fast moving signals like the response to NaCl. A solution to this would be to decrease the time interval between frames in the time-lapse. However, with our current imaging setup we were not able to achieve a high enough frame rate while maintaining a sufficient signal intensity.

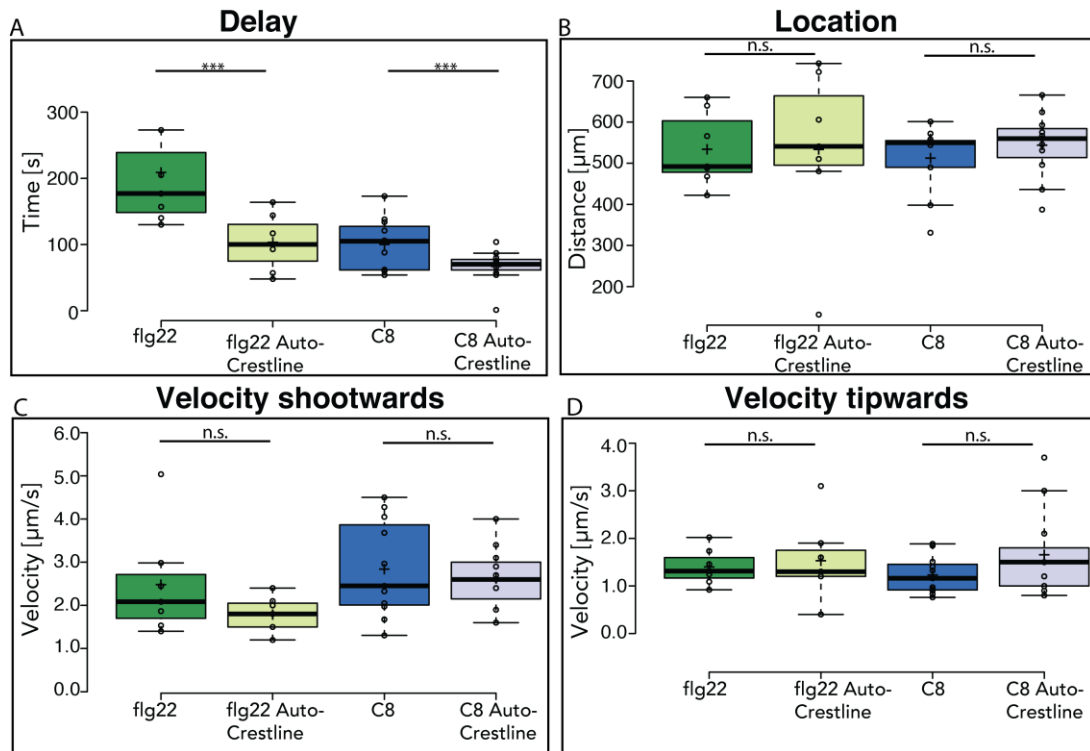


**Figure 24: Comparison of calcium signature parameter quantification by hand and by AutoCrestline algorithm shows comparable quantifications.** The same calcium responses were analyzed by hand and by using the AutoCrestline image analysis pipeline. Measured parameters are: **(A)** delay between the application of the stress and the first detected increase in  $[Ca^{2+}]_{cyt}$ , **(B)** location of the first response measured as the distance from the root tip, **(C)** velocity with which the calcium wave travels towards the shoot and **(D)** velocity with which the calcium wave travels towards the root tip.  $n=13$  for flg22 and  $n=17$  for C8. Asterisks indicate p-values with \*\*\*=  $p < 0,001$  or n.s.=  $p \geq 0,05$  in Student's t-test.



### 3 Discussion

For over 20 years now, the question as to how changes in the concentration of free calcium can trigger a variety of different downstream activities in plants with impressive specificity has not yet been answered satisfactorily. Even though the calcium signature theory has never been proven (Scrase-Field et al. 2003; Plieth 2016), it has been useful in providing a framework to analyze calcium responses to different stresses, and to identify proteins and other factors involved in stress perception and signaling. However, so far, it has been difficult to compare experiments on calcium responses, as a reliable method to quantify both the spatial and the temporal aspects of calcium signatures has been lacking. This has further created a hurdle for research groups to work together in the field of calcium signatures to stress responses. In this thesis a novel method to characterize and quantify the calcium signature is presented that enables easier sharing and comparison of experimental findings on calcium responses. This new method is used to show that there is a unique spatio-temporal calcium signature in response to different stresses in roots of *Arabidopsis*. Furthermore, this new way of quantifying calcium signatures can potentially identify yet unknown factors that play a role in stress responses that lie upstream of calcium signaling, and allow predictions to be made about components involved in the signaling response based on the calcium signature.

#### 3.1: Global stimulation can be used to examine signal propagation pathways

In these experiments the elicitors are applied globally to the whole root. Yet the readout focuses on the way the resulting calcium wave spreads over the root. One could argue that the calcium wave spreading over the root does not represent an actively propagated signaling wave, but rather is an effect of the elicitor diffusing through the root tissue, or the different tissues being differently sensitive to certain elicitors and responding with a different delay time. However, although the

molecular weight of the biotic elicitors is higher than that of the abiotic ones, the weight of the elicitor, and therefore the diffusion coefficient, does not seem to be related to the speed at which the calcium wave propagates through the root (Löffler 2018).

It is clear that there has to be an additional mechanism to propagate the signal as it has been shown that calcium-induced calcium releases will not result in the high velocities that are observed (Evans et al. 2016; Löffler 2018). Calcium waves propagated by calcium-induced calcium releases that propagate at a rate faster than 35  $\mu\text{m/s}$  have never been reported in any organism (Jaffe 2010). Even if there would be no active propagation of the signal, the calcium signature, as defined in this work, could still be used as a readout for the sensed stress since the way calcium waves spread over the root is unique for each stress. In addition, the finding that the velocity with which the calcium wave spreads over the root is slowed down after ROS upon both local (Evans et al. 2016) and global treatment (this study, Figure 18) demonstrates that global treatment can also be used to study the effect of ROS on calcium responses.

### **3.2: The amplitude of the calcium release is not part of the calcium signature**

It has been shown that the amount of calcium released in the whole plant in response to flg22 positively correlates with the concentration of the elicitor, with more calcium being released with higher concentrations (X.-Q. Cao et al. 2017). However, more cells responding to the stimulus could be the cause of this. In this work it is shown that although the calcium response to NaCl results in more calcium being released over the whole root (Figure 4) the maximum amount of calcium released in the root is similar (Figure 19). It would be interesting to define the maximum amount of calcium released per cell in response to different stresses. This could be done by using a ratiometric calcium sensor and would require calibration of the sensor as demonstrated in (Waadt et al. 2017). In addition, the strength of the MAMP immune signaling is independent of the concentration of flg22 used (Poncini et al. 2017). Plants do not respond to the absolute concentration of flg22 and NaCl (Suppl. Figure 1) but rather to the

concentration changes over time, as has already been shown for cold stress (Plieth 1999). In the classic calcium signature theory, the calcium signature is defined as the pattern in the amplitude and the timing of the calcium release in the plant upon stimulation. If amplitude of the release depends on the concentration of the elicitor this would lead to every concentration of every elicitor having a unique calcium signature. This would result in plants having millions of possible calcium signatures. In this work the calcium signature is defined as the spatio-temporal pattern with which the calcium signal spreads over the root (Figure 3), while it is unlikely that a single cell in the root is able to perceive this spatial information, it can be used as a readout and used to test hypothesis in calcium signaling. Preliminary data indicates that the spatio-temporal pattern of the calcium signature is independent of the concentration of flg22 nor by the exposure time.

### **3.3 Calcium signature analysis reveals information about the nature of a stress**

This study has revealed features to distinguish calcium signatures in response to biotic or abiotic stresses. The calcium signatures in response to biotic stresses start, and are restricted to, the elongation zone. It has been proposed that plant roots are most sensitive to a bacterial or fungal infection in this region as cell walls are weakest as they are stretching to accommodate cell elongation (Somssich et al. 2016). Several immune responsive genes are specifically upregulated in the elongation zone upon flg22 treatment, and, in addition, flg22-induced callose deposition is restricted to the elongation zone (Millet et al. 2010). However, the heightened sensitivity of the elongation zone to flg22 does not correlate to the FLS2 receptor being higher expressed in this region, as the expression of FLS2 is higher in the more mature root zones (Wyrsh et al. 2015). The fact that calcium signatures are restricted to the elongation zone does not mean that the resulting immune response is also restricted as it is known that plant hormones act downstream of immune recognition events (Couto et al. 2016). Although the events leading up to the changes in hormone regulation remain largely unknown, hormones potentially start an immune response in the rest of the plant (Denancé 2013). In contrast to biotic stresses like fungi and bacteria that target the

elongation zone, abiotic stresses including salt and cold affect every root zone equally, which is reflected in their response not having a preferred starting point. This study has identified an exception to biotic stresses being restricted to the elongation zone in the form of the allegedly biotic elicitor, cellobiose. Cellobiose is considered a biotic stressor as it leads to an increase of expression of defense related genes that overlap with other pathogen associated elicitors like chitin and oligogalacturonides (Azevedo Souza et al. 2017). The atypical biotic stress-induced calcium signature of cellobiose can be explained by the nature of the fungi that produces enzymes capable of inducing this stress signal. In nature, only wood digesting fungi produce the cellulase that breaks down cellulose into its cellobiose breakdown product (Howard 1997). Fungi that are capable of digesting the cell wall would not need to target the elongating region in the root where there are the weakest cell walls. Instead, every region would be equally sensitive to infection with this pest. Therefore, it seems that the calcium signature in response to cellobiose reflects the nature of the pest it is responding to. Although the majority of the measured parameters by itself do not show a distinct grouping of biotic and abiotic stresses (Figure 10), taken together, it is now possible to distinguish calcium signatures in response to biotic versus abiotic stresses (Figure 11). It is important to keep in mind, of course, that the biotic/abiotic division of stresses is a human classification and plants might distinguish stresses in a whole other way.

### **3.4 Local application of stresses show that the flg22 induced calcium signal is not propagated**

Together with Janos Löffler, I locally applied elicitors in three different ways using the Dual-flow-RootChip (Stanley et al. 2017; Stanley et al. 2018), alginate beads, and by growing roots in agar filled pipette tips. All three methods confirmed that there was active propagation of the calcium signal upon local application of salt or ATP, and that for flg22 and chitin only the cells that are directly exposed to the elicitor showed a calcium response (Löffler 2018). In these studies, fluorescein was used to visualize the presence or absence of the elicitor at the root. However, the diffusion behavior of fluorescein is not the same as the different elicitors

tested. Löffler (2018) used elegant computer models to show that the diffusion of salt was slower than the velocity of the propagated calcium wave. These setups for local application of elicitors can also be used together with mutants in ROS generation or ROS scavengers like Aa to test the role of ROS in the signal propagation mechanism.

### **3.5 Newly produced ROS is not involved in the flg22 calcium signaling response**

ROS accumulation is a typical early MAMP response. ROS production in response to flg22 takes place after the calcium release as the calcium release takes place 5 minutes after exposure to flg22 (this work, Figure 4) and ROS accumulation peaks only after 15 minutes (Chinchilla et al. 2007; Smith et al. 2014; Noshi et al. 2016; Poncini et al. 2017). In addition, it has been shown that pre-treatment with the calcium channel inhibitor lanthanum(III)Chloride prevents the accumulation of ROS (Ranf et al. 2011), showing that the ROS response is downstream of the calcium response.

Despite all these indications that ROS is downstream of calcium, scavenging with Aa affects the calcium response, as it shortens the delay before the first calcium release. Furthermore, it changes the location of the first signal higher up the root and makes the calcium signal spreads further (Figure 18). This discrepancy can be explained by different kinds and sources of ROS. The ROS produced for the MAMP response is produced by the NADPH oxidase RbohD, which is activated by the calcium sensitive CPK5 (L. Li et al. 2014) while the ROS influencing the calcium signal initiation might be already present and allowing cell expansion in the elongation zone. The *RbohD* knockout mutant could be used to selectively block the generation of ROS in response to flg22 but leave the baseline ROS concentrations unchanged.

### **3.6 ROS targets and restricts the biotic calcium signal to the elongation zone**

NADPH-oxidase-derived ROS can both promote and restrict cell wall extensibility (Schmidt et al. 2016). As the elongation zone is the region where the cell wall has to selectively expand, the concentration of ROS is tightly controlled there. ROS concentrations are different in the elongation zone compared to the meristematic zone and the root hair zone (Hernández-Barrera et al. 2015). The unique ROS homeostasis of the elongation zone might play a role in the elongation zone being more sensitive to biotic stresses and being the only region in the lower root responding with a calcium signature to these biotic stresses. Data in this work indicate that the inhibition of ROS results in the release of more calcium in response to C8 (Figure 19). It has been demonstrated that an increase in ROS leads to a dampened calcium release. Upon phosphate starvation the ROS concentration in the elongation zone in the root goes up, which lead to a dampened calcium response in the same area (Matthus et al. 2019).

ROS in the elongation zone might play a role in restricting the MAMP response to the elongation zone as the responses travels further and are initiated in other regions when the ROS is scavenged with Aa (Figure 18). This mechanism would use the baseline ROS distribution to define the responsive region, as we do not see generation of additional ROS in response to the applied biological stresses while the calcium wave seems to spread further over the root after ROS scavenging (Figure 18). This could be explained by the responsive region being expanded after the inhibiting ROS are scavenged. The importance of ROS and calcium in local responses to biotic stresses has been confirmed by an experiment that used nematodes as a biotic stress. In this experiment it was shown that in response to nematode attack cell communicate with their neighbors using a local change in ethylene production that was dependent on calcium channels and NADPH oxidases (Marhavy et al. 2019).

### **3.7 Combinations of stresses result in new calcium signatures and stress responses**

It has been reported that the calcium response to flg22 and NaCl use different calcium channels as the integral of the resulting calcium release is similar to the integral of the two separated responses added together (X.-Q. Cao et al. 2017). Interesting is that in their experiment there still is only one calcium release in response to the combined elicitors and that this calcium release is earlier than the normal calcium release in response to flg22, just like we see in the data presented in this work (Figure 15). While it takes two minutes before the first calcium response to flg22 is visible, the cell already has the information and manages to respond appropriately as soon as 30 seconds after application of a combined salt and flagellin stress. This indicates that there is a feedback between the signaling pathways of NaCl and flg22. To figure out to which stress the plant is responding to, a readout for downstream stress responses is required. Monitoring of gene expression changes in *Arabidopsis* leaves using a microarray after exposure to combinations of salt, heat and mannitol showed that the response to multiple stress conditions does not reflect a simple merge of the single stress response (Sewelam et al. 2014). The new unique calcium signature and stress response indicate that plants treat combinations of stresses as a new stress rather than a simple combination of the two stresses. As hazards to a plant usually consist of several simultaneous stresses, this helps them to mount adequate responses to different dangers. For example, insect herbivory would result in chitin stress among others, while mechanical damage would warrant a different defense response than a fungal infection, which includes chitin stress and cell wall degradation.

In 35% of the responses to combinations of biotic flg22 and abiotic salt stress a second calcium response identical in shape followed after about 50 seconds (Figure 15). This 50-second interval could be a second activation by the additional stress and the time in between waves could represent the refractory period of the involved channels. This refractory period is significantly longer than the refractory period of ion channels in animal neurons, which have a refractory period in the millisecond range before they can respond again (Yeomans 1979). However, ion

channels in plants need between several minutes up to hours before they can respond to the same stress again (Gong et al. 1998; Johnson et al. 2002).

### **3.8 Different branches of signaling pathways influence the calcium signature parameters**

That a single calcium signature parameter in response to two simultaneous stresses can switch between showing measures of both the single responses depending on ROS being present or not (Figure 15, Figure 22) points towards an intricate signaling network that has multiple branches that are intertwined with branches of other signaling networks. For instance, it is known that the salt and chitin stress responses both use the CERK1 receptor and the ANN1 ion channel. In addition, they induce an overlapping set of transcript changes (Espinoza et al. 2016). This could explain why the calcium signature in response to the combined stress displays features of a chitin calcium signature, as the branch of the signaling network that uses calcium results in these transcript changes used in both the chitin and salt response. Having signaling networks in place that share branches between different stresses is an efficient way to reduce the amount of signaling molecules and potential unwanted crosstalk. It has been shown that after forming a complex with LYK5, activated CERK1 starts three different signaling branches: (1) It associates with the calcium permeable channel ANN1 and triggers the calcium release. (2) It phosphorylates GEFs that in turn interact with GTPases and promotes GDP disassociation. Upon GTP binding the GTPase Rac1 interacts with RbohD, which produces ROS. (3) It phosphorylates BIK1 and its homolog PBL27. PBL27 interacts with MAPKKK5, which will start plant defense signaling that leads to chitin-induced immunity (Yuan et al. 2017). Calcium plays a role in only one of the three branches that are activated upon binding of chitin. It is likely that salt and chitin have this branch of their signaling network in common and each have other, non-overlapping branches, to start other more specific downstream responses. qRT-PCR data of salt responsive genes activated in the shoot in response to local NaCl treatment of the roots and after blockage of the calcium wave with lanthanum chloride showed that the increase in transcript abundance was suppressed in six out of nine tested genes (W.-G. Choi et al. 2014). That the other three genes still showed the regular salt responsive increase in transcript



level shows that you can block the signaling in one branch without affecting the effects of the other branches. It would be interesting to see whether the six genes that are affected are part of the subset that also respond to chitin stress, and whether you can block the up-regulation of these genes in response to chitin by preventing calcium releases in the same way. This would prove that the salt and chitin stress responses share a branch in their signaling network. This could, however, also be done in a more systematic way by using transcriptomics to analyze all genes simultaneously.

### **3.9 Is calcium just a chemical switch after all?**

The calcium signature theory is based on a single-file signaling view. This states that after binding an elicitor the receptor opens calcium channels starting a unique calcium transient. In turn, the kinetics of the calcium release are decoded by calcium dependent proteins that start the appropriate physiological response. Unique calcium signatures that appear upon stress application and correlate with an appropriate end response have been reported, but this does not prove that the calcium signature contains information yet. In guard cells, calcium oscillations occur as a response to factors that lead to the closing of stomata (McAinsh et al. 1995). The *deetiolated3* (*det3*) mutant has an abnormal calcium signature and fails to induce normal stomatal closure. However, stomatal closure could be restored by artificially inducing calcium oscillations that mimic the wildtype oscillations (Allen et al. 2000). This proved that the calcium signature itself encodes the information that induces stomatal closure. As of yet this is the only case in which the calcium signature theory has been proven correct in plants. In the case of the guard cells the oscillatory nature of the calcium signature seems to play a major role in the information encoding. However, in the majority of the cases the calcium response is only one burst or a transient increase of calcium. Calcium oscillations have only been reported in single cell systems like guard cells, root hairs, pollen tubes and synergids (Scrase-Field et al. 2003; Denninger et al. 2014). Therefore, it seems unlikely that the encoding and decoding mechanisms will be similar in other cell types.

There has been little success in confirming the calcium signature theory in other cell types in the last 25 years, and some researchers argue that other potential explanations have been ignored in favor of the calcium signature theory (Scrase-Field et al. 2003; Plieth 2016). They argue that outcomes of many experiments can also be explained by calcium acting just as a chemical switch to activate calcium sensitive proteins, and that calcium acts in combination with other signaling components to convey information. An argument for this is that calcium releases often seem to be accompanied by other signaling molecules. This has been shown for a decrease in pH (Behera et al. 2018), ROS (Mittler et al. 2011), ATP (Clark et al. 2018), membrane potential changes (Hedrich et al. 2016) and implicated for nitrogen oxide (NO) (Imran et al. 2018). If the calcium signature itself would contain enough information to start a specific response then it would not need other signaling molecules to be involved. Conversely, if there are other signaling molecules involved, the calcium signature does not have to be unique for every stress.

From the ROS scavenging data presented in this thesis (Figure 18 & 21) we can conclude that ROS plays a role in all the tested stress responses. This points towards calcium not being the only component involved in the response. To disprove the calcium signature hypothesis and to confirm the signaling network hypothesis we have to look at more signaling molecules simultaneously. Biosensors have been employed in plants for calcium (Keinath et al. 2015), pH (Gjetting et al. 2012), ROS (Ermakova et al. 2014), ATP (De Col et al. 2017) and membrane potential changes (Matzke et al. 2013). These sensors can be used in different combinations in multi-parameter imaging to better understand the subcellular location of the signaling responses and to elucidate the order in which they appear. To see whether the signals of the different signaling molecules overlap, the method of creating a kymograph and measuring the parameters can be employed as it works for any fluorescent sensor independent of the signaling molecule it is sensing. In addition to visualizing the signaling molecules, visualizing the downstream defense responses will tell us whether the signals contain information and whether this information is still decoded properly after chemically or genetically taking out parts of the pathway. For this, qRT-PCR (W.-G. Choi et al. 2014), mRNA profiling (Sato et al. 2010) or bio-reporters (Lim et al. 2018) can be used. Alternatively, a FRET-based map kinase activity sensor has recently been

used to show map kinase activation upon treatment with flg22, chitin and salt (Zaman et al. 2018). To figure out what the defense response to different stresses is, positive signaling components (CaMs, CBLs, CIPKs or CDPKs) can be over expressed or knocked out to easily identify downstream response.

## Material and Methods

### 4.1 Plant growth conditions

Seeds of *A. thaliana* plants expressing the R-GECO1 calcium sensor (Keinath et al. 2015; Waadt et al. 2017) were placed on 10  $\mu$ L pipette tips (cut to ca. 5 mm length) filled with  $\frac{1}{2}$  MS-Medium (MS-Salts from Serva, 0.1 % MES, pH 5.7 adjusted with KOH, 0.7% plant agar, Duchefa). The pipette tips were stuck in plates filled with sterile  $\frac{1}{2}$  MS-Medium and placed in a growth chamber (Convion) under long day conditions (16 h light / 8h dark, 70  $\mu$ mol/m<sup>2</sup>/s) at 21 °. After 5 days the tips containing seedlings whose roots had grown close to the end of the pipette tip were transferred to the RootChip16 by gently inserting them into the root inlets of the chip. The flow in the chip was started with liquid  $\frac{1}{2}$  MS-Medium. To prevent the seedlings from drying out the chip was surrounded with moist tissue paper and covered with a transparent plastic lid. After about 36 hours the roots had reached the imaging chambers and were ready for microscopy.

### 4.2 Microscopy

#### 4.2.1 RootChip experiments

The RootChip experiments were performed using the RootChip16 (Jones et al. 2014). Fluorescent imaging was done using a custom-built fluorescent microscope with a Nikon Ti-E stand, equipped with a 20x multi-immersion objective (N.A. 0.75, Nikon), motorized stage (Applied Scientific Instrumentation, USA), motorized filter wheel (Cairn Research, UK), laser launch (Omicron, Germany), two dichroic mirrors (Chroma triple band 440/514/561 and Chroma quad band 405/488/561/640) and an EMCCD camera (Photometrics, USA). Image acquisition was operated through Nikon NIS Elements software or Micro-Manager (Edelstein et al. 2014). For the imaging of the R-GECO1 calcium sensor a 630nm/92

longpass filter (Semrock) and a 561nm laser were used. During the time-lapse recordings a picture was taken every second.

Oxyburst Green coupled to BSA (dihydro-29,4,5,6,7,79-hexafluorofluorescein) (Thermo Fisher) was used in a concentration of 200  $\mu\text{g mL}^{-1}$ . As Oxyburst Green becomes irreversibly fluorescent upon the binding of ROS the flow in the root channel was stopped after medium exchange to allow the fluorescence to build up. Multichannel imaging was done using the 488nm laser and 525nm/45 bandpass filter (Semrock) for the Oxyburst Green-BSA ROS sensitive dye and the 561 nm laser and 630nm/92 longpass filter for R-GECO1 calcium sensor.

#### **4.2.2 Dual-flow-RootChip experiments**

Pressurizable vials with a septum in the lid were filled with  $\frac{1}{2}$  MS-medium or  $\frac{1}{2}$  MS-medium containing an elicitor. A luer-lock stopcock valve set in the “closed” configuration was connected to the end of the tubing coming from each vial. The vials were pressurized using clean, dry air and the tubing was filled with medium by opening each of the stopcocks until the tubing was filled with medium. Once the tubing was filled completely the stopcock was closed again. The vial with  $\frac{1}{2}$  MS-medium was connected to one of the medium inlets of the dual-flow-RootChip and the stopcock was opened. This resulted in a symmetric perfusion of the whole root. To treat the root asymmetrically the vial containing the treatment was connected to the other medium inlet and the stopcock was opened, resulting in an asymmetrical treatment of the root (Stanley et al. 2018).

#### **4.2.3 BalanceSir experiments on meshes**

*A. thaliana* plants expressing the R-GECO1 calcium sensor (Keinath et al. 2015; Waadt et al. 2017) were grown on a 1,5 x 5 centimeter nylon mesh with a pore-width of 100  $\mu\text{m}$  placed on plates containing sterile  $\frac{1}{2}$  MS medium. 1-well on coverglass slides (Sarstedt) were plasma treated in the HAR-040 Diener/Femto Plasma Cleaner. This would create a hydrophilic surface that ensures an equal distribution of the medium during incubation. A mesh with 10-day old plants was placed in the well and 1 mL of  $\frac{1}{2}$  strength MS was added. The slide was placed in

an airtight humidified container for 1 hour to recover. The well containing the seedlings on the mesh was placed on a tilting platform (Figure 25) (Lampou 2015) that enabled trouble free exchange of the medium. Imaging was started, and after 5 minutes of baseline recording the medium was exchanged with medium containing an elicitor. In the case of treatment with ascorbic acid the medium was replaced with medium containing 100  $\mu\text{M}$  ascorbic acid prior to imaging and the medium with the elicitor also contained 100  $\mu\text{M}$  ascorbic acid.

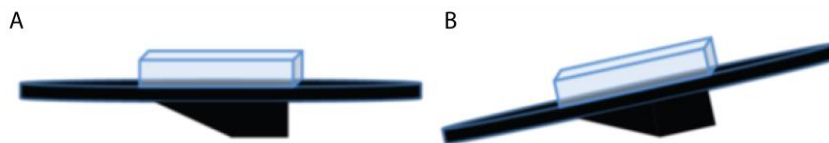


**Figure 25: The tilting platform (BalanceSir) used for treating meshes with 30-40 seedlings simultaneously.** (A) The platform in upright position used for incubation with medium and imaging. (B) The platform in the tilted position which collects all the medium on one side to facilitate medium exchange using a pipette. Image modified from (Lampou 2015).

Imaging was done using a Nikon SMZ18 Stereo Microscope equipped with a SHR Plan Apo 2x (N.A. 0.3) objective (Nikon), 545/25x excitation, 605/70m emission filter (Nikon) and an Orca Flash 4.0 sCMOS camera (Hamamatsu, Japan). Exposure time was 800 milliseconds and images were captured once every second for twenty minutes in total.

### 4.3 Image and data analysis

Image processing, analysis and measurements was done using FIJI (ImageJ) (Schindelin et al. 2012).

#### 4.3.1. Kymograph generation

A line was drawn along the midline of the root. A kymograph was created along this line with a line width of 3 pixels. The kymograph was normalized using

Crestline normalization. A custom lookup table called `wave_tracking` was used to display the kymograph. The LUT `wave_tracking` is a linear interpolation of the following colours: #352A86, #0362E0, #1483D4, #05A5C7, #33B8A0, #8CBE74, #D2BA58, #FDCA30, #F8FA0D.

## 4.4 Data analysis

### 4.4.1 General Data analysis

All data analysis was performed in Microsoft Excel, if not mentioned otherwise. Principal component analysis were performed and plotted in R (Team 2018). Box plots were created using the web-tool BoxPlotR (<http://shiny.chemgrid.org/boxplotr/>) provided by the Tyers and Rappsilber labs.

### 4.4.2 Macros for Image J

To aid in image analysis some macros were created in Image J.

#### 4.4.2.2 Normalize to baseline

```
1 orgID = getImageID();
2 img_title = getTitle();
3 run("Duplicate...", "title=1st duplicate range=1-25"); Set the range of the
baseline here
4 run("Grouped Z Project...", "projection=[Average Intensity] group=25"); This
should match the amount of frames in the baseline
5 imageCalculator("Subtract create 32-bit stack", img_title, "AVG_1st");
6 imageCalculator("Divide create 32-bit stack", "Result of "+img_title, "AVG_1st");
7 selectWindow("Result of Result of "+img_title);
8 run("16_colors");
9 selectWindow("1st");
10 close();
11 selectWindow("AVG_1st");
12 close();
13 selectWindow("Result of "+img_title);
14 close();
```

#### 4.4.2.2 Kymograph creation

This macro expects you to have manually drawn lines through the midlines of all the roots in the time-lapse image and have them added to the ROI manager.

```
1 setBatchMode(true)
2 G_Ddir = getDirectory("Choose Destination Directory");
3 Image = getImageID();
4 for (i=0 ; i<roiManager("count"); i++) {
5 selectImage(Image);
6 roiManager("select", i);
7 run("Multi Kymograph", "linewidth=3");
8 setMinAndMax(-0.15, 0.15);
9 run("greys");
10 img_title = getTitle();
11 dest_filename = img_title+"_kymo_"+i;
12 fullpath = G_Ddir + dest_filename;
13 saveAs("tiff", fullpath);
14 close();
15 }
```

#### 4.4.2.3 Crestline normalization

Created with help from Martin Zauser

```
1 print("Scaling image ...");
2 id = getImageID();
3 getDimensions(width, height, channels, slices, frames);
4 newImage("crestline", "16-bit", width, height, 1)
5 idnew = getImageID();
6 for(col = 0; col < width; ++col) {
7     print("column ", col);
8     selectImage(id);
9     val = getPixel(col, 0); first value = first minimum = first maximum
10    min = val;
11    max = val;
12    data = newArray(height);
13    data[0] = val;
14    for(row = 1; row < height; ++row) {
15        val = getPixel(col, row);
16        min = minOf(min, val);
17        max = maxOf(max, val);
18        data[row] = val; // store values of the row
19    }
20    selectImage(idnew);
21    for(row = 0; row < height; ++row) {
22        setPixel(col, row, (data[row] - min) / (max - min) * 65535); // scale 16-bit =>
min = 0, max = 65535
23    }
24 }
```

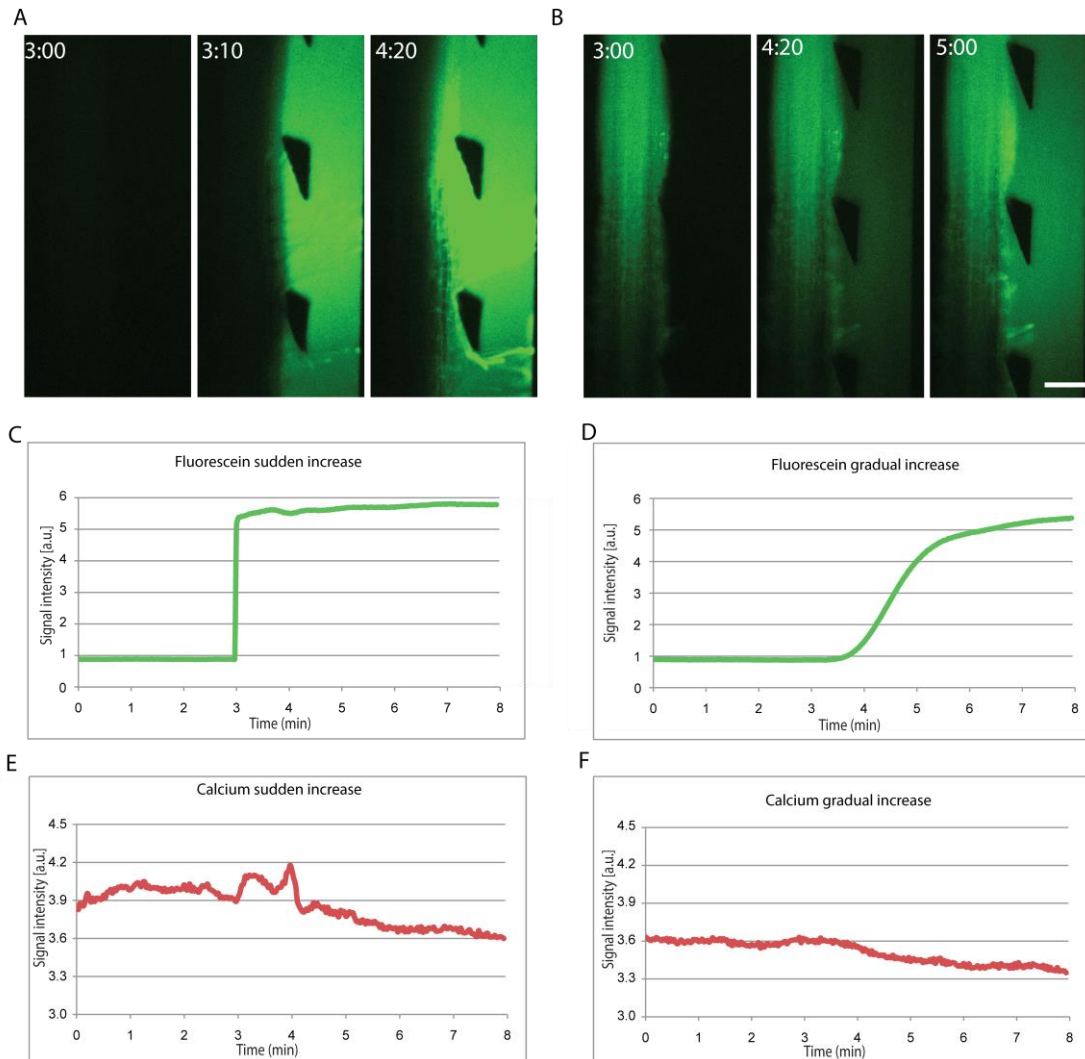


```
25 print("ready.");
```

#### **4.4.2.4 Maxium intensity analysis**

```
1 setBatchMode(true)
2 G_Sdir = getDirectory("Choose the Directory where the file is");
3 list = getFileList(G_Sdir);
4 for(i = 0; i<list.length; i++) {
5   Prop(list[i]);
6 }
7 function Prop(img_filename) {
8   fullpath_image = G_Sdir + img_filename;
9   run("Bio-Formats Importer", " open=["+fullpath_image+"] autoscale
color_mode=Default view=Hyperstack stack_order=XYCZT");
10  run("Gaussian Blur...", "sigma=2");
11  run("Set Measurements...", "mean min redirect=None decimal=3");
12  run("Measure");
13  close();
14 }
```

## Supplemental information



**Supplemental figure 1: Calcium response to a sudden increase or a gradual increase of elicitor.** *Arabidopsis* roots in the Dual-flow-RootChip were treated on one side with an instantaneous burst of a mix of 100 mM NaCl and fluorescein (**A, C, E**) or a slow increase in concentration to 100 mM NaCl and fluorescein (**B, D, F**). Time series of roots showing the concentration of fluorescein in the channel increasing instantaneous (**A**) or gradually (**B**). Scale bar depicts 100  $\mu\text{m}$ . Root in **B** has been treated with fluorescein prior to the experiment. Time format, mm:ss. (**C, D**) Time dependent fluorescent intensities of fluorescein measured in the channel during a sudden (**C**) or gradual (**D**) increase of the concentration. (**E, F**) Time dependent fluorescent intensities of R-GECO1 measured in the epidermis of the treated side of the root during a sudden (**E**) or a gradual (**F**) increase of the concentration.

**Supplemental table 1: First 6 principle components with their eigenvalues, variance percentage and cumulative variance percentage for the dataset containing flg22, C8 and NaCl**

<i>Principle component</i>	<i>Eigenvalue</i>	<i>Variance percentage</i>	<i>Cumulative variance percentage</i>
Dim.1	4.24463313	71.283915	71.28392
Dim.2	0.77346833	12.989544	84.27346
Dim.3	0.43762743	7.349468	91.62293
Dim.4	0.25250975	4.240622	95.86355
Dim.5	0.16101473	2.704064	98.56761
Dim.6	0.08529209	1.432386	100

**Supplemental table 2: p-values of paired Student's t-test of the delay parameter**

<i>Delay</i>	nlp20	C8	flg22	PG3	Cellobiose	ATP	Glutamate	NaCl
nlp20	1							
C8	0.0430191	1						
flg22	5.732E-05	0.147101	1					
PG3	6.237E-48	5.065E-13	5.201E-11	1				
Cellobiose	1.072E-38	7.882E-09	6.557E-08	4.579E-04	1			
ATP	5.704E-65	5.393E-20	6.249E-21	3.043E-25	1.671E-21	1		
Glutamate	5.209E-64	1.280E-19	1.481E-20	6.038E-25	2.751E-21	0.0089811	1	
NaCl	1.940E-43	1.771E-20	6.743E-22	5.040E-04	0.6178939	6.358E-05	6.203E-05	1
cold	1.169E-69	5.023E-22	3.678E-23	7.444E-28	4.191E-24	0.0100820	0.8732051	1.514E-05

**Supplemental table 3: p-values of paired Student's t-test of the location parameter**

<i>Location</i>	nlp20	C8	flg22	PG3	Cellobiose	ATP	Glutamate	NaCl
nlp20	1							
C8	9.480E-04	1						
flg22	4.366E-17	0.0711133	1					
PG3	5.718E-41	0.5634832	0.0018822	1				
Cellobiose	7.609E-28	8.861E-12	4.598E-36	4.428E-18	1			
ATP	1.831E-04	0.0617309	3.091E-05	8.703E-14	9.626E-14	1		
Glutamate	4.238E-13	0.0083686	2.905E-12	8.992E-06	3.615E-06	3.101E-06	1	
NaCl	6.293E-17	4.959E-06	4.974E-18	2.145E-08	1.132E-06	2.911E-08	0.2248854	1
cold	4.014E-22	1.418E-05	1.240E-23	1.311E-11	1.511E-05	8.161E-11	0.1567941	0.814403

**Supplemental table 4: p-values of paired Student's t-test of the duration parameter**

<i>Duration</i>	nlp20	C8	flg22	PG3	Cellobiose	ATP	Glutamate	NaCl
nlp20	1							
C8	0.0801083	1						
flg22	0.7064146	0.0211529	1					
PG3	2.647E-04	4.660E-05	3.234E-04	1				
Cellobiose	4.010E-05	2.101E-04	3.104E-05	0.006045	1			
ATP	5.260E-07	3.996E-06	3.127E-07	0.001905	8.189E-01	1		
Glutamate	2.197E-16	1.687E-11	3.761E-18	7.858E-17	9.594E-11	3.371E-12	1	
NaCl	2.538E-29	6.572E-22	4.985E-32	1.642E-26	5.527E-12	6.089E-15	6.185E-07	1
cold	5.238E-18	9.968E-13	6.321E-20	2.476E-18	1.074E-11	3.727E-13	0.397902	3.470E-06

**Supplemental table 5: p-values of paired Student's t-test of the distance traveled parameter**

<i>Distance traveled</i>	nlp20	C8	flg22	PG3	Cellobiose	ATP	Glutamate	NaCl
nlp20	1							
C8	1.561E-09	1						
flg22	0.040185	5.539E-10	1					
PG3	1.553E-19	3.400E-04	3.801E-22	1				
Cellobiose	2.174E-33	2.394E-08	1.550E-37	0.0051614	1			
ATP	3.932E-27	0.124689	3.523E-16	4.434E-06	3.932E-13	1		
Glutamate	6.844E-14	0.013178	1.428E-15	0.6212202	0.0065637	4.169E-04	1	
NaCl	2.075E-28	2.880E-07	2.398E-32	0.3853633	0.0068767	1.871E-09	0.1926674	1
cold	5.339E-31	1.097E-12	2.474E-36	7.131E-06	2.275E-01	3.268E-13	5.123E-05	1.220E-06

**Supplemental table 6: p-values of paired Student's t-test of the velocity tipwards parameter**

<i>Vtip</i>	nlp20	C8	flg22	PG3	Cellobiose	ATP	Glutamate	NaCl
nlp20	1							
C8	0.009877	1						
flg22	0.056023	0.012666	1					
PG3	7.949E-04	0.276564	0.031166	1				
Cellobiose	3.595E-05	1.097E-04	3.898E-18	2.396E-10	1			
ATP	1.730E-05	1.179E-05	1.677E-20	6.769E-12	0.014075	1		
Glutamate	1.102E-05	2.932E-06	5.384E-22	6.093E-13	6.375E-05	1.326E-04	1	
NaCl	9.696E-04	3.907E-04	7.447E-14	2.608E-08	0.001617	6.145E-04	0.185445	1
cold	6.080E-09	5.136E-10	9.285E-34	2.962E-20	7.344E-09	1.318E-10	6.423E-04	0.194011

**Supplemental table 7: p-values of paired Student's t-test of the velocity shootwards parameter**

<i>Vshoot</i>	nlp20	C8	flg22	PG3	Cellobiose	ATP	Glutamate	NaCl
nlp20	1							
C8	0.016074	1						
flg22	2.347E-12	2.754E-04	1					
PG3	7.650E-27	1.000E-12	2.455E-08	1				
Cellobiose	2.968E-21	2.417E-14	1.331E-19	3.081E-09	1			
ATP	3.868E-21	2.040E-15	4.875E-23	2.806E-12	0.012142	1		
Glutamate	1.408E-18	6.756E-14	6.206E-22	1.106E-12	4.227E-05	1.397E-05	1	
NaCl	1.729E-17	3.148E-13	1.284E-20	3.325E-12	4.009E-05	3.173E-06	0.120401	1
cold	4.884E-24	3.688E-18	1.018E-28	4.706E-17	1.539E-07	9.272E-10	0.00121	0.047562

**Supplemental table 8: First 6 principle components with their eigenvalues, variance percentage and cumulative variance percentage for the dataset containing nlp20, C8, flg22, PG3, Cellobiose, ATP, Glutamate, NaCl and Cold stress**

<i>Principle component</i>	<i>Eigenvalue</i>	<i>Variance percentage</i>	<i>Cumulative variance percentage</i>
Dim.1	3.97613697	66.475395	66.47539
Dim.2	0.96791385	16.182153	82.65755
Dim.3	0.43814506	7.325167	89.98271
Dim.4	0.30570536	5.110962	95.09368
Dim.5	0.195114	3.262031	98.35571
Dim.6	0.09835122	1.644294	100

**Supplemental table 9: p-values of paired Student's t-test of the delay parameter for combinations of elicitors and ROS scavenging**

<i>Delay</i>	flg22	flg22+Aa	C8	C8+Aa	NaCl	NaCl+Aa	flg22+C8	flg22+C8 +Aa	NaCl +flg22	NaCl+ flg22+Aa	NaCl+C8
flg22	1										
flg22+Aa	2.921E-04	1									
C8	0.1471012	5.360E-06	1								
C8+Aa	4.830E-04	0.245437	4.763E-06	1							
NaCl	6.743E-22	1.272E-07	1.771E-20	2.336E-11	1						
NaCl+Aa	1.348E-36	1.757E-42	3.707E-35	4.892E-44	2.421E-07	1					
flg22+C8	2.468E-04	0.133588	9.730E-06	0.018382	1.555E-04	1.326E-40	1				
flg22+C8 +Aa	0.0060858	0.860621	4.598E-04	0.261398	7.818E-05	6.282E-43	0.112472	1			
NaCl+flg2 2	1.653E-05	0.036683	1.087E-06	0.00322	0.0030319	4.708E-22	0.328584	0.093085	1		
NaCl+flg2 2 +Aa	1.476E-11	5.527E-04	2.961E-11	6.800E-06	0.419852	7.751E-07	0.018663	0.010669	0.0894285	1	
NaCl+C8	0.9050233	0.0060860	0.262144	0.009665	4.725E-12	3.270E-23	0.004956	0.035703	0.0012352	1.735E-06	1
NaCl+C8 +Aa	4.741E-10	3.025E-11	4.084E-10	1.923E-12	0.0584571	0.207267	1.551E-09	1.287E-09	3.046E-05	0.059276	2.86E-06

**Supplemental table 10: p-values of paired Student's t-test of the location parameter for combinations of elicitors and ROS scavenging**

<i>Location</i>	flg22	flg22+Aa	C8	C8+Aa	NaCl	NaCl+Aa	flg22+C8	flg22+C8+Aa	NaCl+flg22	NaCl+flg22+Aa	NaCl+C8
flg22	1										
flg22+Aa	4.645E-06	1									
C8	0.0063199	6.895E-05	1								
C8+Aa	4.723E-08	0.9515299	2.205E-06	1							
NaCl	4.974E-18	3.630E-05	1.045E-10	1.190E-06	1						
NaCl+Aa	8.166E-08	0.5395963	1.360E-06	0.4989354	5.160E-08	1					
flg22+C8	0.1569207	0.0283983	0.0310164	0.0081067	9.067E-05	0.0341144	1				
flg22+C8+Aa	1.463E-03	0.5650388	0.0044614	0.4607347	0.001458	0.3664346	0.034224	1			
NaCl+flg22	1.744E-49	1.966E-17	2.793E-24	8.459E-23	2.939E-04	8.666E-25	8.041E-15	6.056E-12	1		
NaCl+flg22+Aa	5.150E-13	0.0028341	5.180E-08	4.383E-04	0.0479830	4.801E-04	0.0013130	0.0152181	2.275E-08	1	
NaCl+C8	3.644E-37	1.362E-12	1.251E-19	1.951E-16	4.712E-04	8.492E-20	1.753E-10	2.641E-08	0.6029727	3.538E-07	1
NaCl+C8+Aa	8.740E-12	0.0109620	4.192E-06	0.002901	0.0517702	0.0820484	1.165E-05	0.0036551	2.533E-08	0.3578829	1.480E-05

**Supplemental table 11: p-values of paired Student's t-test of the duration parameter for combinations of elicitors and ROS scavenging**

<i>Duration</i>	flg22	flg22+Aa	C8	C8+Aa	NaCl	NaCl+Aa	flg22+C8	flg22+C8+Aa	NaCl+flg22	NaCl+flg22+Aa	NaCl+C8
flg22	1										
flg22+Aa	0.031657	1									
C8	0.0211529	0.003603	1								
C8+Aa	0.6940265	0.0979290	0.0469108	1							
NaCl	4.985E-32	7.091E-31	6.572E-22	8.981E-26	1						
NaCl+Aa	1.413E-14	5.725E-06	1.179E-11	2.467E-09	0.0014116	1					
flg22+C8	0.0020515	0.0372421	1.500E-03	0.0073662	5.735E-29	0.0075429	1				
flg22+C8+Aa	6.215E-05	1.951E-04	3.431E-04	3.684E-04	5.596E-15	0.2890315	0.0019468	1			
NaCl+flg22	5.076E-04	0.0426866	5.257E-04	0.003876	2.032E-14	0.0221795	0.6555124	0.2194686	1		
NaCl+flg22+Aa	5.787E-10	2.833E-06	3.892E-08	1.424E-07	2.005E-11	0.2628028	0.004277	0.6424623	0.0609856	1	
NaCl+C8	0.0259235	0.8865413	3.034E-03	0.1077534	1.570E-18	3.787E-05	0.2319443	0.0192535	0.1498217	3.883E-04	1
NaCl+C8+Aa	5.486E-06	3.548E-06	1.511E-04	4.761E-05	1.069E-05	0.9270352	2.279E-06	0.0256369	0.0220965	0.2135288	0.002410



**Supplemental table 12: p-values of paired Student's t-test of the distance traveled parameter for combinations of elicitors and ROS scavenging**

<i>Distance traveled</i>	flg22	flg22+Aa	C8	C8+Aa	NaCl	NaCl+Aa	flg22+C8	flg22+C8+Aa	NaCl+flg22	NaCl+flg22+Aa	NaCl+C8
flg22	1										
flg22+Aa	1.527E-13	1									
C8	9.287E-09	0.9901292	1								
C8+Aa	7.032E-26	2.894E-05	1.003E-04	1							
NaCl	2.398E-32	2.127E-10	3.177E-12	1.050E-06	1						
NaCl+Aa	1.627E-31	2.154E-07	1.901E-07	0.1715997	1.742E-06	1					
flg22+C8	1.050E-26	1.524E-09	6.536E-11	4.108E-08	0.0114299	6.260E-09	1				
flg22+C8+Aa	3.903E-24	2.564E-08	3.350E-09	1.893E-06	0.1148575	1.158E-06	0.6153496	1			
NaCl+flg22	1.022E-24	1.494E-08	9.394E-10	9.676E-07	0.0937445	4.015E-07	0.535032	0.9507086	1		
NaCl+flg22+Aa	8.012E-18	3.649E-05	6.701E-06	0.0090427	0.1623860	0.0255923	0.0064433	0.0474190	0.0325650	1	
NaCl+C8	4.604E-25	5.827E-08	6.718E-09	6.715E-05	0.7935326	1.773E-04	0.0300864	0.1505279	0.1337689	0.3727888	1
NaCl+C8+Aa	3.215E-19	1.927E-06	4.199E-07	8.645E-05	0.3074059	8.158E-05	0.4909057	0.8148766	0.8403566	0.1389657	0.3335963

**Supplemental table 13: p-values of paired Student's t-test of the velocity tipwards parameter for combinations of elicitors and ROS scavenging**

<i>Vtip</i>	flg22	flg22+Aa	C8	C8+Aa	NaCl	NaCl+Aa	flg22+C8	flg22+C8+Aa	NaCl+flg22	NaCl+flg22+Aa	NaCl+C8
flg22	1										
flg22+Aa	0.2106663	1									
C8	0.012666	0.2456232	1								
C8+Aa	4.377E-08	0.0024951	0.2086009	1							
NaCl	7.447E-14	4.409E-06	3.907E-04	7.903E-08	1						
NaCl+Aa	1.183E-09	2.661E-04	0.0057405	3.085E-05	0.001653	1					
flg22+C8	0.8340483	0.2504003	0.056243	4.033E-04	1.059E-04	0.0019993	1				
flg22+C8+Aa	0.0390869	0.3917110	0.8151469	0.1263568	5.538E-04	0.006974	0.0947459	1			
NaCl+flg22	7.083E-09	5.891E-04	0.0096529	8.827E-05	0.0069415	0.7943808	0.0036345	0.0114584	1		
NaCl+flg22+Aa	3.658E-04	0.0367886	0.1199231	0.0181601	0.0012950	0.5820908	0.0774977	0.1284128	0.7870720	1	
NaCl+C8	1.303E-07	0.0020472	0.0258207	0.0014144	1.455E-05	0.0122590	0.0074011	0.0275542	0.0318269	0.2163370	1
NaCl+C8+Aa	5.046E-08	0.0013293	0.015645	1.828E-04	0.1303132	0.5050690	0.0071772	0.0185630	0.4462055	0.3894828	0.0137091

**Supplemental table 14: p-values of paired Student's t-test of the velocity shootwards parameter for combinations of elicitors and ROS scavenging**

<i>Vshoot</i>	flg22	flg22+Aa	C8	C8+Aa	NaCl	NaCl+Aa	flg22+C8	flg22+C8+Aa	NaCl+flg22	NaCl+flg22+Aa	NaCl+C8
flg22	1										
flg22+Aa	0.0306190	1									
C8	2.754E-04	1.689E-04	1								
C8+Aa	0.0164242	0.5444452	2.414E-08	1							
NaCl	1.284E-20	1.367E-08	3.148E-13	3.160E-12	1						
NaCl+Aa	2.180E-20	2.591E-08	2.350E-13	6.438E-12	3.136E-06	1					
flg22+C8	4.917E-09	0.009888	3.806E-09	3.172E-05	3.652E-06	1.333E-05	1				
flg22+C8+Aa	7.606E-13	0.0007071	1.980E-12	2.829E-08	2.215E-05	8.215E-05	0.5442784	1			
NaCl+flg22	2.162E-08	0.0012935	1.677E-05	5.221E-05	0.0386780	0.3019059	0.0118270	0.0229257	1		
NaCl+flg22+Aa	1.336E-08	0.0010349	1.059E-05	3.868E-05	0.0015047	0.660613	0.0110467	0.0220867	0.658919	1	
NaCl+C8	8.778E-08	0.0037081	1.141E-05	1.817E-04	1.402E-07	6.220E-05	0.0743697	0.1394373	0.0092844	0.0120298	1
NaCl+C8+Aa	4.364E-17	1.105E-06	8.990E-11	9.771E-10	0.0371855	0.5218756	1.281E-04	5.074E-04	0.7934728	0.9060088	6.117E-04

## Bibliography

- Albert, I. et al. 2015. An RLP23–SOBIR1–BAK1 complex mediates NLP-triggered immunity. : 1–9.
- Allen, G.J. et al. 2000. Alteration of stimulus-specific guard cell calcium oscillations and stomatal closing in *Arabidopsis det3* mutant. *Science* 289(5488): 2338–2342.
- Azevedo Souza, C. de et al. 2017. Cellulose-Derived Oligomers Act as Damage-Associated Molecular Patterns and Trigger Defense-Like Responses. *Plant Physiology* 173(4): 2383–2398.
- Behera, S. et al. 2016. Two spatially and temporally distinct Ca<sup>2+</sup> signals convey *Arabidopsis thaliana* responses to K<sup>+</sup> deficiency. *New Phytologist* 213(2): 739–750.
- Behera, S. et al. 2018. Cellular Ca<sup>2+</sup> signals generate defined pH signatures in plants. *The Plant Cell*.
- Böhm, H. et al. 2014. A Conserved Peptide Pattern from a Widespread Microbial Virulence Factor Triggers Pattern-Induced Immunity in *Arabidopsis* P. Birch (ed). *PLoS Pathogens* 10(11): e1004491.
- Bush, D. 1995. Calcium regulation in plant cells and its role in signaling. *Annu. R. Plant Physiol. Plant Mol. Biol.*: 1–28.
- Cao, X.-Q. et al. 2017. Biotic and Abiotic Stresses Activate Different Ca<sup>2+</sup> Permeable Channels in *Arabidopsis*. *Frontiers in Plant Science* 8: 83.
- Cao, Y. et al. 2014. The kinase LYK5 is a major chitin receptor in *Arabidopsis* and forms a chitin-induced complex with related kinase CERK1. *eLife* 3.
- Chinchilla, D. 2006. The *Arabidopsis* Receptor Kinase FLS2 Binds flg22 and Determines the Specificity of Flagellin Perception. *The Plant Cell* 18(2): 465–476.
- Chinchilla, D. et al. 2007. A flagellin-induced complex of the receptor FLS2 and BAK1 initiates plant defence. *Nature* 448(7152): 497–500.
- Choi, J., Tanaka, K., Cao, Y., et al. 2014. Identification of a plant receptor for extracellular ATP. *Science* 343(6168): 290–294.
- Choi, J., Tanaka, K., Liang, Y., et al. 2014. Extracellular ATP, a danger signal, is recognized by DORN1 in *Arabidopsis*. *Biochemical Journal* 463(3): 429–437.
- Choi, W.-G., Toyota, M., Kim, S.-H., Hilleary, R., & Gilroy, S. 2014. Salt stress-induced Ca<sup>2+</sup> waves are associated with rapid, long-distance root-to-shoot signaling in plants. *Proceedings of the National Academy of Sciences* 111(17):

6497–6502.

- Clark, G. et al. 2011. Extracellular Nucleotides and Apyrases Regulate Stomatal Aperture in Arabidopsis. *Plant Physiology* 156(4): 1740–1753.
- Clark, G., & Roux, S. 2018. Role of Ca<sup>2+</sup> in Mediating Plant Responses to Extracellular ATP and ADP. *International Journal of Molecular Sciences* 19(11): 3590.
- Couto, D., & Zipfel, C. 2016. Regulation of pattern recognition receptor signalling in plants. *Nature reviews. Immunology* 16(9): 537–552.
- Day, I.S., Reddy, V.S., Shad Ali, G., & Reddy, A.S.N. 2002. Analysis of EF-hand-containing proteins in Arabidopsis. *Genome Biology* 3(10): RESEARCH0056.
- De Col, V. et al. 2017. ATP sensing in living plant cells reveals tissue gradients and stress dynamics of energy physiology. *eLife* 6.
- Demidchik, V., Shabala, S., Isayenkov, S., Cuin, T.A., & Pottosin, I. 2018. Calcium transport across plant membranes: mechanisms and functions. *New Phytologist* 220(1): 49–69.
- Denancé, N. 2013. Disease resistance or growth: the role of plant hormones in balancing immune responses and fitness costs. : 1–12.
- Denninger, P. et al. 2014. Male–female communication triggers calcium signatures during fertilization in Arabidopsis. *Nature Communications* 5: 1–12.
- Dodd, A.N., Kudla, J., & Sanders, D. 2010. The Language of Calcium Signaling. *Annual Review of Plant Biology* 61(1): 593–620.
- Eckardt, N.A. 2008. Chitin Signaling in Plants: Insights into the Perception of Fungal Pathogens and Rhizobacterial Symbionts. *The Plant Cell* 20(2): 241–243. Available at: <http://www.plantcell.org/lookup/doi/10.1105/tpc.108.058784>.
- Edel, K.H., & Kudla, J. 2015. Cell Calcium. *Cell Calcium* 57(3): 231–246.
- Edel, K.H., Marchadier, E., Brownlee, C., Kudla, J., & Hetherington, A.M. 2017. The Evolution of Calcium-Based Signalling in Plants. *Current Biology* 27(13): R667–R679.
- Edelstein, A.D. et al. 2014. Advanced methods of microscope control using µManager software. *Journal of Biological Methods* 1(2): 10.
- Epstein, E. 1973. Mechanisms of Ion Transport through Plant Cell Membranes. In *International Review of Cytology*. International Review of Cytology, 123–168. Elsevier
- Ermakova, Y.G. et al. 2014. Red fluorescent genetically encoded indicator for intracellular hydrogen peroxide. *Nature Communications* 5: 5222.
- Espinoza, C., Liang, Y., & Stacey, G. 2016. Chitin receptor CERK1 links salt stress

- and chitin-triggered innate immunity in Arabidopsis. *The Plant Journal* 89(5): 984–995.
- Evans, M.J., Choi, W.-G., Gilroy, S., & Morris, R.J. 2016. A ROS-Assisted Calcium Wave Dependent on the AtRBOHD NADPH Oxidase and TPC1 Cation Channel Propagates the Systemic Response to Salt Stress. *Plant Physiology* 171(3): 1771–1784.
- Felix, G., Duran, J.D., Volko, S., & Boller, T. 1999. Plants have a sensitive perception system for the most conserved domain of bacterial flagellin. *The Plant Journal* 18(3): 265–276.
- Feng, W. et al. 2018. The FERONIA Receptor Kinase Maintains Cell-Wall Integrity during Salt Stress through Ca. *Current Biology* 28(5): 666–675.e5. Available at: <https://linkinghub.elsevier.com/retrieve/pii/S0960982218300253>.
- Gilroy, S. et al. 2014. A tidal wave of signals: calcium and ROS at the forefront of rapid systemic signaling. *Trends in Plant Science*: 1–8.
- Gilroy, S. et al. 2016. ROS, Calcium, and Electric Signals: Key Mediators of Rapid Systemic Signaling in Plants. *Plant Physiology* 171(3): 1606–1615.
- Gjetting, S.K., Ytting, C.K., Schulz, A., & Fuglsang, A.T. 2012. Live imaging of intra- and extracellular pH in plants using pHusion, a novel genetically encoded biosensor. *Journal of Experimental Botany* 63(8): 3207–3218.
- Gong, M., van der Luit, A., Knight, M.R., & Trewavas, A.J. 1998. Heat-Shock-Induced Changes in Intracellular Ca<sup>2+</sup> Level in Tobacco Seedlings in Relation to Thermotolerance". *Plant Physiology*: 1–9.
- Gómez-Gómez, L., & Boller, T. 2000. FLS2: an LRR receptor-like kinase involved in the perception of the bacterial elicitor flagellin in Arabidopsis. *Molecular Cell* 5(6): 1003–1011.
- Guo, X., Liu, D., & Chong, K. 2018. Cold signaling in plants: Insights into mechanisms and regulation. *Journal of Integrative Plant Biology* 60(9): 745–756.
- Halfter, U., Ishitani, M., & Zhu, J.K. 2000. The Arabidopsis SOS2 protein kinase physically interacts with and is activated by the calcium-binding protein SOS3. *Proceedings of the National Academy of Sciences of the United States of America* 97(7): 3735–3740.
- Hasegawa, P.M., Bressan, R.A., Zhu, J.-K., & Bohnert, H.J. 2000. Plant cellular and molecular responses to high salinity. *Annual review of plant physiology and plant molecular biology* 51: 463–499.
- Hashimoto, K., & Kudla, J. 2011. Calcium decoding mechanisms in plants. *Biochimie* 93(12): 2054–2059.
- Hayashi, T. 1954. Effects of sodium glutamate on the nervous system. *Keio Journal of medicine* 03: 183–192.

- Hedrich, R., Salvador-Recatalà, V., & Dreyer, I. 2016. Electrical Wiring and Long-Distance Plant Communication. *Trends in Plant Science*: 1–12.
- Hernández-Barrera, A. et al. 2015. Hyper, a hydrogen peroxide sensor, indicates the sensitivity of the Arabidopsis root elongation zone to aluminum treatment. *Sensors* 15(1): 855–867.
- Hetherington, A.M., & Woodward, F.I. 2003. The role of stomata in sensing and driving environmental change. *Nature Publishing Group* 424(6951): 901–908.
- Hirschi, K.D. 1999. Expression of Arabidopsis CAX1 in tobacco: altered calcium homeostasis and increased stress sensitivity. *The Plant Cell* 11(11): 2113–2122.
- Howard, R.J. 1997. Breaching the Outer Barriers — Cuticle and Cell Wall Penetration. In G. C. Carroll & P. Tudzynski (eds) *Plant Relationships: Part A*. Plant Relationships: Part A, 43–60. Berlin, Heidelberg: Springer Berlin Heidelberg
- Imran, Q.M. et al. 2018. Transcriptome profile of NO-induced Arabidopsis transcription factor genes suggests their putative regulatory role in multiple biological processes. *Scientific Reports* 8(1): 771.
- Ismail, A., Takeda, S., & Nick, P. 2014. Life and death under salt stress: same players, different timing? *Journal of Experimental Botany* 65(12): 2963–2979.
- Jaffe, L.F. 2010. Fast calcium waves. *Cell Calcium* 48(2-3): 102–113.
- Jammes, F., Hu, H.-C., Villiers, F., Bouten, R., & Kwak, J.M. 2011. Calcium-permeable channels in plant cells. *FEBS Journal* 278(22): 4262–4276.
- Jeworutzki, E. et al. 2010. Early signaling through the Arabidopsis pattern recognition receptors FLS2 and EFR involves Ca<sup>2+</sup>-associated opening of plasma membrane anion channels. *The Plant Journal* 62(3): 367–378.
- Jiang, Z. et al. 2013. Relationship between NaCl- and H<sub>2</sub>O<sub>2</sub>-Induced Cytosolic Ca<sup>2+</sup> Increases in Response to Stress in Arabidopsis G. Muday (ed). *PLOS ONE* 8(10): e76130.
- Johnson, B.R., Wyttenbach, R.A., Wayne, R., & Hoy, R.R. 2002. Action potentials in a giant algal cell: a comparative approach to mechanisms and evolution of excitability. *Journal of undergraduate neuroscience education : JUNE : a publication of FUN, Faculty for Undergraduate Neuroscience* 1(1): A23–7.
- Jones, A.M. et al. 2014. Abscisic acid dynamics in roots detected with genetically encoded FRET sensors. *eLife* 3: 3158.
- Kass, G.E., & Orrenius, S. 1999. Calcium signaling and cytotoxicity. *Environmental health perspectives* 107 Suppl 1: 25–35.
- Keinath, N.F. et al. 2015. Live Cell Imaging with R-GECO1 Sheds Light on flg22- and Chitin-Induced Transient [Ca<sup>2+</sup>]<sub>cyt</sub> Patterns in Arabidopsis. *MOLECULAR*

*PLANT*: 1–13.

- Kiegle, E., Moore, C.A., Haseloff, J., Tester, M.A., & Knight, M.R. 2000. Cell-type-specific calcium responses to drought, salt and cold in the Arabidopsis root. *The Plant Journal* 23(2): 267–278.
- Kim, S.-H., Yang, G., Kim, T.-J., Han, C.-Y., & Suh, J.-W. 2014. Hypertonic Stress Increased Extracellular ATP Levels and the Expression of Stress-Responsive Genes in Arabidopsis thaliana Seedlings. *Bioscience, Biotechnology, and Biochemistry* 73(6): 1252–1256.
- Kim, S.Y., Sivaguru, M., & Stacey, G. 2006. Extracellular ATP in Plants. Visualization, Localization, and Analysis of Physiological Significance in Growth and Signaling. *Plant Physiology* 142(3): 984–992.
- Knight, M.R., Campbell, A.K., Smith, S.M., & Trewavas, A.J. 1991. Transgenic plant aequorin reports the effects of touch and cold-shock and elicitors on cytoplasmic calcium. *Nature* 352(6335): 524–526.
- Konrad, K.R., Maierhofer, T., & Hedrich, R. 2018. Spatio-temporal aspects of Ca<sup>2+</sup> signalling: lessons from guard cells and pollen tubes. *Journal of Experimental Botany* 69(17): 4195–4214.
- Krebs, M. et al. 2011. FRET-based genetically encoded sensors allow high-resolution live cell imaging of Ca<sup>2+</sup> dynamics. *The Plant Journal* 69(1): 181–192.
- Kudla, J., Batistic, O., & Hashimoto, K. 2010. Calcium Signals: The Lead Currency of Plant Information Processing. *The Plant Cell* 22(3): 541–563.
- Kunze, G. 2004. The N Terminus of Bacterial Elongation Factor Tu Elicits Innate Immunity in Arabidopsis Plants. *The Plant Cell* 16(12): 3496–3507.
- Kwaaitaal, M., Huisman, R., Maintz, J., Reinstädler, A., & Panstruga, R. 2011. Ionotropic glutamate receptor (iGluR)-like channels mediate MAMP-induced calcium influx in Arabidopsis thaliana. *Biochemical Journal* 440(3): 355–373.
- Lam, H.M. et al. 1998. Glutamate-receptor genes in plants. *Nature* 396(6707): 125–126.
- Lampou, K. 2015. Visualizing cell-cell communication in roots of A. thaliana. *Bachelorarbeit* Ruprecht-Karls-Universität Heidelberg: 1–80.
- Laohavisit, A. et al. 2012. Arabidopsis Annexin1 Mediates the Radical-Activated Plasma Membrane Ca<sup>2+</sup>- and K<sup>+</sup>-Permeable Conductance in Root Cells. *The Plant Cell* 24(4): 1522–1533.
- Li, L. et al. 2014. The FLS2-associated kinase BIK1 directly phosphorylates the NADPH oxidase RbohD to control plant immunity. *Cell Host and Microbe* 15(3): 329–338.
- Li, Z.-G., Ye, X.-Y., & Qiu, X.-M. 2019. Glutamate signaling enhances the heat



- tolerance of maize seedlings by plant glutamate receptor-like channels-mediated calcium signaling. *Protoplasma* 23: 139.
- Lim, S.D., Kim, S.-H., Gilroy, S., Cushman, J.C., & Choi, W.-G. 2018. Quantitative ROS bio-reporters: a robust toolkit for studying biological roles of reactive oxygen species in response to abiotic and biotic stresses. *Physiologia Plantarum*.
- Liu, J., & Zhu, J.K. 1998. A calcium sensor homolog required for plant salt tolerance. *Science* 280(5371): 1943–1945.
- Löffler, J. 2018. Combining experimental and theoretical approaches to investigate long-range calcium signalling in plants. *Master thesis*: 1–57.
- Lu, D. et al. 2010. A receptor-like cytoplasmic kinase, BIK1, associates with a flagellin receptor complex to initiate plant innate immunity. *Proceedings of the National Academy of Sciences* 107(1): 496–501.
- Lv, X. et al. 2018. The role of calcium-dependent protein kinase in hydrogen peroxide, nitric oxide and ABA-dependent cold acclimation. *Journal of Experimental Botany* 69(16): 4127–4139.
- Ma, L. et al. 2019. The SOS2-SCaBP8 Complex Generates and Fine-Tunes an AtANN4-Dependent Calcium Signature under Salt Stress. *Developmental Cell* 48(5): 697–709.e5.
- Marhavy, P. et al. 2019. Single-cell damage elicits regional, nematode-restricting ethylene responses in roots. *The EMBO Journal*: 1–18.
- Marti, M.C., Stancombe, M.A., & Webb, A.A.R. 2013. Cell- and Stimulus Type-Specific Intracellular Free Ca<sup>2+</sup> Signals in Arabidopsis. *Plant Physiology* 163(2): 625–634.
- Martineau, M., Parpura, V., & Mothet, J.-P. 2014. Cell-type specific mechanisms of D-serine uptake and release in the brain. *Frontiers in synaptic neuroscience* 6: 12.
- Matthus, E. et al. 2019. Phosphate starvation alters abiotic stress-induced cytosolic free calcium increases in roots. *Plant Physiology*: pp.01469.2018.
- Matzke, A.J.M., & Matzke, M. 2013. Membrane ‘potential-omics’: toward voltage imaging at the cell population level in roots of living plants. *Frontiers in Plant Science* 4: 311.
- McAinsh, M.R., & Hetherington, A.M. 1998. Encoding specificity in Ca<sup>2+</sup> signalling systems. : 1–5.
- McAinsh, M.R., & Pittman, J.K. 2009. Shaping the calcium signature. *New Phytologist* 181(2): 275–294.
- McAinsh, M.R., Brownlee, C., & Hetherington, A.M. 1992. Visualizing Changes in Cytosolic-Free Ca<sup>2+</sup> during the Response of Stomatal Guard Cells to Abscisic

- Acid. *The Plant Cell* 4(9): 1113–1122.
- McAinsh, M.R., Webb, A., Taylor, J.E., & Hetherington, A.M. 1995. Stimulus-Induced Oscillations in Guard Cell Cytosolic Free Calcium. *The Plant Cell* 7(8): 1207–1219.
- Michard, E. et al. 2011. Glutamate receptor-like genes form Ca<sup>2+</sup> channels in pollen tubes and are regulated by pistil D-serine. *Science* 332(6028): 434–437.
- Millet, Y.A. et al. 2010. Innate Immune Responses Activated in Arabidopsis Roots by Microbe-Associated Molecular Patterns. *The Plant Cell* 22(3): 973–990.
- Mittler, R. et al. 2011. ROS signaling: the new wave? *Trends in Plant Science* 16(6): 300–309.
- Miura, K., & Furumoto, T. 2013. Cold Signaling and Cold Response in Plants. *International Journal of Molecular Sciences* 14(3): 5312–5337.
- Miya, A. et al. 2007. CERK1, a LysM receptor kinase, is essential for chitin elicitor signaling in Arabidopsis. *Proceedings of the National Academy of Sciences* 104(49): 19613–19618.
- Moeder, W., Van Phan, & Yoshioka, K. 2018. Ca<sup>2+</sup> to the rescue – Ca<sup>2+</sup> channels and signaling in plant immunity. *Plant Science*: 1–26.
- Monshausen, G.B., Bibikova, T.N., Messerli, M.A., Shi, C., & Gilroy, S. 2007. Oscillations in extracellular pH and reactive oxygen species modulate tip growth of Arabidopsis root hairs. *PNAS* 104(52): 20996–21001.
- Monshausen, G.B., Bibikova, T.N., Weisenseel, M.H., & Gilroy, S. 2009. Ca<sup>2+</sup> Regulates Reactive Oxygen Species Production and pH during Mechanosensing in Arabidopsis Roots. *The Plant Cell* 21(8): 2341–2356.
- Mori, K. et al. 2018. -permeable mechanosensitive channels MCA1 and MCA2 mediate cold-induced cytosolic Ca. *Scientific Reports*: 1–10.
- Navarro, L. 2004. The Transcriptional Innate Immune Response to flg22. Interplay and Overlap with Avr Gene-Dependent Defense Responses and Bacterial Pathogenesis. *Plant Physiology* 135(2): 1113–1128.
- Noshi, M., Mori, D., Tanabe, N., Maruta, T., & Shigeoka, S. 2016. Arabidopsis clade IV TGA transcription factors, TGA10 and TGA9, are involved in ROS-mediated responses to bacterial PAMP flg22. *Plant Science* 252: 12–21.
- Pearson, K. 1901. LIII. On lines and planes of closest fit to systems of points in space. *The London, Edinburgh, and Dublin Philosophical Magazine and Journal of Science* 2(11): 559–572.
- Plieth, C. 1999. Temperature sensing by plants: calcium-permeable channels as primary sensors--a model. *The Journal of membrane biology* 172(2): 121–127.
- Plieth, C. 2010. Signal percolation through plants and the shape of the calcium

- signature. *Plant Signaling & Behavior* 5(4): 379–385.
- Plieth, C. 2016. Calcium, Metaphors, and Zeitgeist in Plant Sciences. *Plant Physiology* 171(3): 1790–1793.
- Poncini, L. et al. 2017. In roots of *Arabidopsis thaliana*, the damage-associated molecular pattern AtPep1 is a stronger elicitor of immune signalling than flg22 or the chitin heptamer O. A. Zabolina (ed). *PLOS ONE* 12(10): e0185808.
- Quan, R. et al. 2007. SCABP8/CBL10, a Putative Calcium Sensor, Interacts with the Protein Kinase SOS2 to Protect *Arabidopsis* Shoots from Salt Stress. *The Plant Cell* 19(4): 1415–1431.
- Ranf, S. et al. 2012. Defense-Related Calcium Signaling Mutants Uncovered via a Quantitative High-Throughput Screen in *Arabidopsis thaliana*. *MOLECULAR PLANT* 5(1): 115–130.
- Ranf, S. et al. 2014. Microbe-associated molecular pattern-induced calcium signaling requires the receptor-like cytoplasmic kinases, PBL1 and BIK1. *BMC Plant Biology* 14(1): 379.
- Ranf, S., Eschen-Lippold, L., Pecher, P., Lee, J., & Scheel, D. 2011. Interplay between calcium signalling and early signalling elements during defence responses to microbe- or damage-associated molecular patterns. *The Plant Journal* 68(1): 100–113.
- Richards, S.L. et al. 2013. Annexin 1 regulates the H<sub>2</sub>O<sub>2</sub>-induced calcium signature in *Arabidopsis thaliana* roots. *The Plant Journal* 77(1): 136–145.
- Sanders, D., Pelloux, J., Brownlee, C., & Harper, J.F. 2002. Calcium at the Crossroads of Signaling. *The Plant Cell* 14(suppl 1): S401–S417.
- Sato, M. et al. 2010. Network Modeling Reveals Prevalent Negative Regulatory Relationships between Signaling Sectors in *Arabidopsis* Immune Signaling S. He (ed). *PLoS Pathogens* 6(7): e1001011.
- Schindelin, J. et al. 2012. Fiji: an open-source platform for biological-image analysis. *Nature Methods* 9(7): 676–682.
- Schmidt, R., Kunkowska, A.B., & Schippers, J.H.M. 2016. Role of Reactive Oxygen Species during Cell Expansion in Leaves. *Plant Physiology* 172(4): 2098–2106.
- Scruse-Field, S.A., & Knight, M.R. 2003. Calcium: just a chemical switch? *Current Opinion in Plant Biology* 6(5): 500–506.
- Sewelam, N., Oshima, Y., Mitsuda, N., & Ohme-Takagi, M. 2014. A step towards understanding plant responses to multiple environmental stresses: a genome-wide study. *Plant, Cell & Environment* 37(9): 2024–2035.
- Shi, H., Ishitani, M., Kim, C., & Zhu, J.K. 2000. The *Arabidopsis thaliana* salt tolerance gene SOS1 encodes a putative Na<sup>+</sup>/H<sup>+</sup> antiporter. *Proceedings of*

- the National Academy of Sciences of the United States of America* 97(12): 6896–6901.
- Smith, J.M. et al. 2014. Loss of Arabidopsis thaliana Dynamin-Related Protein 2B reveals separation of innate immune signaling pathways. *PLoS Pathogens* 10(12): e1004578.
- Somssich, M. et al. 2015. Real-time dynamics of peptide ligand-dependent receptor complex formation in planta. *Science Signaling* 8(388): ra76.
- Somssich, M., Khan, G.A., & Persson, S. 2016. Cell Wall Heterogeneity in Root Development of Arabidopsis. *Frontiers in Plant Science* 07(16): 5214.
- Song, C.J. 2006. Extracellular ATP Induces the Accumulation of Superoxide via NADPH Oxidases in Arabidopsis. *Plant Physiology* 140(4): 1222–1232.
- Stael, S. et al. 2012. Plant organellar calcium signalling: an emerging field. *Journal of Experimental Botany* 63(4): 1525–1542.
- Stanley, C. et al. 2018. Fabrication and Use of the Dual-Flow-RootChip for the Imaging of Arabidopsis Roots in Asymmetric Microenvironments. *BIO-PROTOCOL* 8(18).
- Stanley, C.E. et al. 2017. Dual-flow-RootChip reveals local adaptations of roots towards environmental asymmetry at the physiological and genetic levels. *New Phytologist* 217(3): 1357–1369.
- Sun, Y. et al. 2013. Structural Basis for flg22-Induced Activation of the Arabidopsis FLS2-BAK1 Immune Complex. *Science* 342(6158): 624–628.
- Suzuki, N., & Mittler, R. 2006. Reactive oxygen species and temperature stresses: A delicate balance between signaling and destruction. *Physiologia Plantarum*: 1–7.
- Takeuchi, A. 1987. The transmitter role of glutamate in nervous systems. *The Japanese journal of physiology* 37(4): 559–572.
- Tang, W.J., Fernandez, J.G., Sohn, J.J., & Amemiya, C.T. 2015. Chitin Is Endogenously Produced in Vertebrates. *Current Biology* 25(7): 897–900.
- Team, R.C. 2018. R: A language and environment for statistical computing. <https://www.R-project.org/>.
- Tian, W. et al. 2019. A calmodulin-gated calcium channel links pathogen patterns to plant immunity. *Nature Publishing Group*: 1–23.
- Toyota, M. et al. 2018. Glutamate triggers long-distance, calcium-based plant defense signaling. *Science* 361(6407): 1112–1115.
- Tran, D. et al. 2018. Methanol induces cytosolic calcium variations, membrane depolarization and ethylene production in arabidopsis and tobacco. *Annals of Botany* 29: 87.

- Trempel, F. et al. 2016. Altered glycosylation of exported proteins, including surface immune receptors, compromises calcium and downstream signaling responses to microbe-associated molecular patterns in *Arabidopsis thaliana*. *BMC Plant Biology*: 1–16.
- Tuteja, N., & Mahajan, S. 2007. Calcium signaling network in plants: an overview. *Plant Signaling & Behavior* 2(2): 79–85.
- van den Brink, J., & de Vries, R.P. 2011. Fungal enzyme sets for plant polysaccharide degradation. *Applied Microbiology and Biotechnology* 91(6): 1477–1492.
- Vincill, E.D., Bieck, A.M., & Spalding, E.P. 2012. Ca<sup>2+</sup> Conduction by an Amino Acid-Gated Ion Channel Related to Glutamate Receptors. *Plant Physiology* 159(1): 40–46.
- Waadt, R., Krebs, M., Kudla, J., & Schumacher, K. 2017. Multiparameter imaging of calcium and abscisic acid and high-resolution quantitative calcium measurements using R-GECO1-mTurquoise in *Arabidopsis*. *New Phytologist* 216(1): 303–320.
- Walia, A., Waadt, R., & Jones, A.M. 2018. Genetically Encoded Biosensors in Plants: Pathways to Discovery. *Annual Review of Plant Biology* 69(1): 497–524.
- Wan, J. et al. 2012. LYK4, a Lysin Motif Receptor-Like Kinase, Is Important for Chitin Signaling and Plant Innate Immunity in *Arabidopsis*. *Plant Physiology* 160(1): 396–406.
- Wan, W.-L. et al. 2018. Comparing *Arabidopsis* receptor kinase and receptor protein-mediated immune signaling reveals BIK1-dependent differences. *New Phytologist* 1: 15140.
- Webb, A.A.R., McAinsh, M.R., Taylor, J.E., & Hetherington, A.M. 1996. Calcium Ions as Intracellular Second Messengers in Higher Plants. In *Advances in Botanical Research*. Advances in Botanical Research, 45–96. Elsevier
- Weerasinghe, R.R. et al. 2009. Touch induces ATP release in *Arabidopsis* roots that is modulated by the heterotrimeric Gprotein complex. *FEBS Letters* 583(15): 2521–2526.
- Whalley, H.J., & Knight, M.R. 2013. Calcium signatures are decoded by plants to give specific gene responses. *New Phytologist* 197(3): 690–693.
- Wu, S.-J., Liu, Y.-S., & Wu, J.-Y. 2008. The Signaling Role of Extracellular ATP and its Dependence on Ca<sup>2+</sup> Flux in Elicitation of *Salvia miltiorrhiza* Hairy Root Cultures. *Plant and Cell Physiology* 49(4): 617–624.
- Wyrsh, I., Domínguez-Ferreras, A., Geldner, N., & Boller, T. 2015. Tissue-specific FLAGELLIN-SENSING 2 (FLS2) expression in roots restores immune responses in *Arabidopsis fls2* mutants. *New Phytologist* 206(2): 774–784.

- Yang, Y., & Guo, Y. 2017. Elucidating the molecular mechanisms mediating plant salt-stress responses. *New Phytologist* 217(2): 523–539.
- Yang, Y., & Guo, Y. 2018. Unraveling salt stress signaling in plants J. Li (ed). *Journal of Integrative Plant Biology* 60(9): 796–804.
- Yeomans, J.S. 1979. The absolute refractory periods of self-stimulation neurons. *Physiology & behavior* 22(5): 911–919.
- Yuan, P., Jauregui, E., Du, L., Tanaka, K., & Poovaiah, B.W. 2017. Calcium signatures and signaling events orchestrate plant–microbe interactions. *Current Opinion in Plant Biology* 38: 173–183.
- Zaman, N. et al. 2018. A FRET sensor for live-cell imaging of MAP kinase activity in Arabidopsis. *The Plant Journal*.
- Zhang, L. et al. 2014. Fungal endopolygalacturonases are recognized as microbe-associated molecular patterns by the arabidopsis receptor-like protein RESPONSIVENESS TO BOTRYTIS POLYGALACTURONASES1. *Plant Physiology* 164(1): 352–364.
- Zipfel, C. et al. 2006. Perception of the Bacterial PAMP EF-Tu by the Receptor EFR Restricts Agrobacterium-Mediated Transformation. *Cell* 125(4): 749–760.

## Acknowledgements

Last but not least, I want to thank all the people who supported me during my PhD. The successful completion of this thesis would not have been possible without the support of colleagues and friends.

First of all, I would like to express my gratitude to Guido Grossmann for the opportunity to work on my PhD in 'our' group and for the many opportunities to work on other projects and visits to (international) conferences he provided. I also want to thank Prof. Dr. Karin Schumacher for all the helpful discussions and ideas.

Philipp, when I met you for the first time in Carnegie in 2012 my first thought was "what a silly German". I am happy to conclude that while our love has grown over time, this thought is still as relevant as it was back then. I'm happy to have started the PhD adventure with you at my side. And although I had to give you away to your lovely wife on your wedding day you will always have a special place in my heart.

Aaron, you were the senior scientist in the neighboring lab, but graciously adopted us too. You taught me that failed experiments happen and that it's nothing to get hung up on. You helped all of us through many bad days and were always happy to join for a Feierabend beer. Thank you for all your advice and tips, both in the lab and in the kitchen (my mushrooms taste so much better now!).

My other colleagues, Anna, Vanessa, Linda and Alan. It was a pleasure working besides you in the lab and to keep the whole circus running together. You guys made the lab feel like a team and we tackled many problems together that would have been near impossible alone.

This thesis has been in the making for quite some time and could not have been finished without friends who helped me with proofreading. Thank you Philipp, Anna, Vanessa, Rainer and Victor! An especially big 'thank you' goes out to Nina.

Your moral support was indispensable in the final phase of writing up. You cheered me on when I needed it the most and knowing you were coming over with a bottle of wine motivated me to get the day's work done.

21 E-street, my home, my tribe. Thank you for all the distractions and all the friendships. You guys don't even know how many times it cheered me up to come home to this wonderful community after a hard day at work. We have created so many great memories over the years and we keep making more even after most of us moved away.

The dinner club, Victor, Philipp V, Sara and Marie. We did a lot of things together, but somehow we always managed to include food. Thanks for trying so many different foods (and beers!) with me and for all our culinary themed city trips.

Duizend maal dank gaat uit naar mijn Nederlandse vrienden die regelmatig duizend kilometer reden om mij in Heidelberg te bezoeken. Ellard, Nick, Kobus, Gonda, Robert, Stephan and Yin. Onze weekenden gevuld met Alexander Marcus en bier op de brug gaven me hernieuwde energie en zorgden ervoor dat ik meteen weer uitkeek naar de volgende keer dat jullie langskwamen. Ik ben blij dat we elkaar ondertussen al zo lang kennen en dat alhoewel onze levens veranderen we van binnen nog steeds hetzelfde stelletje idioten zijn.

Guido en Carlijn, als er een prijs zou zijn voor wie me het meest bezocht heeft in Heidelberg dan zouden jullie die makkelijk winnen. Jullie zijn het schattigste koppel dat ik ken. Bedankt voor alle steun, liefde, feestjes, tournooien, BBQs, biertjes, potten pindakaas en alle keren dat ik op de bank bij Jordan mocht slapen!

Lieve Papa, mama, Lex en Ella. Bedankt voor jullie niet aflatende steun. Bedankt voor al het advies, en de ruimte om mn eigen keuzes te maken. Bedankt voor alle interesse in wat ik nou eigenlijk aan het doen was, al kon ik dat niet altijd even goed uitleggen. Bedankt voor alle hulp met de fietsen, computers en medische vraagstukken. Jullie zijn de solide basis die me het zelfvertrouwen geeft om naar een ander land te verhuizen, en de reden om uiteindelijk weer terug te komen.